END-TO-END WELL PLANNING STRATEGIES FOR ALASKA NORTH SLOPE DIRECTIONAL WELLS

By

Neeraj Hemant Mahajan, B.E.

A Project Submitted in Partial Fulfillment of the Requirements

For the Degree of

MASTER OF SCIENCE

in

Petroleum Engineering

University of Alaska Fairbanks

May 2018

APPROVED:

Dr. Santanu Khataniar, Committee Chair

Dr. Shirish Patil, Committee Co-chair

Dr. Abhijit Dandekar, Committee Member

Mr. Ashish Fatnani, Committee Member

Dr. Abhijit Dandekar, Chair

Department of Petroleum Engineering

Abstract

Directional well planning has gained special attention in the Alaska North Slope (ANS) as operators are being compelled to drill increasing numbers of wells from already congested pads because of low oil prices, Capex restrictions, and environmental regulations. This research focuses on two major components of directional well planning: anti-collision and torque and drag analysis in Schrader Bluff, Milne Point. The drilling pattern at the ANS implies very high wellbore collision risk, especially at the shallower section, which affects the safety of drilling operations. However, satisfying anti-collision norms is not the solitary step towards successful well planning. Integration of anti-collision results with torque and drag analysis is essential in evaluating the safety and feasibility of drilling a particular well path and avoiding drill string failures.

In the first part of the study, three well profiles (horizontal, slant, and s-shaped) were planned for each of the two new targets selected in the Schrader Bluff OA sand. Initially, this part of the research compared the performance of the newly developed Operator Wellbore Survey Group (OWSG) error model and the industry-standard Industry Steering Committee for Wellbore Surveying Accuracy (ISCWSA) error model. To provide effective guidelines, the results of error model comparison were used to carry out sensitivity analyses based on four parameters: surface location, well profiles, survey tools, and different target locations in the same sand. The results of this study aid in proposing an improved anti-collision risk management workflow for effective well planning in Arctic areas.

The second part of the study investigates the drillability of the well paths planned using the improved anti-collision risk management workflow. Furthermore, this part of the research aims at defining the end point limits for critical well planning parameters, including inclination and dogleg, such that within these limits, the well path satisfies anti-collision as well as torque and drag considerations. These limits were generated using a drill string optimized in terms of steerable tool, drill pipe size, mud rheology, trip speed, rotational speed, and weight on bit (WOB) during drilling and tripping out operations. The

results of this study would help reduce the cumbersome iterative steps and narrow down the design domain for any well to be drilled on the North Slope of Alaska.

Dedication

I dedicate this work to my parents, my family, and the almighty God.

Table of Contents

List of Figures

Page

List of Tables

Acknowledgements

I would like to express my sincere gratitude to my committee chair, Dr. Santanu Khataniar, for his mentoring, support, and availability throughout my time at the University of Alaska Fairbanks (UAF). He gave me an incredible opportunity to serve as a teaching assistant, which broadened my experience. His mentoring skills as an advisor and instructor have taught me how to carry out research with minimal guidance. Thank you for believing in me, encouraging me, and motivating me at every stage of my studies.

I would like to extend my gratitude to my committee co-chair, Dr. Shirish Patil, for the time he spent with me for this research. He provided valuable assistance from King Fahd University of Petroleum and Minerals (KFUPM) in Saudi Arabia, where he is now Saudi Aramco Chair Professor of Petroleum Engineering. His assistance and contributions, even across a 12-hour time difference, are highly appreciated. Also, I would like to thank KFUPM for allowing Dr. Patil to dedicate his time to this effort.

I would like to thank my committee member, Dr. Abhijit Dandekar, for spending his valuable time and providing helpful tips and suggestions in completing this work. I would also like to thank Mr. Ashish Fatnani for providing software support and agreeing to serve on my committee despite his commitments to Halliburton. I am indebted to my entire committee for always giving me opportunities to grow professionally and personally.

I am greatly indebted to all faculty members who taught me the courses required for my master's program. I am also thankful to Leanne, office manager at the Department of Petroleum Engineering, for her timely help with paperwork and paychecks. I would also like to acknowledge Mr. Chirag Raisharma (DNR, Alaska) for generously providing the field data required for my research.

I would like to thank all the funding sources that have supported me throughout my graduate studies: the Department of Petroleum Engineering for providing me teaching and travel support; the Associated Students of University of Alaska Fairbanks (ASUAF) for travel support; and the Department of Residence Life and the Department of Mathematics and Statistics for providing me an opportunity to fund myself through on-campus student jobs.

I would certainly like to thank the UAF Namaste India community and its extended family. Even though being miles away from home, they have always treated me as a family member and made me feel at home. During my stay in Fairbanks, I was also blessed to have made numerous lifelong friends. They have always encouraged and motivated me through the kind words of wisdom during the hours of need. Thank you for making my stay in Fairbanks one of the most memorable and enjoyable experiences of a lifetime.

Last but not the least, I remain grateful to my father, Mr. Hemant Mahajan, my mother, Mrs. Kalpana Mahajan, and my maternal uncle, Mr. Mukund Dhake, for their endless emotional and financial support. Thank you for believing in me and standing by me through all the thick and thin. You are my strength and I owe everything to you!

CHAPTER 1: INTRODUCTION

1.1 Overview

This report is divided into four chapters. ***Chapter 1*** describes the operational issues related to drilling in the Alaska North Slope (ANS). It also discusses the conventional well planning steps undertaken incorporate these issues and to make a well plan executable. However, it focuses on the well planning steps considered in the current study, namely, anti-collision and torque and drag analysis. This chapter briefly introduces these concepts and states the motivation for selecting these specific well planning steps. Finally, it describes the objectives of the project.

Chapter 2 addresses three research objectives. First, it shows how the confidence level in wellbore positioning degrades in higher latitude areas like Alaska. Second, it analyzes the effects of location, survey tools, and well profiles as a function of error model to determine the best survey tool that will help well planners increase their confidence in wellbore positioning. As a final point, Chapter 2 puts forth an improved anti-collision risk management workflow that would aid effective well planning in Arctic areas.

Chapter 3 is a follow up study and challenges the drillability of the well paths planned using the improved anti-collision workflow proposed in Chapter 2. During this process, it addresses the remaining two goals of the research. Initially, it optimizes the drill string design for its operational limits as a function of steerable tool, drill pipe size, mud rheology, and trip and rotational speed. In the second phase, it uses this optimized drill string to define the limits for variation of inclination and dogleg for the present well density scenario in Milne Point, S-Pad.

Finally, ***Chapter 4*** discusses the overall conclusions drawn from the study with future recommendations for carrying forward the present research.

1.2 Features of Drilling in the Alaska North Slope

The oil and gas operations, particularly the drilling operations, in the ANS are constrained by the rigorous Arctic climate and the presence of thick permafrost (Davies et al., 1979).

1.2.1 Climate

The climate in the ANS is classified as Arctic. Figure 1.1 shows the annual average temperature variation observed at Prudhoe Bay, from a maximum of 55°F during the summer to a minimum of -23°F during the winter, for one climate normal (period of 30 years) from 1971 to 2000. This type of extreme climate has many limitations on oil and gas operations in Alaska. One of the major limitations is that the drilling operations are restricted to the winter months, i.e., October through March (Zarling, 2016). This limitation can be described by two terms: first, the active layer, which is the layer (or depth from the surface) that freezes in winter and thaws in summer; and second, the Arctic rule of thumb: "If it is frozen, keep it frozen" and "If it is thawed, keep it thawed" (Zarling, 2016). These two conditions describe the limitations of the drilling operations in any Arctic conditions because during the winter, the active layer is frozen and thus, the operational challenges and permafrost-related hazards like thermokarst and thermal erosion are less severe. This is because there is no phase change through the vertical section, as both the active layer and permafrost are frozen. However, the severity of the operational challenges and the permafrost hazards increases greatly during the summer because the active layer is thawed, causing a phase change through the vertical section and thus making it difficult to set up a rig to commence the drilling operations. To solve such problems, drilling pads are developed so that the operations can be carried out year-round. The rig and the equipment are also protected from the rigorous climate with the help of rig winterization, which works on the basis of covering and subsequently warming the equipment. The rig floor is covered with wind walls which are insulated and coated with an anti-freezing foam to ensure the safety of the rig, as well as the personnel working on the rig, from the Arctic climate (Fletcher, 2011). The equipment on the rig or the pad generally consists of pipelines, for example mud line, electrical line, stand pipe line, etc., and the well control and the drilling equipment. To protect the various pipelines, special containers called as rig suitcases are used. These containers are kept warm with the help of heated air blowers installed at specific intervals. Degassers are used to protect the equipment related to well control and are kept warm with the help of tarpaulin and hot air blowers (Fletcher, 2011).

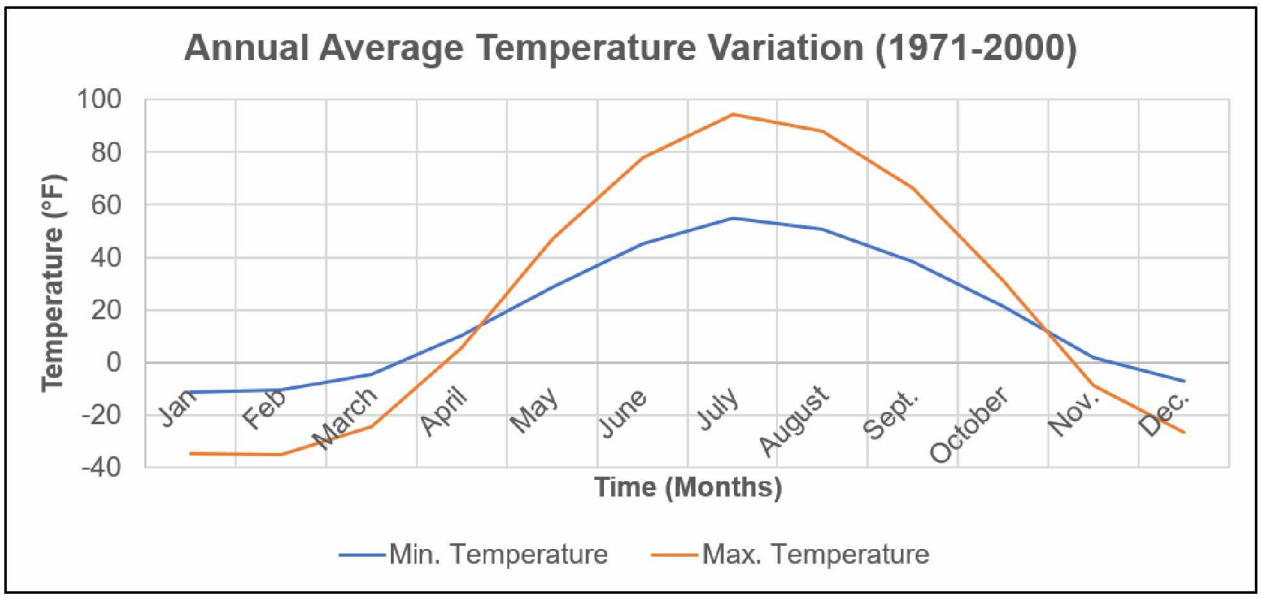

Figure 1.1: Variation of annual average temperature observed at Prudhoe Bay (Zarling, 2016).

1.2.2 Permafrost

Permafrost is defined as soil that is frozen continuously for two or more years (Zarling, 2016). Figure 1.2 shows the distribution of permafrost in Alaska. This figure also shows that all the oil and gas operations in Alaska are in the region of continuous permafrost, defined as the area in which permafrost is present in all directions (Everdingen, 1998). The presence of continuous permafrost creates limitations for well trajectory planning. To maintain permafrost stability, all the wells from a pad are drilled in close proximity, up to 2500 ft. As a result, anti-collision (or collision avoidance) becomes a primary challenge in such areas. Although most of the research about permafrost stability and challenges faced during the drilling operations has been carried out in Prudhoe Bay, the results can be applied in Milne Point. This is because first, the thickness of the permafrost in Milne Point (~ 1800 ft) is similar to that observed in Prudhoe Bay (Smith and Clegg, 1971) and second, the lithology through the permafrost is same as observed in Milne Point as well as in Prudhoe Bay (Shur, 2016).

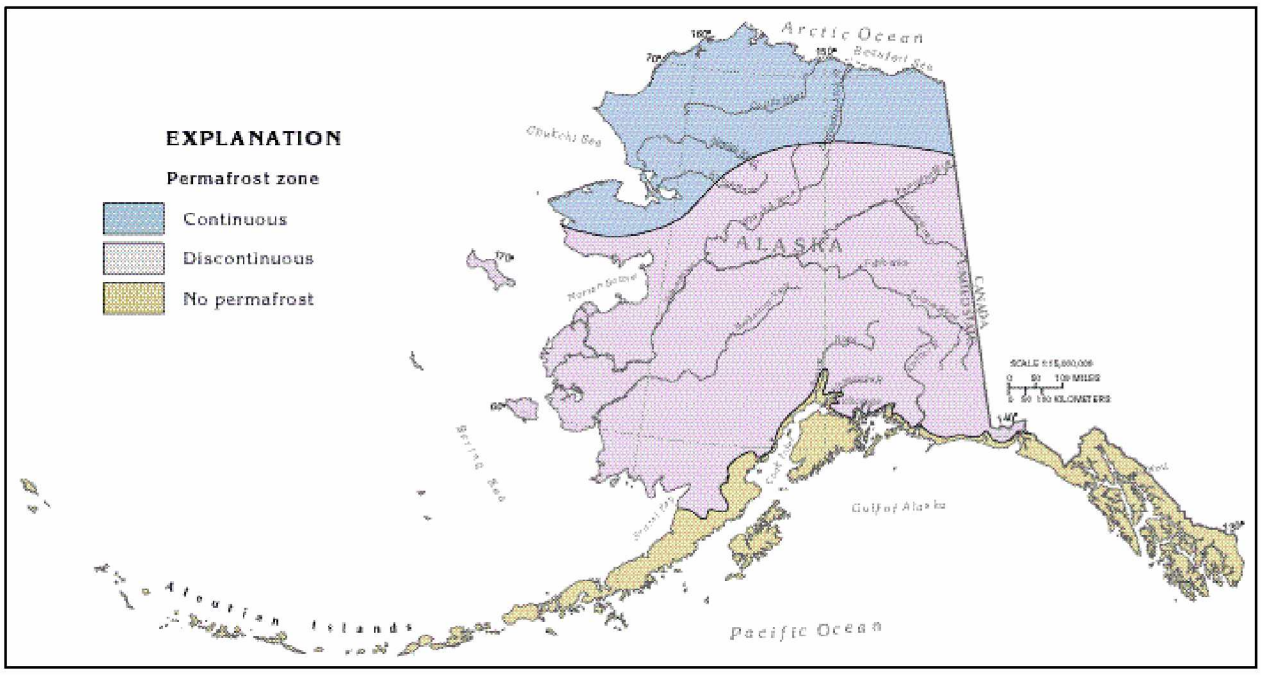

Figure 1.2: Distribution of permafrost in Alaska (USGS, 2017a).

In order to overcome these constraints, it is important to understand the typical challenges encountered while drilling a new well in the ANS so that these challenges can be incorporated in the planning phase to ensure that the drilling operations can be carried out with minimal impact on permafrost.

1.3 Operational Challenges While Drilling Through the Permafrost

1.3.1 Permafrost Thaw Subsidence

The major operational challenge for drilling operations in thick permafrost is the thawing of the frozen permafrost, called as permafrost thaw subsidence. This is a four-step process beginning with melting of excess ice, followed by thaw consolidation and fluid expulsion, which cause pore pressure reduction as well as stiffness reduction (Goodman, 1978). As a result, the casing losses its stability either due to collapse or buckling (Goodman, 1978).

Melting of excess ice is a phenomenon that occurs near the surface. For the frozen soils, ice acts as a cementation material, keeping the pores together. During drilling operations, the soils containing excess ice near the surface are heated due to the circulation of drilling

mud. This causes melting of excess ice as well as cementation ice, which reduces the strength of the soils around the wellbore (Kutasov and Caruthers, 1988). This process causes a phase change of soil from the frozen state to the thawed state, and subsequent reduction in the volume by ~9%. Due to this, the weak thawed soil tries to slump downwards (Goodman, 1978).

The phase change from a frozen state to a thawed state leads to the second step, where the thawed state consolidates followed by fluid expulsion. In this step, pressures greater than the hydrostatic pressures are generated, causing the fluid to expel out of thawed state leading to soil compaction.

The third and most crucial step is the pore pressure reduction. Thawing of pore ice in the shallow permafrost causes an increase in pore pressure due to thaw consolidation and fluid expulsion, but in the deep permafrost causes a decrease in the pore pressure (Goodman, 1978). This process causes intergranular stresses and soil compaction, which in turn generate loads on the casing in the vertical direction.

According to Goodman (1978), stiffness reduction is believed to be the result of all three mechanisms discussed above. As pore ice melts, it causes soil consolidation accompanied by fluid expulsion because of pore pressure reduction. All these processes cause the soil to become weak and soft because the soil loses its support from the pore ice and deforms easily.

1.3.2 Hole Stability

Due to the complex interactions between the casing and the formation (permafrost), drilling operations face other operational challenges like washout or hole enlargement. Hole washout is generally experienced within the first 500 ft of the permafrost and can extended up to 4 ft in radius (Goodman, 1978). The main reason for this phenomenon is the presence of excess ice in the soils near the surface. During the drilling operation, heat transfer between the circulating drilling fluid and the soils near the surface causes the excess ice to melt. This creates a situation of hole enlargement which is technically called washout (Kutasov and Caruthers, 1988). According to Kutasov and Caruthers (1988), the diameter of hole enlargement depends on the properties of the drilling fluid and the soil

in contact with the drilling fluid, temperature, duration of mud circulation, and, most importantly, the amount of fluid infiltration from the drilling fluid into the frozen soil. Washouts not only create issues related to hole stability, but also affect hole cleaning and solid control. Furthermore, they can also cause problems for mud displacement, positioning of insulating packer fluid, and placing of the cement behind the casing also arise due to washout (Goodman, 1978).

1.3.3 Sloughing

Sloughing in the permafrost is a process in which the thawed unconsolidated soil falls down in the hole, causing problems like blocked circulation and fill on the bottom (Kutasov and Caruthers, 1988). From a drilling operation standpoint, frozen soil impermeability and lateral loads are the two main causes of sloughing (Goodman, 1978).

1.3.3.1 Frozen Soil Impermeability

Frozen soil has limited permeability. This restricts the penetration of the filtrate from the drilling mud into the thawed section. As a result, inadequate amount of filter cake is formed on the surface of the wellbore. This causes issues related to hole stability, as hole stability is directly proportional to the amount of mud cake formed on the walls of the wellbore (Rabia, 1985). Hole stability is also related to the pressure differential between the hydrostatic pressure and the formation pressure across the mud cake. However, as the filtrate penetrates into the thawed zone, the pore pressure in the section increases, which in turn increases the formation pressure. Thus, the resulting pressure differential is negative, which causes the wellbore to lose its stability and collapse, leading to sloughing (Goodman, 1978).

1.3.3.2 Lateral Loads

These loads arise from the pore pressure reduction across the frozen soil-thawed soil interface, causing the thawed zone to apply compressive forces on the casing in the inward direction. During the drilling operation, the thaw zone created is very small. As a result, field data regarding the lateral load during drilling operations is not available (Goodman, 1978). Thus, to estimate the effect of lateral loads on hole stability, Goodman (1978) considered a system, shown in Figure 1.3, where the thawed zone across an open

hole is represented as a thick elastic cylinder. The radial inward displacement of the thawed zone, u, caused by the lateral load acting across the thaw front, ΔL is given by Eq. 1.1 (Goodman, 1978)

$$u = \frac{\Delta L}{E_t} \frac{2a}{\left(1 - \frac{a}{b}\right)^2} \tag{1.1}$$

where, a is the wellbore radius, b is the radius of the thaw front, and E_t is the Young's modulus of the thawed material. As seen from Figure 1.3, radial inward displacement, u, will destabilize the hole by exerting the lateral loads on the casing. This is also clear from Eq. 1.1, which shows that as the radius of the thaw front, b, increases, the radial inward displacement, u, decreases (Goodman, 1978). This indicates that when the radius of the thaw front is small, i.e., small thaw, the lateral loads acting on the casing will be large, and thus the radial inward displacement will be large. Since such small thaw zones are encountered only in the drilling operations, the lateral loads pose a significant challenge to hole stability over the total depth of permafrost.

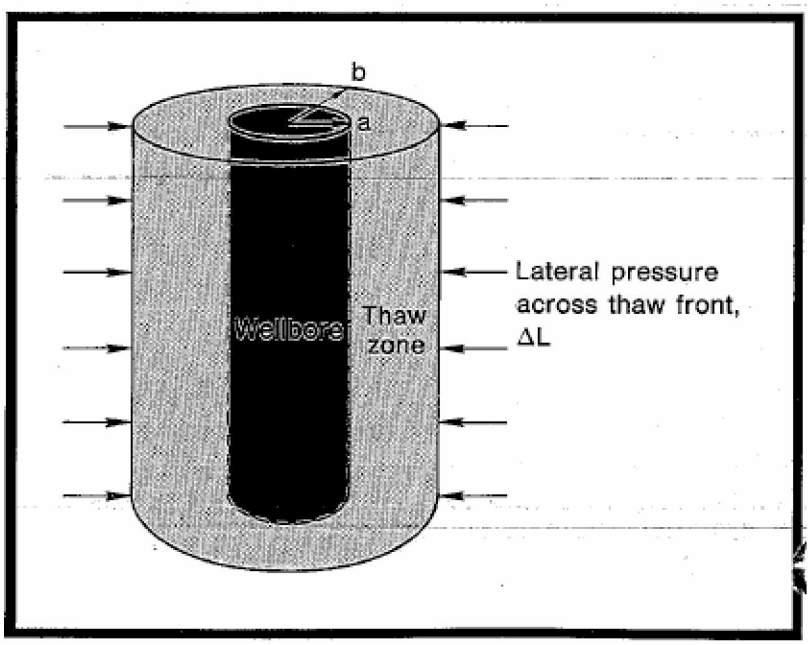

Figure 1.3: Representation of a system of wellbore and surrounding thawed zone to estimate the effect of lateral load during drilling operations (Goodman, 1978).

1.4 Well Planning

As design and operations go hand in hand, it is very important to design a well incorporating all the challenges mentioned in the previous section. This goal is achieved with the help of a thorough and orderly well planning process. Well planning is defined as a process which describes the geometry, orientation, depth, completion and evaluation of a proposed wellbore (Schlumberger glossary, 2017). It is an integrated process which requires a team wherein the geologists work with the drilling engineers to understand the subsurface lithology and its specific characteristics like formation tops, presence of shales, abnormal conditions (pressures and temperatures), and possible production zones (Azar and Samuel, 2007). The drilling engineers subsequently work with the well planning engineers to develop the well plan, with the help of their experience related to the different aspects of drilling operations, engineering tools, and specific well planning software.

1.4.1 Objectives of Well Planning

Apart from designing the well for all operational challenges, the objective of formulating an orderly and step-wise process of well planning is to make sure that the resultant drilling program has the following characteristics (Adams, 1985):

1.4.1.1 Safety

In all the drilling operations, safety of the personnel and rig equipment is considered the most important aspect. Amongst these, the first priority is assigned to the personnel, over all other aspects of the plan (Shanker and Saktavat, 1994). In unfavorable situations, the well plan must be altered to ensure the safety of the personnel. The second priority is assigned to the safety of rig equipments and the well. The well plan must be designed to minimize the risk of blowouts by designing an appropriate size and quality of a blowout preventer (BOP).

1.4.1.2 Minimum Costs

Figure 1.4 describes this objective of well planning accurately. It indicates that if the time required for well planning is long, it will reduce well cost, as the plan will incorporate all

the expected challenges and thus the chances for deviation from the plan and the corresponding increases cost will be eliminated (Adams, 1985).

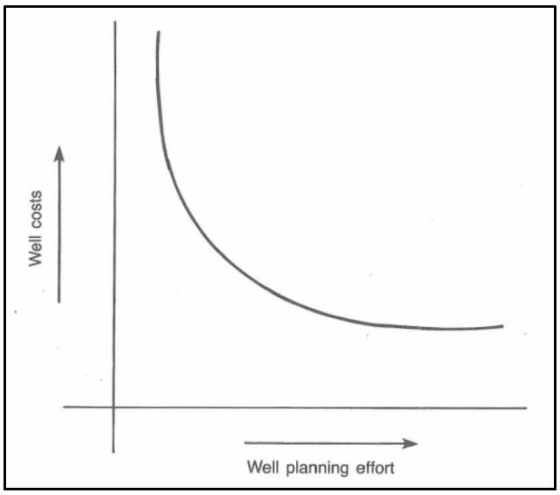

Figure 1.4: Minimized well costs as a result of effective well planning (Adams, 1985).

1.4.2 Conventional Steps of Well Planning

Figure 1.5 outlines the general flow path as well as the steps involved in the process of conventional well planning. However, this order can be altered for various cases depending upon the terms of operator companies (Adams, 1985). This section briefly describes a few of the important steps in this process in terms of their functions and widely used procedures.

1. Data Collection: Data collection is the first step and involves a team of drilling engineers and geologists completing two objectives. First, to understand the sub-surface geology with the help of seismic maps and geological anomalies (for example, faults) with the help of contour maps and correlation logs that would be encountered while drilling the prospect well. Second, to select a suitable offset well based on the similarity of geology expected to be encountered in the prospect well, which can be used as a reliable source for the data requirements during drilling.

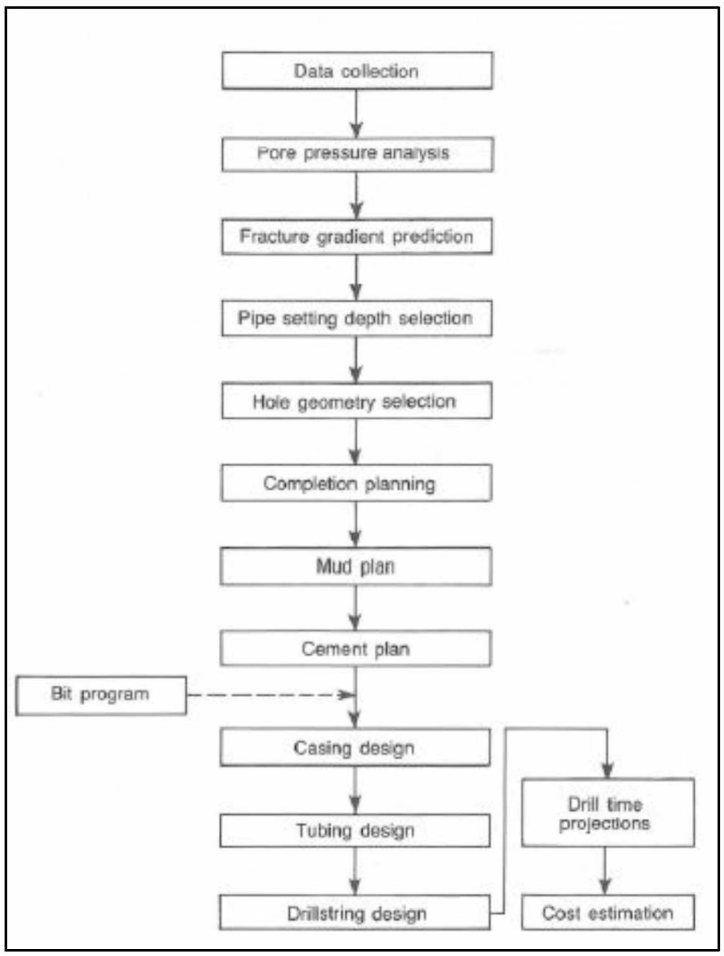

Figure 1.5: Steps involved in conventional well planning (Adams, 1985).

2. Pore and Fracture Pressure Analysis: The next step is to carry out pressure analysis to obtain near accurate values of formation pore pressures and fracture pressures for the expected geology of the prospect well. Estimation of formation pore pressure is critical not only for developing the mud and cement program, but also for classifying the areas in terms of sub-normal and abnormal pressured zones, which possess a great level of difficulty during the drilling operations. Similarly, estimation of the fracture pressure is important for determining the casing setting depths to prevent the formation from getting fractured at the casing shoe while drilling through the next section. When both these pressures are estimated properly, challenges such as lost circulation, stuck pipe, and blowouts can be prevented (Adams, 1985).

3. Casing Setting Depth: Deciding the casing setting depth is the first actual task of a well planning engineer wherein he must select a depth to which the necessary casing will be run and cemented. According to Rabia (1985), the most important geological parameters required for selection of casing setting depths are obtained from pressure analysis. In most of the cases, the process of selecting the casing setting depth has three objectives. First, to cover the zones of lost circulation; second, to cover the zones where differential sticking is likely to be encountered; and third, to protect the weak shallow zones from abnormal pressures (Shanker and Saktavat, 1984).
4. Hole Geometry Selection: The purpose of hole geometry is to select the appropriate bit and casing or liner sizes. According to Rabia (1985), improper size selection can result in small holes which may lead to abandonment of the well. Figure 1.6 describes the combinations of casing and bit sizes generally used in the industry.

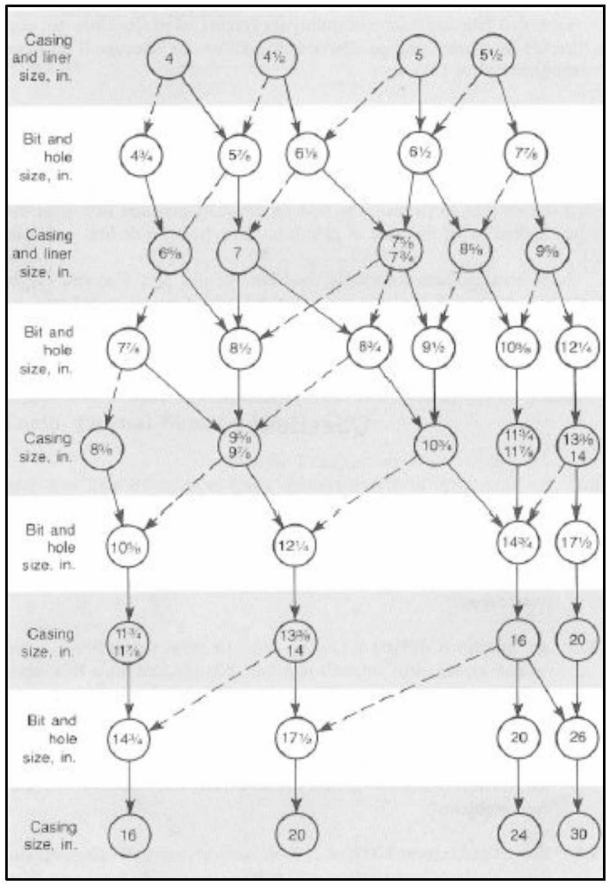

Figure 1.6: Casing and bit sizes chart (Adams, 1985).

5. Mud Design: The first part of mud design deals with estimating the mud weight required to drill through a particular formation. This part depends on the accuracy of the pore pressure data, obtained from either offset well data or seismic analysis. The second part deals with selection of the type of mud that will exert the determined pressures. According to Siddique, Mangla, and Pandey (1985), mud selection depends on factors like clay composition, formation temperature, water content, degree of compaction, and tectonic stresses.
6. Drill String Design: According to Dhar and Gandhi (1985), designing the drill string depends on anticipated depth of the string, expected mud weight, hole size, and size, length, and weight of drill pipe and drill collars. However, the conventional process of drill string design involves designing only the drill pipe and the drill collar (Rabia, 1985 and Adams, 1985).

A similar planning sequence is followed in the ANS (AOGCC, 2017). However, while drilling through the permafrost, there are additional recommendations that are required to be followed to maintain its integrity. These recommendations include (AOGCC, 2017):

1. Maintain low temperature of drilling mud (less than 60°F)
2. Circulate the connections thoroughly
3. Limit Rate of Penetration (ROP)
4. Reduce pump rates

1.5 Well Planning Steps Considered in the Study

1.5.1 Anti-Collision

All the steps mentioned in the previous section can be carried out under the assumption that the well path is executable. In other words, these steps are used to condition the well path so that the target can be reached. However, before questioning the drillability of the planned well path, it is imperative to study how the existing well paths affect the inclination, dogleg, and azimuth of the new planned well trajectories. In this research, this was studied through a pre-conventional well planning step called anti-collision using COMPASS©, a Landmark-Halliburton software.

1.5.1.1 What is Anti-Collision?

In simple words, anti-collision is a process that helps well planning engineers design the inclination, azimuth, and dogleg of the planned (or reference) well path such that it does not collide with the existing (or offset) wells which are already drilled in its vicinity. This points out the fact that the results of anti-collision are greatly dependent on the accuracy of measuring the subsurface wellbore position, which is accomplished by survey measurements (Bang et al., 2009; Bang and Torkildsen, 2011). The inclination, azimuth, and dogleg of the reference well path are planned for each section and are converted to continuous and definitive measurements using surveys. Thus, anti-collision helps in checking the separation between these surveyed wellbores and the offset wellbores wherein the definition of limits for separation vary from company to company. This is because every operator has different error models, which define how positional uncertainty is calculated, and different scanning methods, which define how well path separation is calculated (Compass User Guide, 2011). This process becomes even more complicated because the surveys themselves are a function of error models and survey tools. Hence, it becomes essential to study anti-collision as a function of these properties, such that the best error model and survey tool can be selected to decrease the uncertainties and thus increase the positional accuracy of the wellbore.

1.5.1.2 Importance of Anti-Collision Study

Anti-collision studies are important for a variety of reasons. The most important reasons are increased resource value which causes operators to increase the complexity of well trajectories and lack (or inaccuracy) of survey data for previously drilled wells (Poedjono et al., 2009).

For most cases in the past, operators could tap the reservoirs by drilling vertical wells without being concerned about their surface locations and subsequent anti-collision issues. However, with the wide growth in directional drilling activities, operators are now encountering increasingly complex drilling environments to tap the same reservoirs. This has become a prominent scenario for mature fields like Milne Point, where the existing well density is high, and several wells are often drilled from a single pad. Furthermore,

the operational constraints surrounding the stability of continuous permafrost in Milne Point force the operators to plan and drill wells at very close proximities in a congested environment, potentially leading to wellbore collisions at shallow depths. Hence, in such areas, anti-collision studies become even more crucial, because the well planners have very limited abilities to vary the inclination, azimuth, and dogleg of the reference well path. The entire process occupies a significant portion of the non-productive time (NPT), which might delay the actual drilling process. For multilateral wells in Milne Point, the collision risk scenarios are not confined to shallow depths but extend to the lower 6-1/8" hole section of the wells. In the case of wellbore collision, this combined with the location of Milne Point can cause safety, environmental and financial consequences ranging from minor to catastrophic leading to huge economic losses for the operators (Poedjono et al., 2006; Poedjono et al., 2007a, b).

Many researchers have also stated that the old wells of mature fields like Prudhoe Bay and Milne Point lack the survey data or have very low-quality survey data (Poedjono et al., 2006; Poedjono et al., 2007a, b; Poedjono et al., 2009). In many cases, such data were recorded by hand, which raises questions about their accuracy. To add to this, majority of the wells in Milne Point were surveyed using a magnetic survey tool (AOGCC, 2017). Such tools depend on the geomagnetic properties of the Earth, which changes with time. When the borehole position of such wells is mapped in the present time frame, it may not indicate its actual location. Hence, evaluation of potential hazards is extremely difficult and, in some cases, requires a complete resurvey of the nearby offset wells, which again adds to the NPT. In such scenarios, anti-collision studies are essential so that the uncertainties associated with the reference well can be reduced and can be used to compensate for the unknown uncertainties of the offset wells.

1.5.1.3 Current Anti-Collision Risk Management Models in the Industry

According to Chatar and others (2015), the industry uses two anti-collision risk management models. The first is the risk-based collision avoidance model and the second is the hazard and risk management model.

The risk-based collision avoidance model is followed via an anti-collision policy, a governing document for wellbore collision risk management (Hawkinson, 2014). This policy includes a set of rules that describe how closely a reference well can be drilled to an offset well (McNair et al., 2005). These rules are based on the separation factor (SF) criterion, defined in Eq. 1.2 as (Samuel and Liu, 2009):

$$Separation\ Factor\ (SF) = \frac{C - C\ Distance}{Minimum\ Separation} \tag{1.2}$$

where, C -- C distance is the center to center distance between the reference and offset wells in ft and minimum separation is the sum of the radii of the Ellipse(s) of Uncertainty (EoU) of both wells in ft.

Figure 1.7 shows the SF and EoU used to describe the uncertainties at a particular depth. For the case shown in Figure 1.7, the SF will be 1, which indicates a very high probability of the subject well colliding with the offset well.

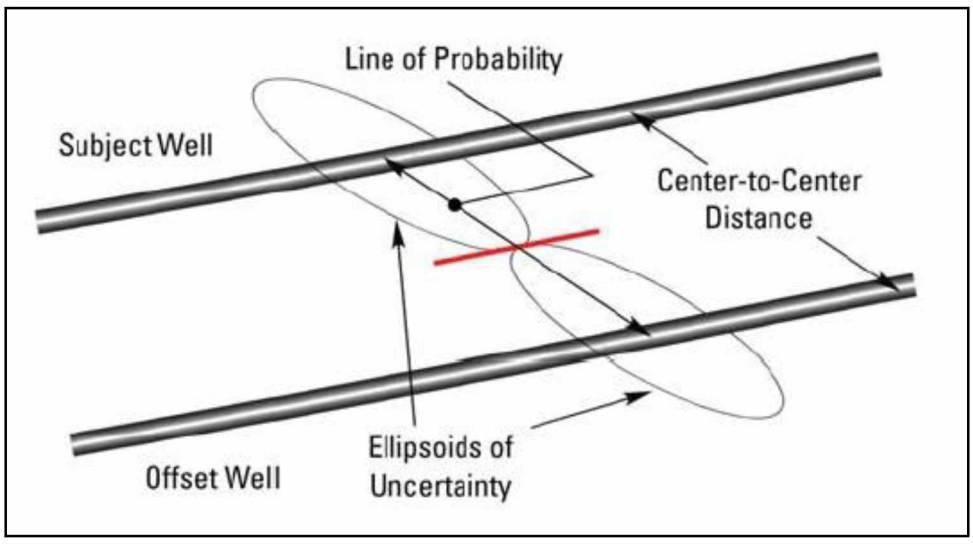

Figure 1.7: Separation Factor (SF) calculation (Poedjono et al., 2007a).

Table 1.1 shows the well planning matrix for the risk-based collision avoidance model and its corresponding limiting SF values. This model is used in the well planning phase because it does not require any additional actions, like drilling manager approval, and the collision issues can be resolved by changing the well trajectory (McNair et al., 2005).

During the planning phase, most of the operators and directional drilling companies plan well paths with a standard SF cut-off value of 1.5.

Table 1.1: Well planning matrix for risk-based collision avoidance model with limiting SF values (Modified from McNair et al., 2005).

Level/Category	Limiting SF value	Action
3	≥1.5	Safe to drill. (Standard SF cut-off value used in the study)
2	1.5 to 1.0	Drillable with mitigation. Mitigation polices vary from company to company.
1	≤1.0	Not drillable. Risk to personnel or facility.

The hazard and risk management model deals with the likelihood and severity of risks expected during the drilling phase. This model is followed via a Hazard Analysis and Risk Control (HARC) matrix, shown in Figure 1.8 (Poedjono et al., 2007a). The main purpose of the HARC matrix is to quantify the severity of every risk associated with drilling a well (HSE, financial, planning, and operational). Another objective of the HARC matrix is to provide solutions on how to reduce these potential risk levels which vary from -25 (maximum risk) to -1 (minimum risk). For the purpose of this study, the potential risk is focused on the probability of collision, whereas the severity of the risk deals with the remedial actions that can be implemented during the operational phase (Chatar et al., 2015). According to Chatar and others (2015), this potential risk of wellbore collision can be reduced either by reducing the likelihood or the severity. In other words, the likelihood of collision can be lowered by reducing the uncertainties associated with wellbore position and the severity can be reduced by shutting the offset wells. However, this process can lead to significant financial loss to the operators. Hence, Chatar and others (2015) have specified various operational remedies which can be used to reduce the severity.

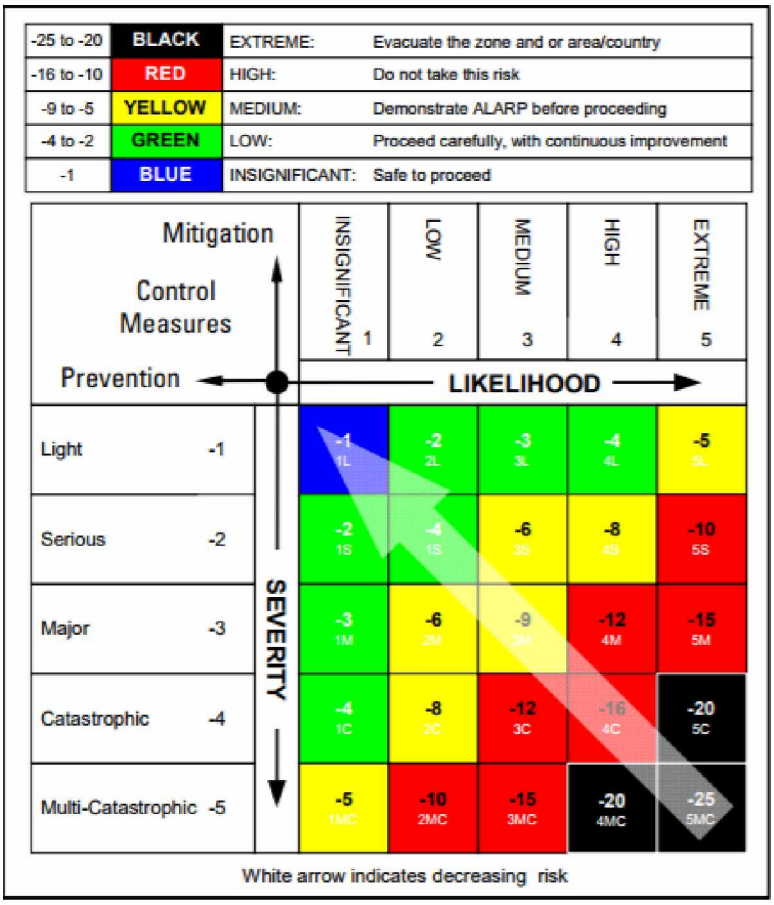

Figure 1.8: Hazard Analysis and Risk Control (HARC) Matrix (Poejdono et al., 2007a).

In summary, the hazard and risk management model is a mix of well planning considerations to reduce the uncertainties and operational considerations to mitigate the problem in real time. Even though this model has been implemented successfully in the industry, it is very subjective and time-consuming, as it requires authorization from the drilling manager at all times. Since this study focuses on well planning considerations, the risk-based collision avoidance model was used. Furthermore, due to the presence of permafrost, this study focuses on anti-collision considerations in the shallower surface hole sections. In such cases, the risk-based collision avoidance model is superior to the hazard and risk management model because mitigation techniques like well control may not be possible in shallower sections (McNair et al., 2005). Moreover, the risk-based collision avoidance model was applied at low latitude, in the Gulf of Thailand (McNair et al., 2005). According to Chatar and others (2015), anti-collision risk management

strategies cannot be transferred directly from low to high latitudes. Hence, this model was selected to examine its performance at high latitude areas like the ANS.

1.5.2 Torque and Drag

During the anti-collision study, azimuth, inclination, and dogleg were used to define the planned well paths. In certain cases, setting a particular magnitude of these quantities would yield a satisfactory well path from the anti-collision standpoint, but the critical question to be answered is the drillability of that well path. Torque and drag is one of the first parameters used to check the drillability of a well path. This study used the torque and drag module of WELLPLAN©, a Landmark-Halliburton software.

However, checking the drillability and optimizing the drill string was not sufficient, because a significant amount of time would be required to perform anti-collision analysis and finalize the azimuth, inclination, and dogleg of the planned well paths. Thus, using the optimized drill string, torque and drag analysis was also used to find the limits for azimuth, inclination, and dogleg such that within these limits, the well path will not only satisfy anti-collision considerations, but will also be drillable from the torque and drag standpoint.

1.5.2.1 Torque

Torque is the moment required to rotate the pipe and is only observed when the pipe is rotated. During drilling operations, this rotational force is usually generated from three sources within the wellbore. These are: 1) frictional torque; 2) mechanical torque; and 3) bit torque (Mims and Krepp, 2003).

Frictional torque is generated by the contact load between the drill string and casing or open hole section. Since the contact load is the major cause of frictional torque, all the parameters which cause contact load to increase will determine the magnitude of frictional torque. Some of these parameters are tension/compression in the drill string, string weight, dogleg severity, inclination, and friction factor (Payne and Abbassian, 1997). Mechanical torque is generated by the interaction of the drill string with cutting beds and unstable formations like sloughing and swelling formations (Caglayan, 2014).

Bit torque or torque at the bit is generated by the interaction between the drilling bit and the formation being drilled. Payne and Abbassian (1997) showed that bit torque is influenced by parameters such as weight on bit (WOB), RPM, formation characteristics, bit design variations, bit wear and hydraulics. Since these are real-time parameters, downhole torque subs are used to measure the torque at the bit. Due to unavailability of real-time data, Eq. 1.3 was used to estimate the torque at the bit (Ulterra, 2017):

$$Torque\ at\ bit = \frac{\mu * D_b * WOB}{36} \tag{1.3}$$

where, torque at bit is in ft-lbf, μ is friction factor, D_b is the bit diameter in inches, and WOB is weight on bit in lbf.

In this study, mechanical torque was considered to be negligible. Hence, the torque values generated in this study are a function of frictional and bit torque.

1.5.2.2 Drag

Drag force is an axial force that replaces torque when the drill string stops rotating and, when the pipe is moved in the axial direction only (Mims and Krepp, 2003). It always acts in the opposite direction to that in which the drill string moves. In other words, drag is the amount of drill string weight being supported by the formation due to friction and contact forces (WellPlan User Guide, 2014).

There are two types of drag forces, depending upon the motion of the drill string: 1) upward drag; and 2) downward drag. Upward drag is experienced during tripping out operations of the drill string, which increase the measured weight of the string at the surface. Upward drag forces are influenced by well trajectory, lubricity, friction factor, wellbore condition, and tortuosity (Payne and Abbassian, 1997). Downward drag is experienced during tripping in operations. Downward drag forces are even more critical during motor drilling operations because they tend to lower the measured weight of the drill string at the surface which limits the motor drilling operations.

In this research, downward drag is studied during drilling operations explicitly using mud motor BHA, whereas upward drag is studied as a function of effective tension and Margin

of Overpull (MOP) during tripping out operations for mud motor as well as Rotary Steerable System (RSS) BHA.

1.5.2.3 Torque and Drag Models

There are numerous mathematical models developed to evaluate the torque and drag behavior of the drill string inside the wellbore. Even though these models are predominantly used in well planning before spudding, they also aid the well planners and directional drillers in troubleshooting during unfavorable situations (McCormick et al., 2011). The industry uses only two types of models for torque and drag analysis: 1) soft string model; and 2) stiff string model.

The soft string model, also called the cable or chain model, is the most commonly used torque and drag model. This model was developed by Johancsik and others (1984) and is based on the assumption that the entire drill string is supported by the wellbore, which makes the drill string behave like a cable or chain. To model torque and drag, the drill string (or cable) is divided into small elements, typically 30 ft intervals. The tension, compression, and torsional forces acting on the entire drill string are calculated by summing up these forces generated across the small elements from the bottom of the drill string to the surface (McCormick et al., 2011). The major disadvantage of the soft string model is the fact that it does not consider the stiffness of the drill string (WellPlan User Guide, 2014). As a result, the bending moment, a function of drill string stiffness and radial clearance of the drill string, is also disregarded which leads to overestimation of the torque and drag estimations (Tikhonov et al., 2014).

The stiff string model, as the name suggests, accounts for the bending moment by taking into consideration the actual stiffness and radial clearance of the drill string (WellPlan User Guide, 2014). Even though there have been many stiff string models developed, none of them have been used as a standard in the industry (Ho, 1988; Cernocky and Scholibo, 1995; Menand et al., 1996; Rezmer-Cooper et al., 1999; Aslaksen et al., 2006; McSpadden et al., 2012; Tikhonov et al., 2014). The requirement of additional inputs and calculations to incorporate the bending forces increases the complexity of the stiff string model. According to Mason and Chen (2007), the majority of stiff string models use either

finite difference, finite element analysis or semi analytical techniques, which leads to their complexity. Hence, the use of such models is justified for wells with high tortuosity, high doglegs, or stiff tubulars (McCormick et al., 2011).

Even though the stiff string models are designed to be more accurate than the soft string model, their disadvantages include selection of appropriate model and high computational time. Hence, in this study, the soft string model is used to predict the torque and drag behavior of the drill string because of its simplistic algorithm, rapid calculation time, and sufficiently accurate results for most common drilling situations (Tikhonov et al., 2014).

1.6 Objectives of the Study

The main aim of this research was to put forth end-to-end well planning guidelines for the directional wells to be drilled in the ANS using Milne Point S-pad as the focal point. This research was carried out in two phases. The initial phase couples the uncertainties associated with wellbore positioning with the risk-based collision avoidance model for Milne Point, S-Pad as a function of survey tools and error models. The second phase deals with checking the drillability of the well paths planned to satisfy the anti-collision criteria using torque and drag analysis. Thus, the key objectives of this research were to:

1. Investigate the effect of location and survey tool on positional uncertainties for all the planned trajectories of horizontal, s-shaped, and slant wells.
2. Examine the performance of the risk-based collision avoidance model at high latitude areas like the ANS.
3. Develop an improved anti-collision risk management workflow for effective well planning in Arctic areas.
4. Narrow down the design search domain of the operational drilling parameters by optimizing the drill string design in terms of steerable tool, drill pipe size, mud rheology, trip speed, and rotational speed.

5. Develop a systematic approach to determine the end point limits for variation of inclination and dogleg such that, within these limits, the well paths satisfy anti-collision and torque and drag considerations.

CHAPTER 2: ANTI-COLLISION RISK MANAGEMENT GUIDELINES FOR ALASKA NORTH SLOPE DIRECTIONAL WELLS[1]

2.1 Abstract

The complex process of anti-collision in directional well planning has gained attention in the Alaska **N**orth Slope (A**N**S) as economic and environmental constraints have compelled operators to drill from already congested pads. The accuracy of the anti-collision study is highly dependent on the positional accuracy of the wellbore, which is associated with the ellipse of uncertainty (EoU). The dimensions of the EoU are based on the error models assigned to the survey tools. Initially, this study compares the performance of the newly developed Operator Wellbore Survey Group (OWSG) error model and the industry-standard Industry Steering Committee for Wellbore Surveying Accuracy (ISCWSA) error model to address their software validation challenges. The main goal of the study was to develop potential anti-collision guidelines for the A**N**S. To achieve this, the results of the error model comparison were coupled with a thorough sensitivity analysis based on four parameters. First, location, to understand the effect of latitude on the ellipse of uncertainty. Second, type of well to be drilled, to understand if anti-collision considerations are well-type specific. Third, survey tools, to understand the limits of the specific survey tool to be used. Fourth, different target locations in the same sand, to understand the differences, if any, among the first three parameters. There are two substantial findings from the study. First, there is a significant change in positional uncertainty with a change in latitude, which implies that higher separation factors should be used for high latitude areas. Second, the uncertainties for the gyroscopic tool are greater than for the Measurement While Drilling (MWD) tool for Arctic locations. The results of this study can serve as potential guidelines for anti-collision planning strategy in the A**N**S.

---

[1] Published as Mahajan **N**.H., Khataniar, S, Patil. S.L., Dandekar, A.Y., Fatnani, A.K. 2017. "Anti-collision risk management guidelines for Alaska **N**orth Slope directional wells" *J. Petrol. Sci. Eng.* 2018 March 20. doi.org/10.1016/j.petrol.2018.03.069 (Modified)

2.2 Introduction

Anti-collision (also called collision avoidance) is a measure taken by every drilling operator to ensure that wells are drilled in a safe manner. Anti-collision monitoring is a complex and demanding process that often was not given the high priority it required in drilling programs. However, as well density increased from one well per 25 acres (101171 m^2) to one well per 5 acres (20234 m^2), anti-collision monitoring was considered a prime objective of well planning (Poedjono et al., 2007a). Generally, this process is carried out via a set of rules called collision avoidance policies. In most cases, the industry uses the separation factor (SF) as the leading collision avoidance indicator. The separation factor is defined in Chapter 1 by Eq. 1.2.

Table 1.1 shows the limiting SF values and subsequent actions that should be carried out to mitigate them. However, like the SF criterion, all other collision avoidance policies require an accurate understanding of the magnitude of uncertainty associated with the positioning of planned (or reference well) and offset wells. These uncertainties are defined and measured by a combination of survey tool that measures inclination, azimuth, and depth of the wellbore, and error model which is applied to the survey tool to quantify the uncertainties. In terms of wellbore placement, the uncertainties are represented by the ellipse of uncertainty (EoU). This EoU is generated at every survey station, usually defined as a point at every 100 ft of measured depth. As seen from Figure 2.1, there are five components of this EoU (Bang et al., 2009). These are:

1. Vertical, uncertainty in depth measurement
2. Horizontal, uncertainty in determining the size of the EoU
3. Along-hole, uncertainty in determining the stretch of the EoU
4. High-side, uncertainty in determining the high side of the borehole
5. Lateral, uncertainty in determining the orientation of the EoU

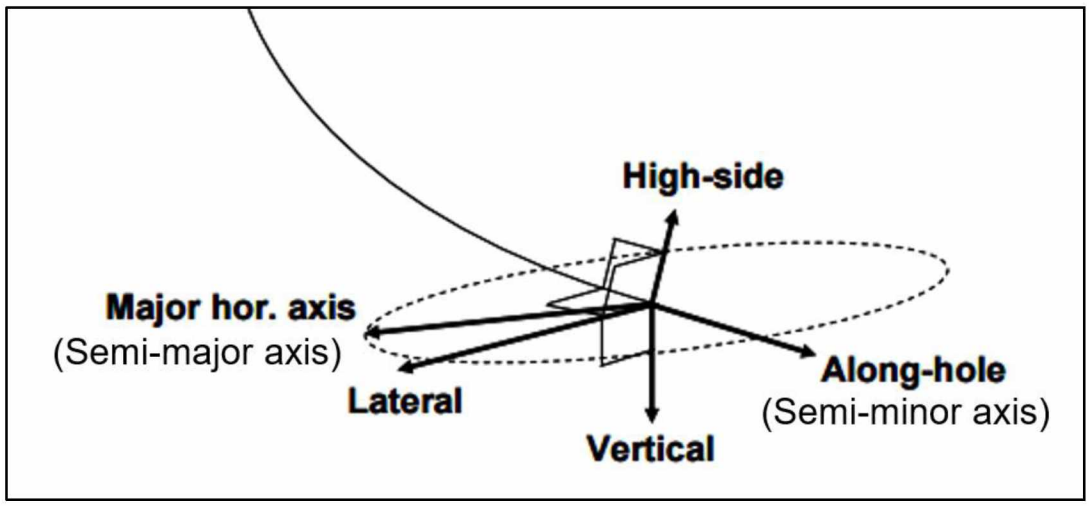

Figure 2.1: Components of Ellipse of Uncertainty (Modified from Bang et al., 2009).

The actual location of the wellbore could be anywhere within this EoU. Thus, smaller the uncertainties, smaller are the dimensions of the EoU and more accurate the positioning of the wellbore. The vertical uncertainties, corresponding to depth measurements, and high-side uncertainties, corresponding to inclination measurements, are independent of geographic location (Bang et al., 2009; Bang and Torkildsen, 2011). However, the horizontal, lateral, and along-hole uncertainties, which correspond to azimuth measurements, depend on geographic location and hence are considered more critical than other types of uncertainties (Bang et al., 2009; Bang and Torkildsen, 2011; Chatar et al., 2015).

Several researchers have described uncertainties associated with survey tools at the well planning phase (Maus and DeVerse, 2015; Bang et al., 2009) and anti-collision considerations in the operational phase using the hazard and risk management model (Poedjono et al., 2009; Chatar et al., 2015; McNair et al., 2005). However, there was a need to integrate these aspects at the core well planning level. In other words, there was a need to understand how the uncertainties in the survey tool affect the SF limits as defined by the risk-based collision avoidance model at higher latitude areas. To fill this gap, the objective of this work was to select new and realistic targets in an actual oil field, namely, Schrader Bluff, Milne Point, and carry out a thorough sensitivity analysis with the goal of developing potential guidelines that can be followed for any well to be drilled in the ANS.

2.3 Anti-Collision in the Alaska North Slope

A critical concern in directional drilling is ensuring collision avoidance while drilling multi-well scenarios from pad locations. Figure 2.2 highlights the importance of anti-collision in the ANS. The existence of several wellbores from one pad implies very high collision risk at the shallower section (Costeno et al., 2014). From the standpoint of well design, this is a unique feature of the ANS because of the presence of permafrost up to ~ 1800 ft. As a result, almost all wells are drilled in close proximity to each other up to 2500 ft. Hence, all our results are defined for the depth of 2500 ft. Due to the constraints of the Arctic location (defined as regions having latitude greater than 66.5°N), including environmental, economic and lack of infrastructure, the operators are forced to drill from already congested pads. To top this, the recent decline of the oil market and subsequent capex restrictions have forced the operators to drill very tortuous well paths from these already congested pads, which further complicates the safety of drilling new wells. Hence, an improved process of anti-collision risk management has become essential in ANS as well as in other areas requiring directional drilling.

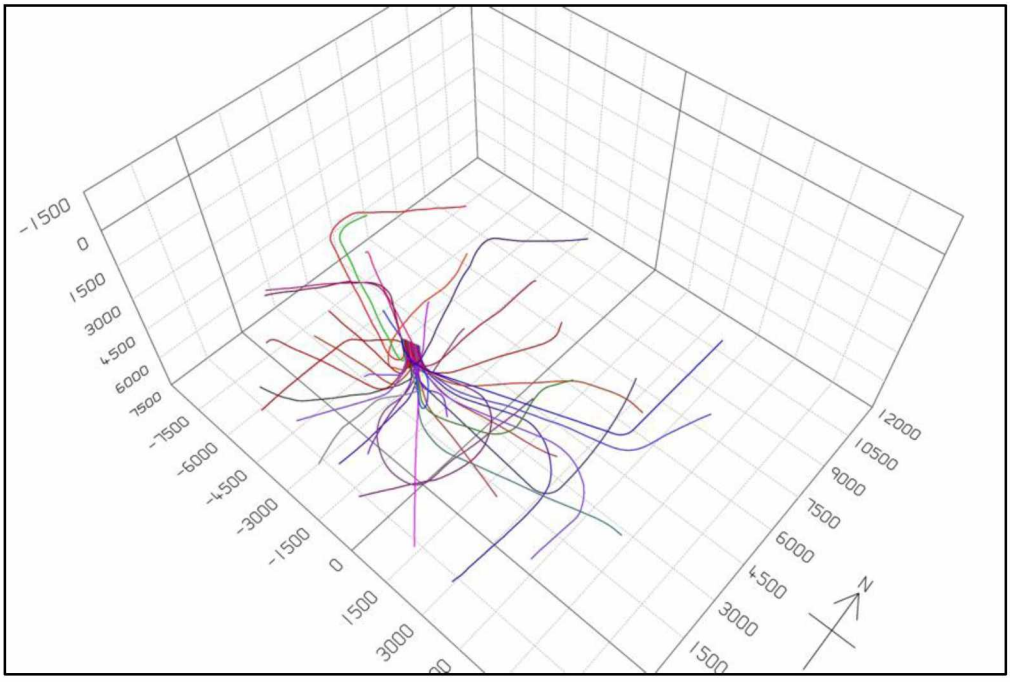

Figure 2.2: Well density of S-Pad, Schrader Bluff, Milne Point.

Along with such complexities, the ANS possess challenges in terms of azimuthal (or lateral) uncertainty because of its latitude and magnetic dip. The changes in azimuthal uncertainty for magnetic survey tools and gyroscopic survey tools are a function of magnetic dip and latitude and are given by Eq. 2.1 and Eq. 2.2, respectively (Bang et al., 2009; Bang and Torkildsen, 2011):

$$\Delta A_{Magnetic} = \frac{K_1}{cosine\ (Magnetic\ Dip)} \tag{2.1}$$

$$\Delta A_{Gyroscopic} = \frac{K_2}{cosine\ (Latitude)} \tag{2.2}$$

where, K_1 and K_2 are constants and magnetic dip and latitude are in degrees.

Table 2.1 shows the geomagnetic properties for the two locations considered in the study. The high latitude of 70°N corresponds to Prudhoe Bay, Alaska, whereas the low latitude of 55°N corresponds to a field in Africa. From Table 2.1, the values of magnetic dip and location for the higher latitude show that azimuthal uncertainties are going to be high for both tools compared to values at the lower latitude. For higher latitude areas like Alaska, this indicates that the type of tool used influences the uncertainties and the subsequent anti-collision considerations. Hence, in such areas, it becomes critically important to select the appropriate survey tool, not only to increase the positional accuracy, but also to avoid enormous economic losses due to wellbore collisions.

Table 2.1: Geomagnetic properties for the locations considered in the study.

Parameter	**Higher Latitude (70°N)**	**Lower Latitude (55°N)**
Magnetic Dip (deg)	81	70
Magnetic Declination (deg)	17.63	16.69
Horizontal Component of Magnetic Field (B_H, nT)	8792	17863
Horizontal Component of Earth's Rotation (E_H, deg/hr)	5.14	8.63

2.4 Methodology

We chose a sensitivity analysis approach to develop potential anti-collision guidelines. Location was selected as the first important parameter to understand the severity of uncertainties as a function of survey tool in higher latitude areas like Alaska. For this parameter, the tools taken into consideration were legacy tools, generic gyroscopic tools, and magnetic tools. The working principles and reasons for their selection will be discussed in the later sections. The second parameter focused on evaluation of the risk-based collision avoidance model at higher latitude locations as a function of survey tools. The third parameter was well profile, to understand if the survey tools have any preference towards a particular well profile. The fourth parameter was different targets in the same sand, to investigate if we can generalize the uncertainty characterization for a particular sand. A summary of parameters for sensitivity analysis is given in Table 2.2.

Table 2.2: Summary of parameters for sensitivity analysis considered in the study.

Parameter	Approach	Aim
Location (Latitude)	High latitude (70°N) vs. Low latitude (55°N)	Investigate the effect of lateral and horizontal uncertainty.
Survey tool	Legacy vs. Generic Gyroscopic vs. Magnetic	Evaluate the performance of the model as a function of survey tools for high latitude areas.
Types of wells	Horizontal Well vs. Slant Well vs. S-Shaped Well	Check preference for uncertainties as a function of well type.
Different targets in same sand	Target 1 vs. Target 2	Analyze the variation in uncertainties for Target 2 for scenario 3.

2.4.1 Selection of Targets

Selection of target is the first and the foremost step in well trajectory planning and hence in anti-collision monitoring. However, due to the unavailability of seismic and geological data for Schrader Bluff OA sand, the target selection was based on the following assumptions:

1. The entire surface of the Schrader Bluff OA sand satisfies all the geologic settings required to classify it as an oil reservoir.
2. The Schrader Bluff OA sand does not contain any faults.
3. The average thickness of the OA sand pay zone is 27 ft. Thus, the new target to be selected should have a thickness of at least 27 ft.
4. The selected target should have maximum possibility of oil accumulation. For example, the selected target should be in the vicinity of a well that is already producing.

Based on the assumptions stated above, the details of the targets selected are described in Table 2.3. Figure 2.3 shows the location of both targets on the OA structure map.

Table 2.3: Position details of selected targets in OA sand.

Target No.	Northing (ft)	Easting (ft)	Depth (ft)	Thickness (ft)	Comments on Location
1	6004166.03	570249.37	4276	43.6	Extended reach target
2	6001316.03	569949.37	4250	29.4	Between two producers

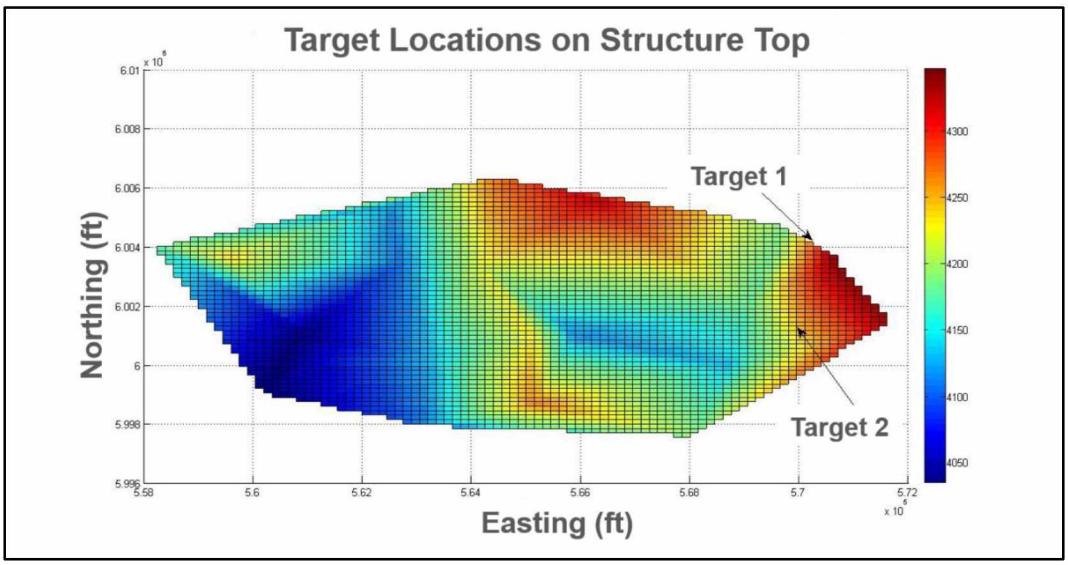

Figure 2.3: Location of targets on 2-D structure map of Schrader Bluff, Milne Point.

2.4.2 Anti-Collision Parameters Considered in the Study

2.4.2.1 Survey Tools

As mentioned in section 2.2, survey tools are used not only to characterize the position of the well path, but also to quantify the corresponding positional uncertainty so that this information can be utilized for collision avoidance among planned and offset wells. The knowledge of positional uncertainty will help the well planners and directional drillers to plan and drill relief wells safely, minimize the risk of crossing lease lines, and hit the target accurately to maximize production (Samuel and Liu, 2009). Hence, it is critical to select the appropriate survey tool that will generate minimum uncertainties and therefore increase the confidence level of positional accuracy.

To determine best survey tool, a broad range of survey tools was chosen spanning from the old legacy tools to recently used generic north seeking gyroscopic and magnetic tools. The legacy tools, including camera based gyroscopic multi shot (CB-Gyro-MS) and camera based magnetic multi shot (CB-Mag-MS), were selected based on the well history report for Schrader Bluff, Milne Point, which indicates that these tools, though considered outdated, were still used in the ANS (AOGCC, 2017). The generic gyroscopic tools included in the study were north seeking gyro (NS-Gyro) and continuous gyro (Gyro-CT).

These tools were selected to compare the functioning of stationary and continuous gyroscopic tools, respectively, especially at high latitude. The magnetic tools include a standard MWD tool and an improved MWD tool with enhanced geomagnetic in-field referencing (IFR) and multi-station analysis (MSA). The main reason for selecting these specific magnetic tools was the fact that improved MWD gives higher positional accuracy than the standard MWD tool (Lowdon and Chia, 2003; Miller et al., 2003; Maus and DeVerse, 2015). However, in our approach, the objective was to check the validity of these results at higher latitudes. Hence, by comparing the uncertainties generated by each tool at higher latitudes, we will be able to determine which survey tool should be used to increase positional accuracy.

The CB-Mag-MS survey tool uses a combination of film disc, pendulum, ring glass with scale, and a compass card to measure the inclination and azimuth by referencing itself to Magnetic North (Inglis, 1987). This tool is greatly affected by nearby magnetic instruments like casing (Inglis, 1987). Furthermore, since this tool uses Magnetic North to measure the azimuth, it must be corrected for magnetic declination which is defined as the angle between True North and Magnetic North. The CB-Gyro-MS survey tool consists of a spinning wheel driven by an electric motor which generates speeds up to 40,000 rpm. The axis of gyroscope is aligned to the True North using an onsite telescope which overcomes the disadvantages of CB-Mag-MS (Inglis, 1987).

The standard MWD tool uses the horizontal component of Earth's main magnetic field to measure the azimuth (Bang et al., 2009). However, like the CB-Mag-MS tool, standard MWD tool must also be corrected for magnetic declination. COMPASS© uses Eq. 2.3 to measure the horizontal component of Earth's magnetic field, B_H, corrected for magnetic declination:

$$B_H = B_{equator} * Cosine\ (latitude) * Cosine\ (declination) \tag{2.3}$$

where, $B_{equator}$ is the magnetic field at the equator in nanoTesla (nT) and declination is in degrees.

In our study, the horizontal component of Earth's main field and magnetic declination were estimated using the International Geomagnetic Reference Field (IGRF) 2015 predictive model.

The improved MWD tool works on the similar principles of standard MWD tool. However, it uses local in-field referencing (IFR) as opposed to the main magnetic field used by standard MWD and CB-Mag-MS tool to measure azimuth. Apart from the main magnetic field, the IFR measurements are dependent on Earth's crustal field and are derived from magnetic surveys by vessels or airplanes that are location specific (Bang et al., 2011). For high latitude areas, these measurements are derived from magnetic observatories which allow for the treatment of magnetic storms caused due to Earth's crustal field by accurate estimation of magnetic declination (Lowdon and Chia, 2003). In Alaska, the observatories at Barrow and Dead horse are used for this purpose (USGS, 2017b). As a result, this method reduces the global magnetic anomalies, which gives more accurate positioning of the wellbore. This tool also uses MSA to reduce the uncertainties arising from axial magnetization. Nyrnes and others (2009) give a detailed mathematical description of the working of the improved MWD tool with MSA correction.

The NS and CT gyroscopic tools use the horizontal component of Earth's rotation to measure the azimuth (Bang et al., 2009; Chatar et al., 2015). This component, E_H, is a function of Earth's rotational rate and is given by Eq. 2.4 (Hawkinson and Mullin, 2014).

$$E_H = 15.041 \frac{deg}{hr} * Cosine\ (latitude) \tag{2.4}$$

2.4.2.2 Error Model

The error model is a mathematical framework for evaluating position uncertainty at every survey station (Jamieson, 2012). Tool error models (also called Instrument Performance Model (IPM) in Compass©, Landmark) provide an estimate of uncertainty of wellbore location based on survey tools (ICF International, 2016). Every survey tool has a discrete error model based on a standardized error model framework defined by Williamson (2000) for MWD and Torkildsen (2008) for gyroscopic tools. For example, there are a total of 27 terms that define the OWSG standard MWD tool error model. However, the critical

terms are azimuthal errors for axial interference (AMIL) and B_H dependent declination (DBHR), given by Eq. 2.5 and Eq. 2.6, respectively:

$$AMIL = \frac{Sin\ (Inclination)\ *\ Sin\ (Azimuth)}{\left(B_{Total}\ *\ Cosine\ (Magnetic\ Dip)\right)} \tag{2.5}$$

$$DBHR = \frac{1}{\left(B_{Total}\ *\ Cosine\ (Magnetic\ Dip)\right)} \tag{2.6}$$

where, B_{Total} is the total magnetic field of the Earth, which is a combination of the main, crustal and external fields, in nanoTesla; and inclination and azimuth are in degrees.

Even though the ISCWSA error models have been standardized in the industry, there have been many issues in their implementation for common practice (Okewunmi and Brooks, 2011; Grindrod et al., 2016). Some of the issues include an excessive number of models (4 revisions for MWD error model and 5 for gyro error model), the complexity associated with each respective model, and the validity of the models (Grindrod et al., 2016).

To overcome these issues, OWSG, a subcommittee of SPE-Wellbore Positioning Technical Section (WPTS), developed a standardized series of five sets of error models called OWSG error models (Grindrod, 2017). In our study, we focus on set A, which is a standard set including the tools that we have selected for the study. However, we use IGRF, a low definition geomagnetic model, as opposed to the default British Geologic Survey Global Geomagnetic Model (BGGM) used in set A of the OWSG error model. Furthermore, one of the challenges mentioned by Grindrod and others (2016) was comparison of the ISCWSA standard error model and the OWSG error model. To address this challenge, we compared the error sources and their magnitudes for both error models. These differences for the respective survey tools are outlined in Table 2.4. For the remaining survey tools, there were no changes in parameters or magnitudes for both the ISCWSA and OWSG error models.

Table 2.4: Differences in parameters and their magnitude for ISCWSA and OSWG error model.

Tool	Terms	ISCWSA Error Model	OWSG Error Model
Standard MWD	AMIL	300 nT	220 nT
	DECR	-	0.1 deg
	DBHR	-	3000 dnT
CB-Gyro-MS	DRFS	3.28084 ft	0.656168 ft
Improved MWD (MWD + IFR1 + MS)	DECG	0.36 deg	0.15 deg
	DBHG	5000 dnT	1500 dnT
	AMIL	200 nT	100 nT
	mbxy	70 nT	35 nT
	mbz	70 nT	35 nT
	msxy	0.00016	0.0008
	msz	0.00016	0.0008

Next, we compared the performance of both error models. Figures 2.4 and 2.5 highlight the comparison results for lateral and horizontal uncertainties generated by both error models at 95% confidence level for a Target 1 horizontal well at 70°N. It is important to note that all the horizontal uncertainties shown in this chapter are generated at 2500 ft. These results indicate that the OWSG error model is in compliance with the ISCWSA error model. However, we prefer the OWSG error model as the default model because it provides a complete range of error model modifications used in the industry and delivers an equivalent single model for both gyroscopic and MWD tools.

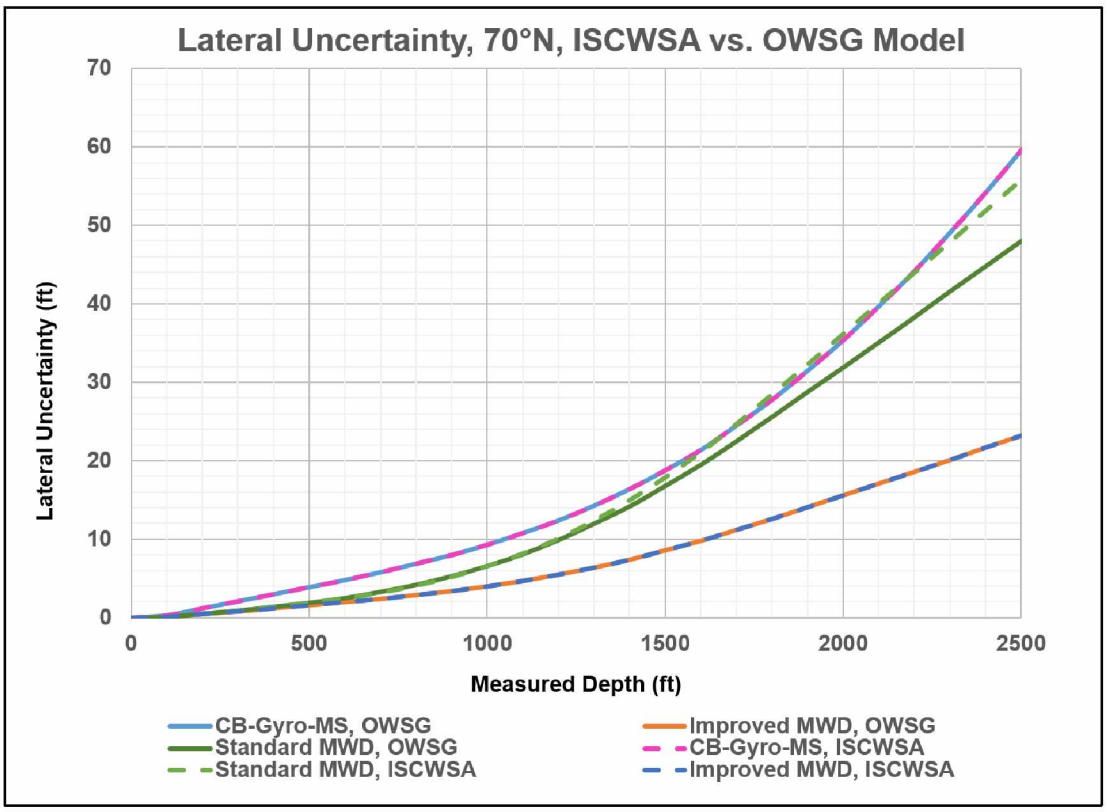

Figure 2.4: Lateral uncertainty comparison, ISCWSA vs. OWSG error model for target 1 horizontal well at 70°N.

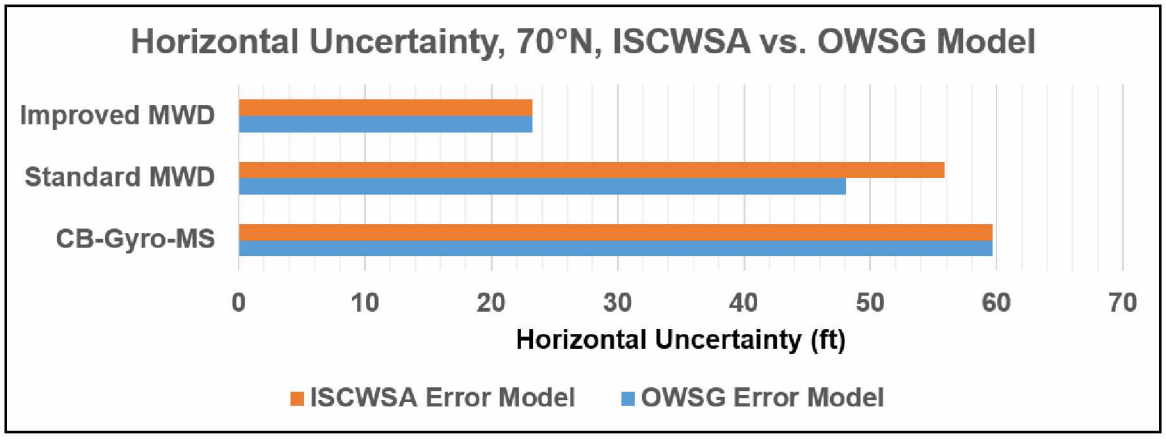

Figure 2.5: Horizontal uncertainty comparison, ISCWSA vs. OWSG error model for target 1 horizontal well at 70°N.

2.4.3 Well Trajectory Planning for Target 1 and Target 2

Before designing the well trajectory, COMPASS© requires the well planner to define the anti-collision settings to be followed while generating the SF plot. Table 2.5 defines the settings used in this study.

Table 2.5: Anti-collision settings used in the study.

Setting name	Aim	Model selected for well planning
Error model	How is positional uncertainty evaluated?	OWSG error model
Survey tool	How is positional uncertainty quantified?	Improved MWD survey tool
Scan method	How is well path separation calculated?	3-D closest approach
Warning type	What criteria is used to issue warnings?	Ratio based (or SF) warning
Error surface	How is SF calculated?	Elliptical conic

This section discusses well trajectory design for slant, s-shaped, and horizontal wells for target 1. A similar approach was used to design the wells for target 2.

2.4.3.1 Slant Well

Slant well design is also called hold-build-hold well design. COMPASS© requires any two parameters from kick-off point (KOP), build-up rate (BUR), maximum inclination, and length of tangent to define the slant well trajectory. In the initial stages of slant well trajectory design, an average KOP and BUR of 473 ft and 3.84 deg/100ft, respectively, were selected from slant well offset data for S-Pad. However, this approach was not able to satisfy the SF plot, as shown in Figure 2.6. Figure 2.6 shows that when the slant well trajectory is planned using the offset data, four of the existing wells will collide with the

well path, because the SF value falls below the acceptable risk levels defined in Table 1.1. This indicates a need to change the planning method. To address such scenarios, nudging is used to offset the trajectory so that it can land at the desired MD, azimuth, or inclination (Compass User Guide, 2011). These properties are finalized based on a trial and error approach.

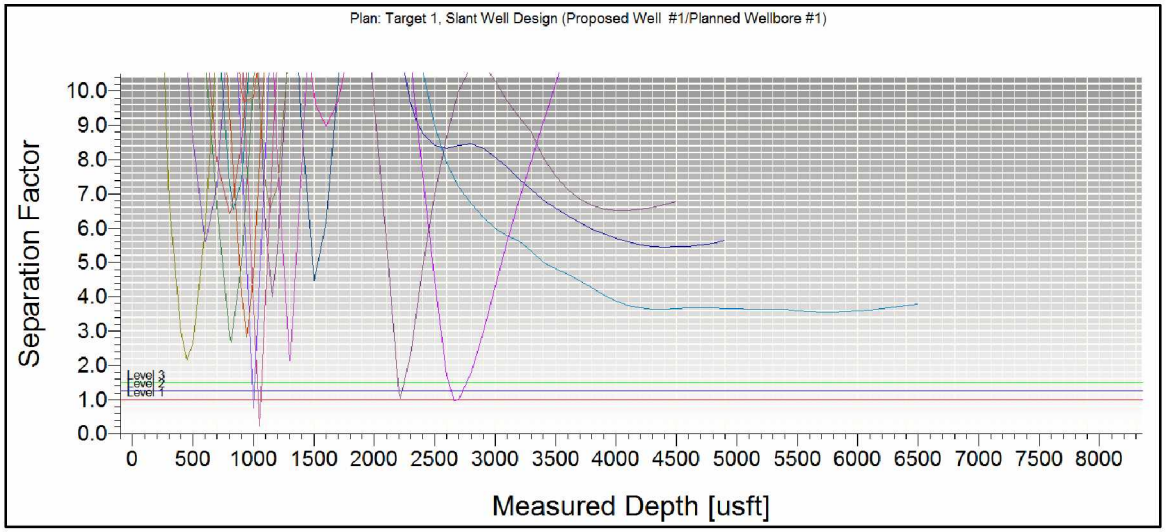

Figure 2.6: Initial SF plot for slant well design for target 1.

Figure 2.7 shows the finalized plan section for a Target 1 slant well generated using nudging technique.

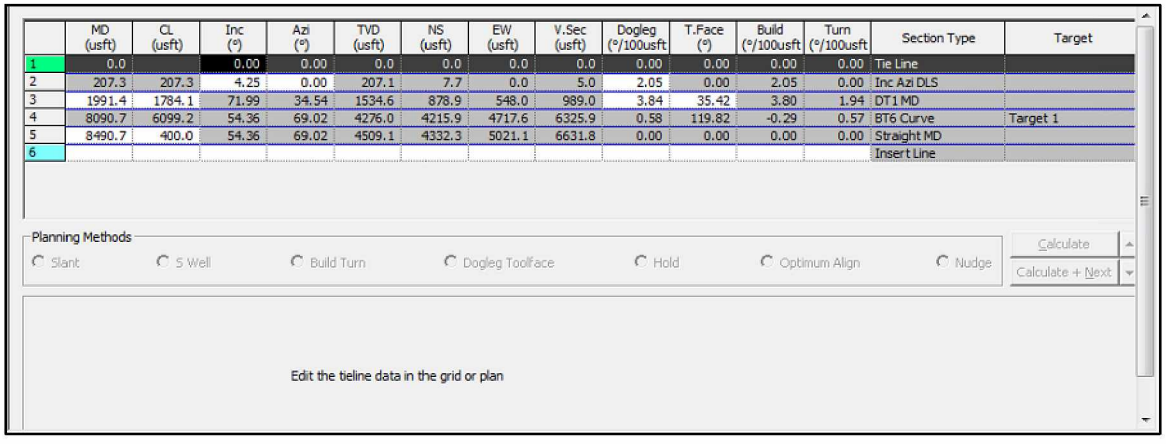

	MD (usft)	CL (usft)	Inc (°)	Azi (°)	TVD (usft)	NS (usft)	EW (usft)	V.Sec (usft)	Dogleg (°/100usft	T.Face (°)	Build (°/100usft	Turn (°/100usft	Section Type	Target
1	0.0		0.00	0.00	0.0	0.0	0.0	0.0	0.00	0.00	0.00	0.00	Tie Line	
2	207.3	207.3	4.25	0.00	207.1	7.7	0.0	5.0	2.05	0.00	2.05	0.00	Inc Azi DLS	
3	1991.4	1784.1	71.99	34.54	1534.6	878.9	548.0	989.0	3.84	35.42	3.80	1.94	DT1 MD	
4	8090.7	6099.2	54.36	69.02	4276.0	4215.9	4717.6	6325.9	0.58	119.82	-0.29	0.57	BT6 Curve	Target 1
5	8490.7	400.0	54.36	69.02	4509.1	4332.3	5021.1	6631.8	0.00	0.00	0.00	0.00	Straight MD	
6													Insert Line	

Figure 2.7: Final plan section for slant well design for target 1.

This plan section is finalized based on Figure 2.8, which shows that none of the existing well paths fall below the cut-off SF value of 1.5 used in the study.

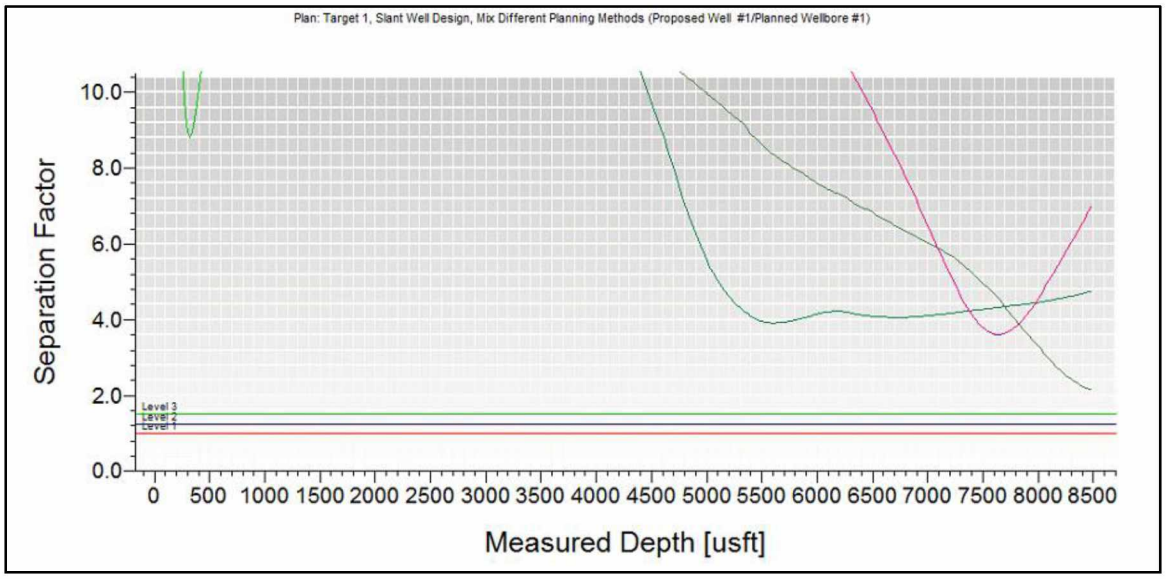

Figure 2.8: SF plot for finalized slant well design for target 1.

2.4.3.2 S-Shaped Well

An S-shaped well design is typically called a build-hold-drop-hold well profile. COMPASS© requires any two parameters from KOP, BUR, maximum inclination, length of tangent, drop rate, final inclination, and length of final hold to define the S-shaped well trajectory. In the initial stages, an average KOP of 404 ft, BUR of 3.73 °/100 ft, drop rate of -3.37 °/100 ft (negative for drop), final inclination of 32°, and length of final hold length of 400 ft were selected from S-shaped well offset data for S-Pad. However, similar to the slant well design, this approach was not able to satisfy the SF plot. Next, a nudging technique was used to plan the well trajectory from an anti-collision standpoint. Figure 2.9 shows the resulting SF plot generated using the nudging technique. As seen from Figure 2.9, this technique was unable to clear the SF criterion due to the very high density of existing wells in the shallower section (~1200 ft MD).

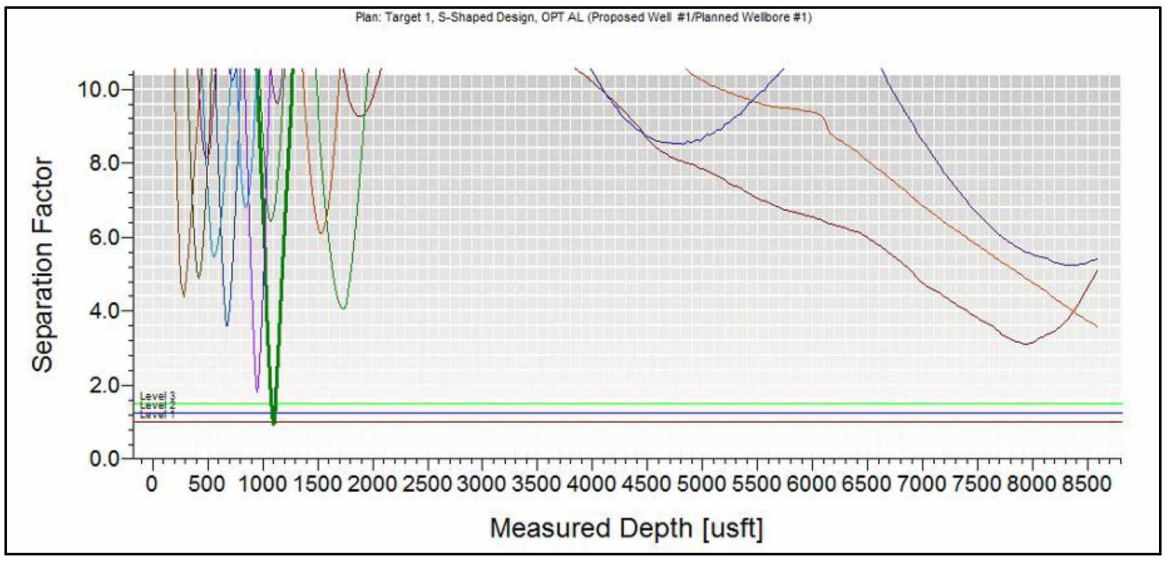

Figure 2.9: SF plot generated using nudging technique for target 1 S-shaped well.

Hence, a new optimum align technique was used to plan the S-shaped well for target 1. This is a curve-hold-curve technique and allows the well planner to reach a target at a specific inclination or azimuth by changing either the dogleg for each curve, TVD for start and end of hold, or length of the hold (Compass User Guide, 2011). The S-shaped well was designed using 4.2 °/100 ft and 3.0 °/100 ft as the doglegs for the build and drop sections, respectively, with a final inclination of 32°. Figure 2.10 shows the plan section generated using the optimum align method.

	MD (usft)	CL (usft)	Inc (°)	Azi (°)	TVD (usft)	NS (usft)	EW (usft)	V.Sec (usft)	Dogleg (°/100usft	T.Face (°)	Build (°/100usft	Turn (°/100usft	Section Type	Target
1	0.0		0.00	0.00	0.0	0.0	0.0	0.0	0.00	0.00	0.00	0.00	Tie Line	
2	300.0	300.0	6.00	0.00	299.5	15.7	0.0	10.8	2.00	0.00	2.00	0.00	Inc Azi DLS	
3	1852.4	1552.4	68.76	52.59	1483.1	601.0	645.9	882.2	4.20	54.64	4.04	3.39	OPT AL DLS	
4	6408.3	4555.9	68.76	52.59	3133.4	3181.0	4018.7	5105.3	0.00	0.00	0.00	0.00	(ditto)	
5	8161.8	1753.5	32.00	0.00	4276.0	4215.9	4717.6	6324.3	3.00	-148.01	-2.10	-3.00	(ditto)	Target 1
6	8633.5	471.7	32.00	0.00	4676.0	4465.8	4717.6	6496.1	0.00	0.00	0.00	0.00	Straight TVD	
7													Insert Line	

Planning Methods
Slant | S Well | Build Turn | Dogleg Toolface | Hold | Optimum Align | Nudge
Calculate
Calculate + Next

Figure 2.10: Plan section using optimum align method for target 1 S-shaped well.

Figure 2.11 shows the anti-collision results for this well plan. Since no existing well paths fall below the SF value of 1.5, the well path shown in Figure 2.10 is finalized from an anti-collision standpoint.

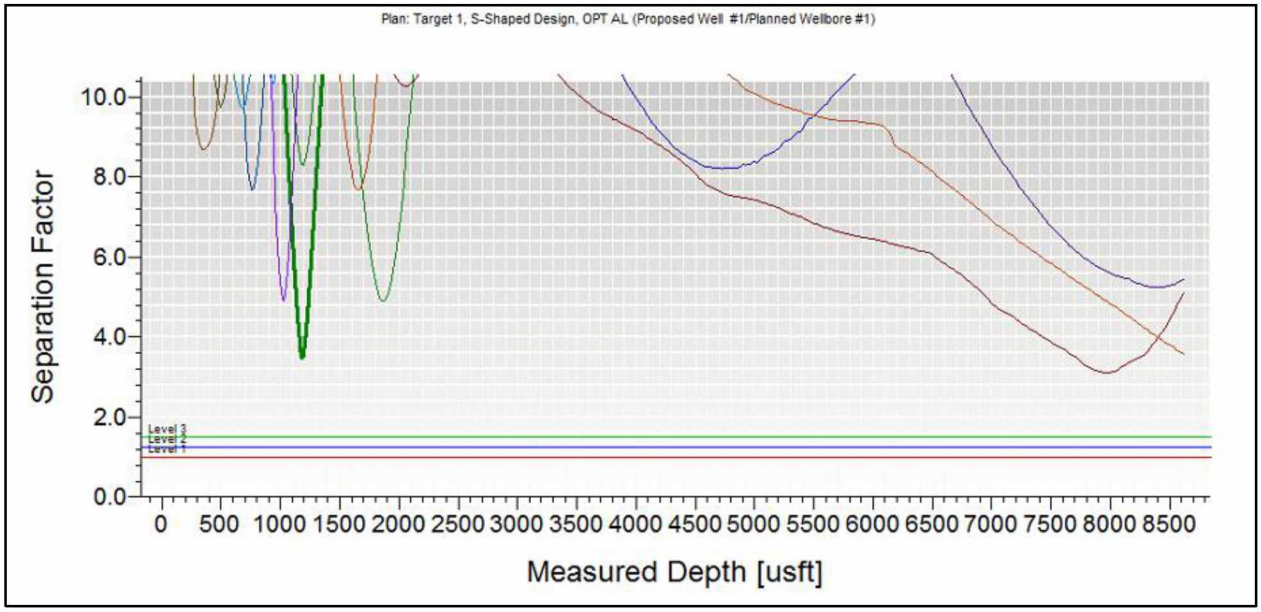

Figure 2.11: SF plot using optimum align method for target 1 S-shaped well.

2.4.3.3 Horizontal Well

COMPASS© does not offer a pre-defined technique for planning a horizontal well. Hence, a combination of nudging and the optimum align method was used to plan the horizontal well. The approach for planning the horizontal well was similar to that for the slant and S-shaped wells. The planning of a horizontal well is based on two assumptions. First, the targets defined in section 2.4.1 are considered the heel of the horizontal well, and second, the length of the horizontal lateral was assumed to be 4500 ft MD (Dunn et al., 2005). Like the S-shaped well, the section above KOP required nudging to prevent collisions with existing wells. The section from KOP to heel was planned using the optimum align method with a desired inclination of 88°, which was achieved using doglegs of 4.5 °/100 ft for the first build section below the KOP and 8.0 °/100 ft for the second build section above the heel. Figures 2.12 and 2.13 show the final plan section and corresponding SF plot for the horizontal well.

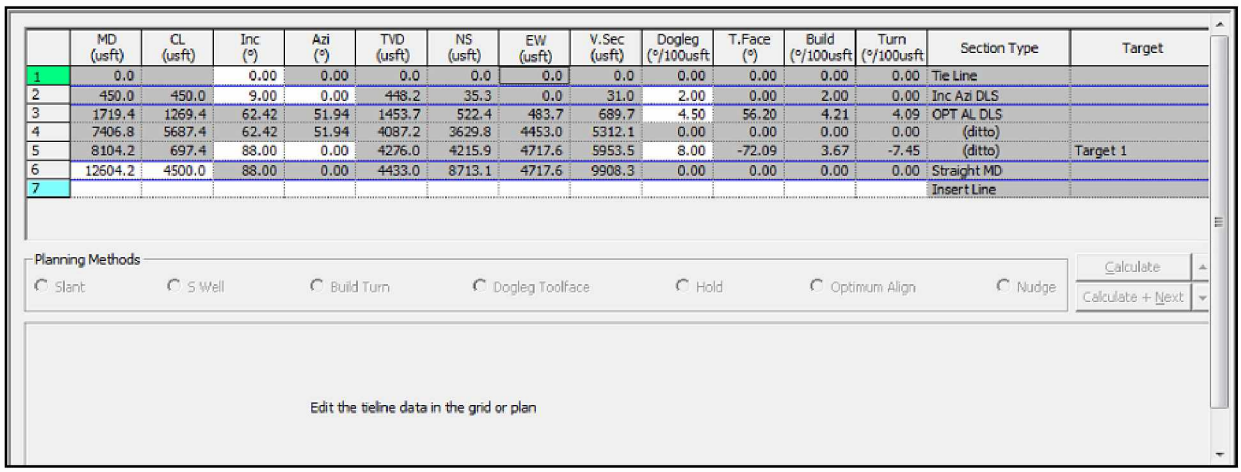

	MD (usft)	CL (usft)	Inc (°)	Azi (°)	TVD (usft)	NS (usft)	EW (usft)	V.Sec (usft)	Dogleg (°/100usft	T.Face (°)	Build (°/100usft	Turn (°/100usft	Section Type	Target
1	0.0		0.00	0.00	0.0	0.0	0.0	0.0	0.00	0.00	0.00	0.00	Tie Line	
2	450.0	450.0	9.00	0.00	448.2	35.3	0.0	31.0	2.00	0.00	2.00	0.00	Inc Azi DLS	
3	1719.4	1269.4	62.42	51.94	1453.7	522.4	483.7	689.7	4.50	56.20	4.21	4.09	OPT AL DLS	
4	7406.8	5687.4	62.42	51.94	4087.2	3629.8	4453.0	5312.1	0.00	0.00	0.00	0.00	(ditto)	
5	8104.2	697.4	88.00	0.00	4276.0	4215.9	4717.6	5953.5	8.00	-72.09	3.67	-7.45	(ditto)	Target 1
6	12604.2	4500.0	88.00	0.00	4433.0	8713.1	4717.6	9908.3	0.00	0.00	0.00	0.00	Straight MD	
7													Insert Line	

Planning Methods

Slant | S Well | Build Turn | Dogleg Toolface | Hold | Optimum Align | Nudge

Calculate

Calculate + Next

Edit the tieline data in the grid or plan

Figure 2.12: Plan section using nudge and optimum align method for target 1 horizontal well.

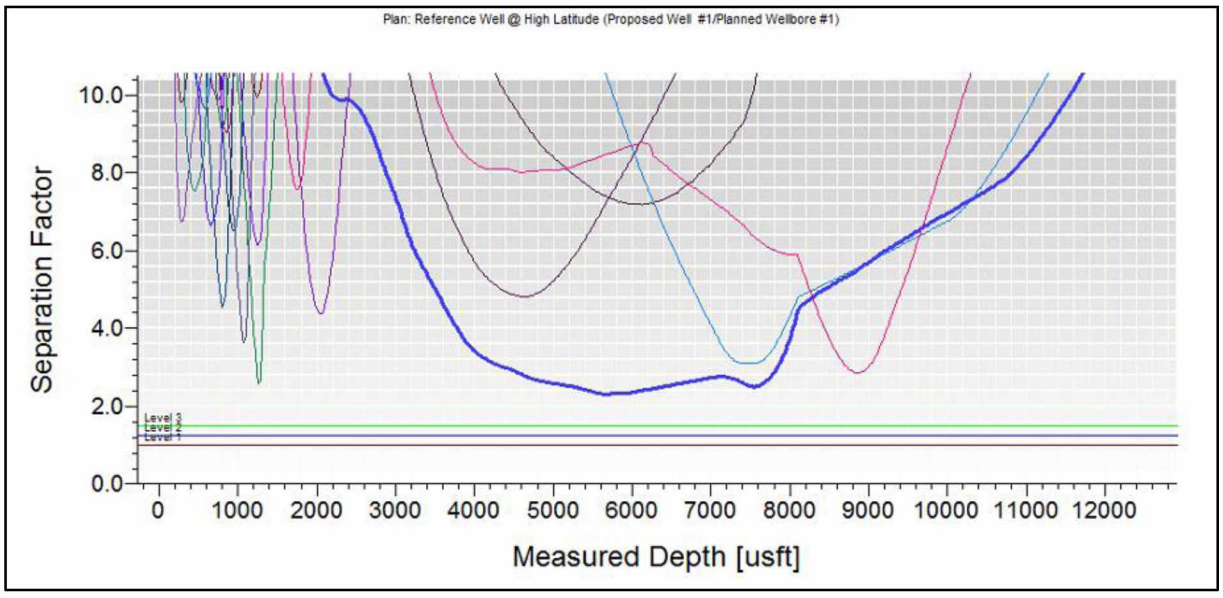

Figure 2.13: SF plot using nudge and optimum align method for target 1 horizontal well.

2.5 Results and Discussion

2.5.1 Effect of Location

Figure 2.14 shows the variation of lateral uncertainty as a function of location and survey tools for a horizontal well. As seen from the figure, the lateral uncertainties at higher latitudes are almost double than those at lower latitudes. The exponential nature of the

curve implies that the uncertainties increase rapidly as MD increases. Figure 2.15 shows the variation of horizontal uncertainty as a function of location and survey tool for a horizontal well. Like the lateral uncertainties, the horizontal uncertainties are also greater at higher latitudes. This is critical because the higher the horizontal uncertainty, higher will be the size of the EoU, which indicates a reduced safety margin for drilling new wells.

In case of magnetic tools, the improved MWD tool generates least uncertainties. This is because it uses both, main and crustal field to measure the horizontal component of Earth's magnetic field. Furthermore, the azimuth measurements are based on real-time declination measurements that are location specific which leads to near accurate uncertainty quantification. On the other hand, standard MWD tool uses only the main field to measure the horizontal component of Earth's magnetic field. As a result, the resolution of the estimated magnetic field is weak. Although the readings for this tool are corrected for magnetic declination, the correction is static. In other words, a single, constant declination value is used to correct these measurements. Hence, the systematic errors which are a function of continuous declination measurements are not accounted in case of standard MWD tool. The CB-Mag-MS tool generates very high uncertainties. This is because COMPASS© does not correct its azimuth measurements for declination error since it falls under the category of legacy tools (Compass User Guide, 2011).

In case of gyroscopic tools, NS-Gyro generates very high uncertainties compared to the other tools. This is due to the combination of Earth's rotation rate and the tool's operating principle. As shown in Table 2.1, Earth's rotation rate decreases at high latitude areas, and, this coupled with the stationary operating mode of NS-Gyro tool, affects its ability to seek North, which decreases its accuracy to measure the azimuth (Bang et al., 2009; Buchanan et al., 2013). The Gyro-CT tool generates least uncertainties because this tool directly and continuously measures the Earth's rotation by finding the True North in real-time. The continuous operating principle overcomes the effect of decrease in Earth's rotation rate which lead to reduced uncertainties (Stockholm Precision Tool, 2017; Huracan, 2017). Furthermore, since the measurements are based on True North, the errors due to magnetic field are eliminated. On the other hand, CB-Gyro-MS tool uses indirect methods to measure True North because the tool is aligned to onsite True North

before running in the wellbore. As a result, the drift errors, which arise when the True North alignment changes, are significant leading to greater uncertainties than Gyro-CT. Furthermore, the drift errors lead to magnetic declination errors, which also contributes to the increased uncertainties.

As shown in Table 2.1, the magnitude of the properties defined by Eq. 2.3 and 2.4 respectively, decreases at higher latitudes. This coupled with the findings from Figures 2.14 and 2.15 indicates that the uncertainties associated with the measurement of azimuth increase in such areas. Hence, Figures 2.14 and 2.15 can be used to conclude that wellbore positioning accuracy degrades in areas of higher latitudes because of increased uncertainties.

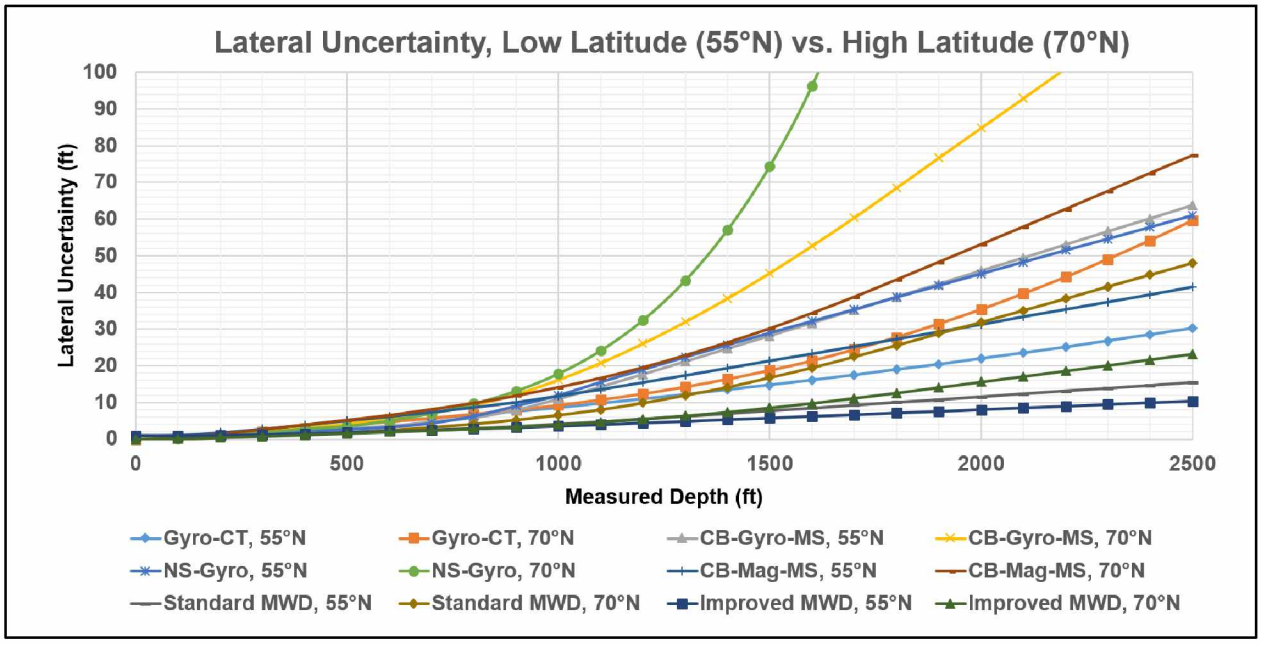

Figure 2.14: Lateral uncertainty as a function of location and survey tools with OWSG error model.

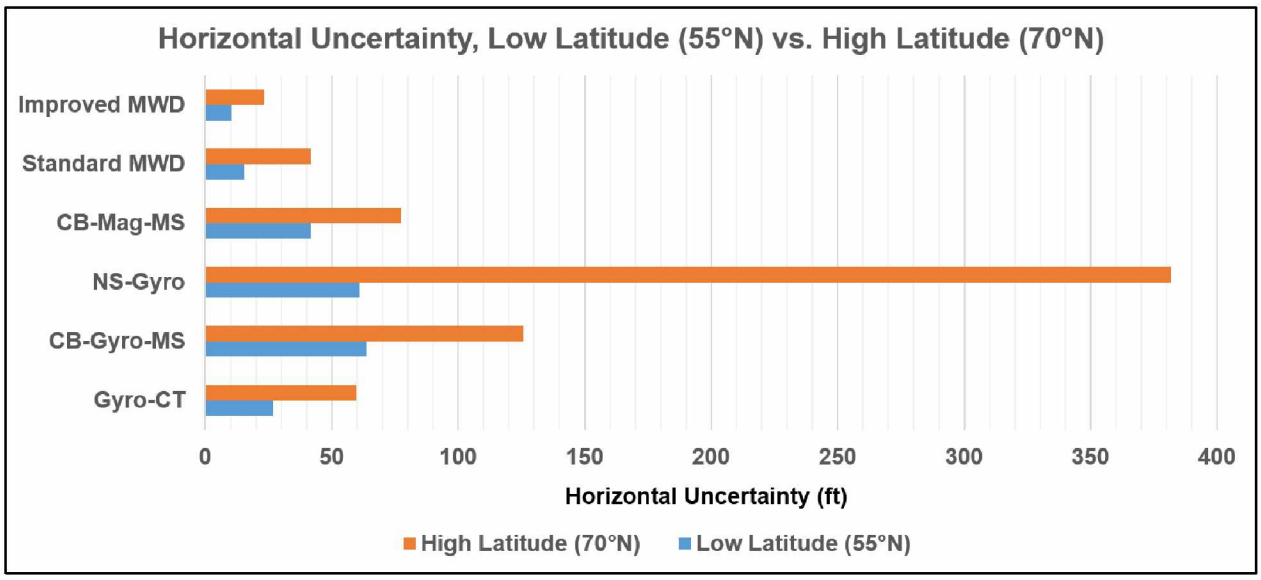

Figure 2.15: Horizontal uncertainty as a function of location and survey tools with OWSG error model.

Although several researchers have concluded that Gyro-CT tool generates higher positional accuracy than both, standard MWD and improved MWD, our results show that these magnetic tools provide more reliable positional accuracy, which is similar to the results reported by Miller and others (2003) and ICF International (2016). We attribute the validity of our results to the working principle of these tools. As mentioned previously, Gyro-CT, standard MWD, and improved MWD use the horizontal component to measure azimuth. From Table 2.1, when we compare the magnitude of E_H and B_H for the same latitude, B_H is significantly higher, meaning that the horizontal component of Earth's magnetic field is significantly stronger than that of its rotation. This indicates that for any latitude where B_H is higher than E_H, the uncertainties generated by magnetic tools will be smaller than those of gyroscopic tools.

Previous studies have shown that gyroscopic tools not only cause cessation of drilling operations, but also require additional rig costs (Miller et al., 2003; Chia and de Lima, 2004; Poedjono et al., 2010). These reasons can have negative impacts on drilling economics, especially in the Arctic, where the average rig cost is around $350,000 per day. Hence, the results presented in the study are critical for economic drilling

considerations in the Arctic, allowing operators to have greater confidence in positional accuracy during real time drilling operations using a magnetic MWD tool.

To keep our study universal, we selected one tool from each of the survey tool categories explained in section 2.4.2.1, which generated smaller uncertainties. This includes CB-Mag-MS from legacy tools, Gyro-CT from generic gyroscopic tools, and improved MWD from magnetic tools.

2.5.2 Evaluation of Risk Based Collision Avoidance Model

As mentioned in section 1.5.1.3, the risk-based collision avoidance model is studied using a ratio-based SF defined by Eq. 1.2. Figure 2.16 shows that the minimum separation for a set of horizontal reference and offset well is higher at higher latitude. This points out that the anti-collision criterion given by the risk-based collision avoidance model will give results, but at a very high risk. The results shown in Figure 2.16 are for a constant c-c distance of 26 ft. Even though this number was arbitrarily chosen, the same trend is seen for all other distances, provided that they are kept constant for both reference and offset wells at high latitude and low latitude, respectively. The higher minimum separation implies that the size of the associated EoU at that depth is high. Thus, based on Eq. 1.2, the SF will be smaller for high latitude areas, which ultimately increases the risk of collision. As shown in Table 1.1, the SF cut-off limit for safe planning, defined at the well planning level by the risk-based collision avoidance model, is 1.5. However, this limit does not incorporate the effect of the increase in minimum separation because its value used in the industry remains the same (1.5) irrespective of location. Hence, these results indicate that the industry should use a SF greater than 1.5 as the cut-off limit for safe well planning, especially in areas like Alaska, the North Sea, and the Barents Sea.

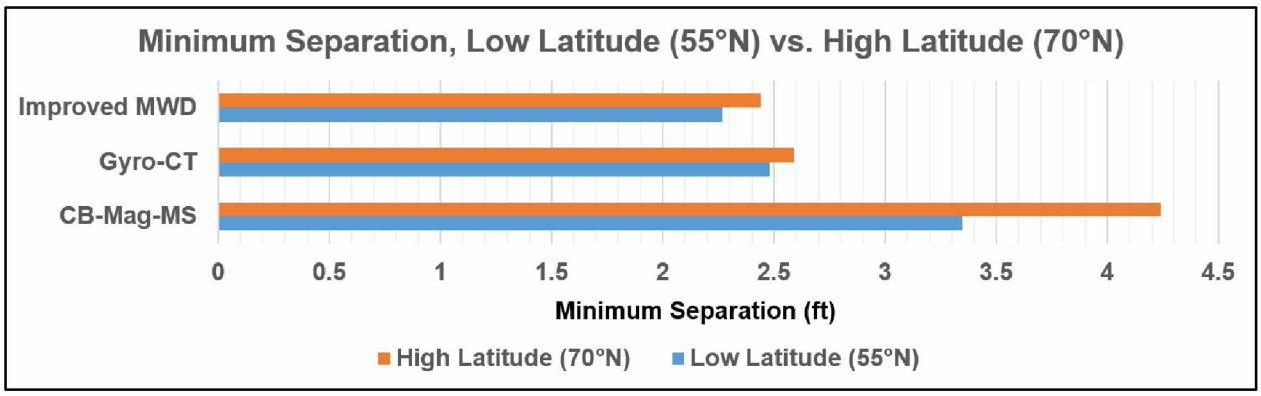

Figure 2.16: Minimum separation for different survey tools at 70°N and 55°N.

Bang and Torkildsen (2009) have shown a way to address the large uncertainties associated with high latitudes using the concept of the wellbore separation expansion factor (F). They defined F as the ratio of the minimum separation at high latitude (75°N) to the minimum separation at low latitude (60°N), with an average magnitude of 1.70. The magnitude of F can be considered the new SF cut-off limit because it scales the smaller uncertainties associated with lower latitudes to higher latitudes, provided that the c-c distance and the confidence level remain constant. In our study, generating an F value for the ANS was not possible for several reasons. Firstly, Bang and Torkildsen (2009) were able to derive this value from a very large data set (281 cases) as a function of various well profiles (spanning vertical to deviated to horizontal) and four combinations of survey tools. In our case, we only had access to one horizontal well with three combinations of survey tools. Secondly, the choice of lower latitude plays a crucial role in determining the value of F. The lower the latitude, the smaller the minimum separation, which will increase the magnitude of F. In some cases, it might also lead to a very unrealistic value. The choice of lower latitude can vary from company to company, but we recommend selecting the latitude based on similarity of well density. For example, based on the well density of Milne Point S-Pad, any field from the Gulf of Mexico with 25°N latitude can serve as a good lower latitude candidate. Thirdly, the value of minimum separation for both latitudes changes with the c-c distance. Bang and Torkildsen (2009) did not provide any justification for selecting 196.8 ft and 492 ft as the two choices for c-c distances for the 281 cases. One way to solve this dilemma is evaluating the minimum separation at minimum c-c distance (Chatar et al., 2015). However, even though F = 1.70

cannot be used for the ANS directly, it can serve as a base for a new SF cut-off value to be used in higher latitude areas.

2.5.3 Effect of Well Profiles

Figures 2.17 and 2.18 indicate the variation of horizontal and lateral uncertainties at 70°N with survey tools and well profiles including horizontal, slant, and S-shaped wells. By comparing them with Figures 2.14 and 2.15, it is clear that even though there is a slight change in the magnitude of uncertainties, the trend is similar. Hence, we can conclude that both uncertainties are independent of well profile and depend only on survey tool. Regarding the survey tool, the improved MWD tool outperforms all the other tools as it decreases the uncertainties by an average of 73% for all well profiles when used with the OWSG error model. This average decrease to 63% when used in conjunction with the ISCWSA error model. This not only highlights the better performance of the OWSG error model, but also clarifies the reason for using it as a default error model.

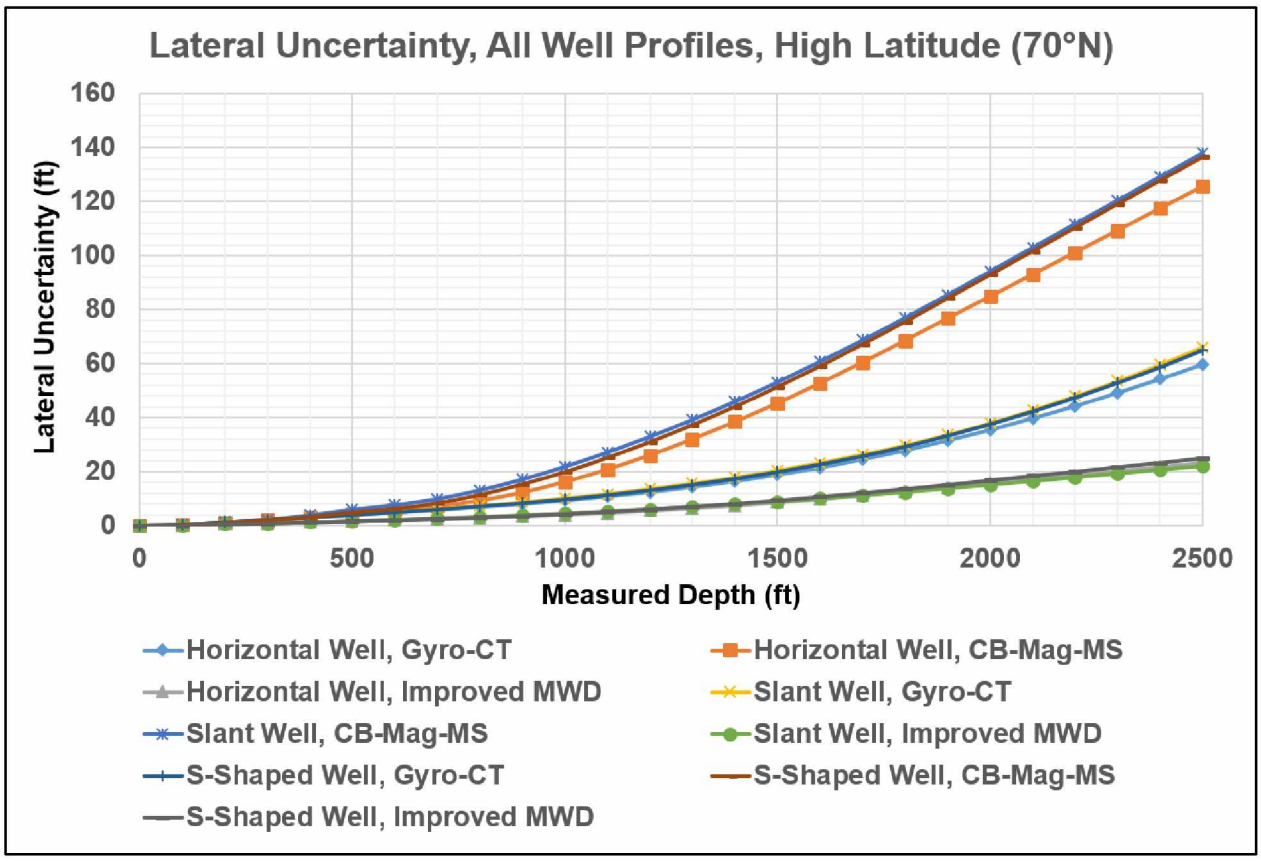

Figure 2.17: Lateral uncertainty for all well profiles for target 1 at 70°N.

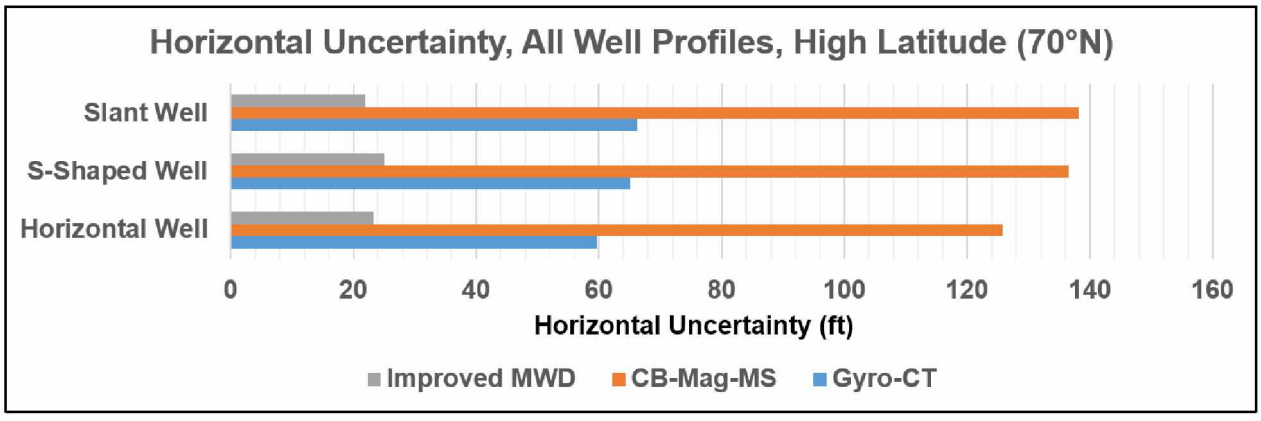

Figure 2.18: Horizontal uncertainty for all well profiles for target 1 at 70°N.

2.5.4 Different Targets in same Sand

Next, to investigate if we could generalize the uncertainties in the same sand, we selected two targets. The locations of these targets are shown in Figure 2.3. Both targets are realistic from the standpoint of drilling engineering, having an MD/TVD ratio of 2.84. Figure 2.19 shows that we can generalize the uncertainties to some extent because the lateral and horizontal uncertainties for each target overlap. However, this is possible only in 2-D wellbores where the semi-major axis is equal to the lateral axis (Bang et al., 2011). For Figure 2.19, our results are focused on the horizontal well because 47% of the wells drilled in S-Pad are horizontal (AOGCC, 2017). The uncertainties are characterized only by the improved MWD tool because of its performance superiority over other tools as shown by Figures 2.17 and 2.18.

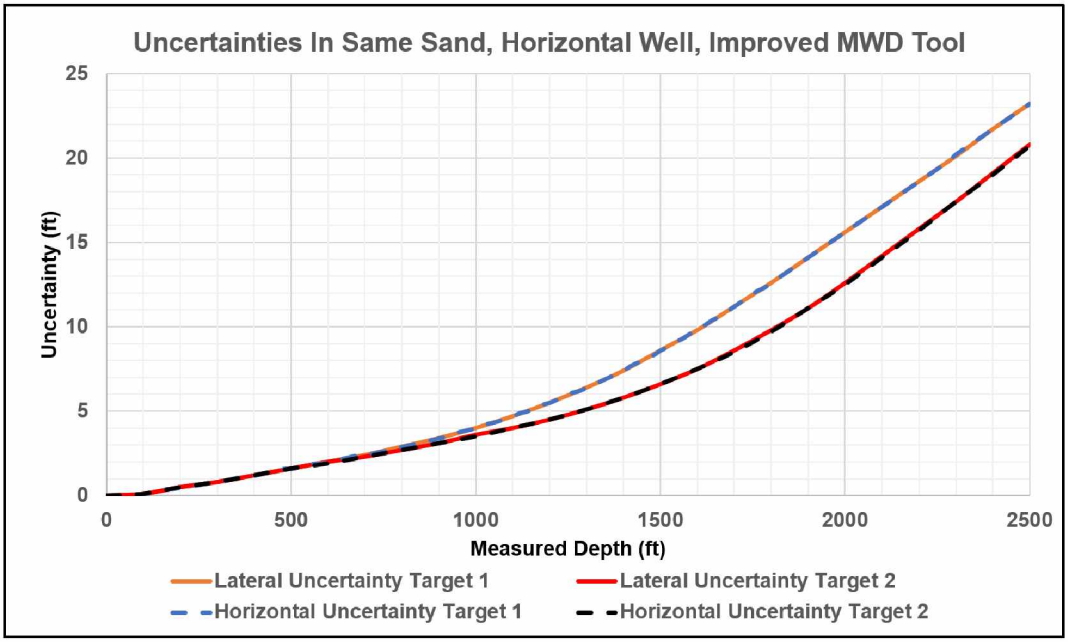

Figure 2.19: Horizontal and lateral uncertainty for horizontal well at target 1 vs. target 2.

2.6 Application

The results of this study have led to the development of an improved flowchart to integrate anti-collision and survey tools at the well planning level for higher latitude areas (Figure 2.20). In the initial stages, well planners design the well paths to the targets assigned by geologists. These well paths can either be horizontal, slant, or S-shaped. Our results

indicate that the uncertainties have no preference over a particular well profile. Hence, there is no limitation over selection of a specific well path. In the next step, the well planner will select the appropriate survey tool and error model that will characterize the uncertainties at every survey station. For the survey tool, our results show that the magnetic tools provide higher positional accuracy than the gyroscopic tools do for higher latitude areas. In terms of economics, operators can combine the results of this study with their proprietary cost data to optimize their choice of tools. Though this would depend on company policies, we recommend using the improved MWD tool throughout the entire drill path. For error model, we recommend using the OWSG error model with the magnitudes defined by Grindrod (2017). Once the survey tool and error model have been selected, the next step for the well planner would be to select the offset wells that are in close proximity to the planned well. The most critical step in terms of anti-collision would be to check the SF between the planned and offset wells using the SF plot. In this step, we recommend using a higher SF than the widely-used value of 1.5, however, the actual value may vary from company to company. It is important to note that directly using the SF cut-off limit of 1.70, as defined by Bang and Torkildsen (2009) could lead to a conservative well planning approach. If the SF criterion is satisfied for all survey stations, all the anti-collision criterions are satisfied, and the well is ready to drill. However, if the SF is not satisfied, the well planners should optimize the well path by changing either azimuth, inclination, or dogleg. Simultaneously, the well planner should recheck the optimized well path for the acceptable separation factor.

This procedure will serve as an effective well planning workflow, as it highlights all the crucial steps involved in the process, including selecting the appropriate survey tool, error model, and separation factor required for well planning in Arctic areas like the ANS, the Barents Sea, and the North Sea. It also states the minimum requirements essential for mitigating the high risks associated with such areas. In case of unfavorable scenarios from the anti-collision standpoint, this procedure shows the corrective measures that can be adopted by the well planner to maintain safety standards in drilling operations.

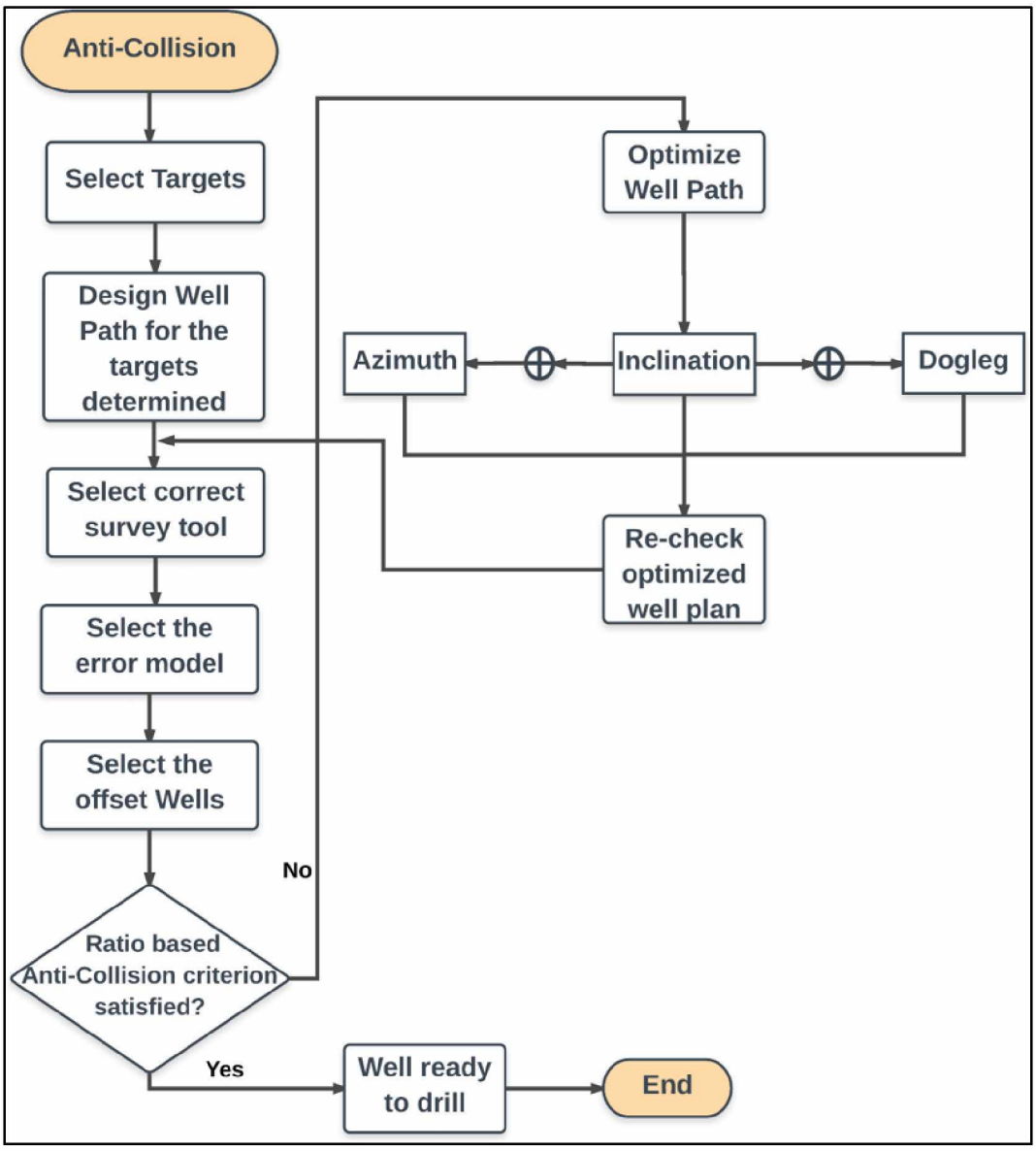

Figure 2.20: Improved anti-collision workflow for well planning at high latitude areas.

2.7 Conclusion

The following findings can be put forward for high latitude areas like ANS with 2-D well profiles:

1. The OWSG error model agrees with the ISCWSA error model. However, the OWSG error model should be used for two reasons:
    a. It provides a complete range of error model modifications used in the industry.
    b. It delivers an equivalent single model for both gyroscopic and MWD tools.

2. The lateral and horizontal uncertainties increase by a factor of approximately 2 at higher latitudes due to Earth's geomagnetic properties. This shows that the positional accuracy of the wellbore degrades in such areas.
3. The improved MWD tool should be employed throughout because it reduces the uncertainties by almost 73% compared to legacy and generic gyroscopic tools.
4. The separation factor criterion should be higher than the industry standard of 1.5 for enhanced safety of operations at higher latitude areas like Alaska, the North Sea, and the Barents Sea.
5. The nature of uncertainties is almost independent of well profiles but strongly dependent on the survey tool.
6. The uncertainties for targets in the same sand can be generalized for 2-D wellbores because the lateral uncertainty is equal to the horizontal uncertainty.

2.8 Acknowledgements

The authors would like to extend their sincere thanks to Landmark Solutions, Halliburton for the software support throughout the process, and the Oil and Gas Division of the Department of Natural Resources (DNR) for providing the data for the study.

CHAPTER 3: OPTIMIZED WELL PLANNING USING TORQUE AND DRAG ANALYSIS FOR ALASKA NORTH SLOPE DIRECTIONAL WELLS[2]

3.1 Abstract

The geo-environmental constraints of the Alaska **N**orth Slope (A**N**S), including surface location and well proximity issues, have compelled well planners to plan tortuous well paths with large departures, high inclinations, and doglegs. As a result, accurate torque and drag analysis of these well paths is an absolute necessity to prevent drill string failures and premature termination of drilling operations. In this study, we use a soft string model to investigate the drillability of the well paths planned to satisfy the anti-collision criterion in Schrader Bluff, Milne Point. There were two objectives of the study: first, to narrow down the design search domain of the drilling parameters; and second, to define the end point limits for critical well planning parameters, including inclination and dogleg, such that within these limits, the well path satisfies anti-collision as well as torque and drag considerations. In our approach to reduce the design search domain, we optimized the drill string in terms of its operational parameters for steerable tool, drill pipe size, mud rheology, trip speed, rotational speed, and weight on bit (WOB) for drilling and tripping out operations. The optimized drill string design was then tested on three different well profiles: horizontal, s-shaped, and slant. The surface torque parameter was identified as the crucial indicator for initiating the change in well planning parameters. The inclination and dogleg of the well profiles were varied only when the surface torque rating exceeded the API recommendation. In other cases, the drillability of the well path was confirmed using the optimized drill string design. The results show higher WOB capacity for the Rotary Steerable System (RSS) BHA than mud motor BHA. The analysis of combined motion for both BHAs indicated that optimal combination was possible with low trip speeds and high rotational speeds. In terms of drill pipe sizing, the results show that higher margin of overpull (MOP) and lower torque and drag were obtained for larger drill

---

[2] Submitted as Mahajan **N**.H., Khataniar, S, Patil. S.L., Dandekar, A.Y., Fatnani, A.K. 2018. "Optimized well planning using torque and drag analysis for Alaska **N**orth Slope directional wells" *J. Petrol. Sci. Eng*. Under Review. (Modified)

pipes. Overall, the results indicated superiority of RSS BHA over mud motor BHA. The most significant result was the formulation of optimized drill string design in terms of operational parameters for the most common 9-7/8" hole section in Schrader Bluff, Milne Point for all well profiles. The results of this study would help reduce the cumbersome iterative steps involved not only in anti-collision planning strategies but also in torque and drag considerations in Arctic.

3.2 Introduction

Torque and drag refers to the effects encountered during rotating and pulling the drill string from or into a wellbore during the operating modes of drilling and tripping (Mitchell, 1995). The drilling operation is carried out in two modes. The first is slide drilling, wherein the drill string undergoes only axial movement and no rotation. Since the drill string is not rotated, the torque is expected to be low, equal to the torque at bit. However, due to the axial movement, the axial drag is expected to be high. This indicates a possibility of drill string buckling, causing problems related to the weight transfer to the bit. The second mode is rotary drilling, wherein the drill string undergoes continuous rotation from the surface. As a result, the torque is expected to be high, but the drag and subsequent buckling forces are expected to be insignificant. In the case of tripping, the two operating modes are tripping in and tripping out. During these operations, if the drill string is rotated, a significant amount of torque is expected due to rotation. As a result, the drill string can undergo fatigue and twist off failures. When the drill string is not rotated, the axial drag determines the measured weight at the surface depending on the type of mode in consideration. During tripping in, the drag will lower the measured weight at the surface, whereas during tripping out, the drag will increase the measured weight at the surface. In such a scenario, the drill string can undergo tensile failures. It is also important to note that the drag forces during tripping in and out operations are not exact counterparts of each other because of the different contact points (Ismayilov, 2012).

Aarrestad and Blikra (1994) showed that excessive torque and drag are associated with each other and are expected to play a major role in extended-reach and horizontal wells. In most of the cases, the causes for excessive torque and drag are hole instabilities, key seating, differential sticking, poor hole cleaning, and wellbore friction (Johancsik et al.,

1984; Sheppard et al., 1987, Lesage et al., 1988). For extended reach and horizontal wells, Rae and others (2005) showed that high friction factors generate higher drag forces, which ultimately limits the ability to push the drill string to the target depth (TD). In the case of torque, Johancsik and others (1984) showed that sliding friction was the primary factor causing increased surface torque. Such scenarios can lead to problems like fatigue and twist off failures of the drill string in the operational phase or changing the rig capabilities in the well planning phase to accommodate the large make up torque (MUT), which may not be feasible during real time operations.

To overcome these challenges, torque and drag modeling is considered a primary step which allows well planners to not only foresee possible problematic areas but also optimize the drill string to reduce the surface torque (Rae et al., 2005; Ugochukwu et al., 2014). During this process, parameters such as casing and open hole depths, drill string components and their weights, friction factors, drilling fluid density and its composition, well profile, and rig capabilities are considered to make a realistic and effective torque and drag model. Even in the case of extended reach and horizontal drilling, close monitoring and accurate calculations are necessary to keep torque and drag within permissible limits to prevent drill string failures.

3.3 Objective of the Study

In the North Slope of Alaska, the geo-environmental constraints of location and anti-collision issues have compelled well planners to plan tortuous well paths with large departures, high inclinations, and dogleg. Furthermore, in Schrader Bluff, the shallow depth of the reservoir (~ 4000 ft TVD) has forced operators to drill shallow extended reach wells. This might create situations wherein setting a particular magnitude of azimuth, inclination, and dogleg would yield a satisfactory well path from the anti-collision standpoint, but the critical question is the drillability of a particular well path. Hence, the main purpose of torque and drag analysis was to check the drillability of the well paths planned in the previous study through the anti-collision phase. This was done using the Torque and Drag Module of WELLPLAN©, a Landmark-Halliburton software. Thus, this process would not only lead to optimization of the drill string but would also help narrow down the design search domain for drilling parameters.

However, checking the drillability of the planned well paths and optimizing the drill string is not sufficient, because a significant amount of time is required to perform anti-collision analysis and finalize the well planning parameters, viz., azimuth, inclination, and dogleg. Thus, using the optimized drill string, torque and drag analysis was also aimed at finding the limits for azimuth, inclination, and dogleg such that when these parameters are varied within specified limits, the well path will not only satisfy anti-collision considerations but will also be drillable from a torque and drag standpoint.

3.4 Methodology

We identified two methods to investigate the drillability of the planned well paths. In the first approach, the well path is kept constant and the drill string is optimized. In the second approach, the drill string is kept constant and the well planning parameters, including inclination and dogleg, are varied to satisfy the surface requirements. In our study, we adopted a combined approach to solve the problem on a case-by-case basis.

In order to simulate drilling operations, we focused on the drilling and tripping modes of the drill string. In the drill string optimization process, we used a soft string model and integrated it with the effects of weight on bit (WOB), trip and rotational speed, mud rheology, and drill pipe size. We used WELLPLAN© to simulate each of these parameters separately as a function of rotary steerable system (RSS) and mud motor BHAs to cover the complete spectrum of torque and drag issues associated with their use. The WOB parameter was selected based on a study conducted in Alpine, Alaska, which concluded that WOB was one of the leading cause for wear and failure of the drill string (Alvord et al., 2007). Hence, the objective of studying the effects of WOB was to generate a range that would allow operators to reach the TD for the given configuration of the drill string. Due to inaccessibility of historical torque and drag data, the trip and rotational speeds were derived from previous studies. The trip speeds used in the study were based on the study conducted by Fazaelizadeh (2010), whereas the rotational speeds were based on the study conducted by Hoan Van Luu (2015). Mud rheology was studied by analyzing the effect of hydrodynamic viscous force. The selection was based on the study conducted by Mason and Chen (2007), which showed that in the case of soft string

models, the effects of mud rheology should be included to make a more realistic torque and drag model. The drill pipe sizes and grades were selected based on case studies conducted in Umiat and Nikaitchuq, Alaska by Sayers and others (2015) and Chaudhary and others (2016), respectively. These case studies verified the availability and usability of the selected drill pipe sizes and grades in the ANS.

The optimized drill string design was then tested on the three different well profiles. During this process, the surface torque parameter was identified as the crucial indicator in changing the well planning parameters. The limits for well planning parameters were defined for the well profiles in which the surface torque rating exceeded the API recommendation which states that the surface torque rating should be less than 80% of the MUT of the drill string. In the case of the remaining well profiles, the drillability of the well path was confirmed using the optimized drill string design. A summary of all the parameters considered in the study in given in Table 3.1.

Table 3.1: Summary of parameters considered in the study.

Parameter	**Cases**			
Directional tool	Mud Motor (Bent housing and PDM)			
	Rotary Steerable System (RSS)			
Combined Motion	**RSS BHA**		**Mud Motor BHA**	
	Trip speed (ft/min)	Rotary Speed (rpm)	Trip speed (ft/min)	Rotary Speed (rpm)
	60	50	60	20
	180	100	180	40
	300	200	300	80
Mud Rheology	**Yield Point (lb/100 ft^2)**		**Plastic Viscosity (cP)**	
	20		10	
	24		12	
	40		25	

Drill Pipe size	4 ½" S-135, 22.8 ppf
	5" S-135, 25.6 ppf
	6-5/8" S-135, 27.7 ppf
Well Trajectories	Horizontal Well
	S-shaped Well
	Slant Well

3.5 Well Design

Figures 3.1a, 3.1b, and 3.1c show the planned trajectories of the horizontal, S-shaped, and slant wells used in the study. All the wells were planned for Target 1 described in section 2.4.1, with a drill floor elevation (DFE) of 71 ft. To compare the performance of the well profiles as a function of the drilling parameters mentioned in the previous section, we used a common 9-7/8" vs. 7-5/8" hole section in our torque and drag analysis for all the well profiles.

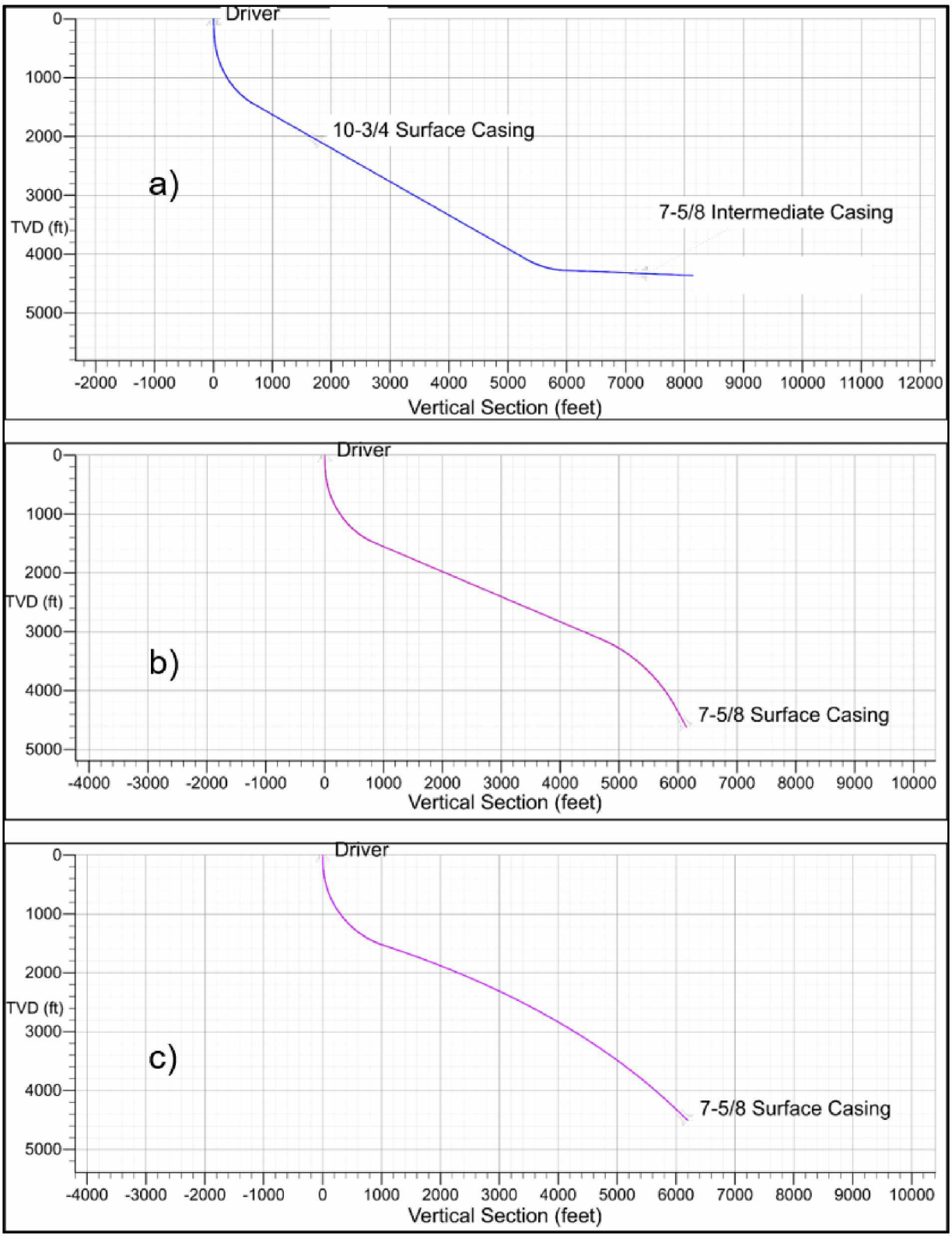

Figure 3.1: Well trajectories and planned sections for a) Horizontal b) S-shaped c) Slant well profiles.

The horizontal well for a 9-7/8" vs. 7-5/8" hole section was planned for a MD/TVD ratio of 2.4. The hole depths, casing grade, and mud weight were derived from the offset well, MPU SB 01 (AOGCC, 2017). The selection of the offset well was based on well trajectory and distance. A 20", H-40, 94 ppf driver pipe was set at 112 ft MD. The 13-1/2" surface hole was drilled and cased with 10-3/4", H-40, 32.75 ppf casing at 3100 ft MD. The planned intermediate 9-7/8" open hole section extended from 3100 ft MD to 9700 ft MD. Based on the offset well data for the intermediate hole section, we used the Bingham Plastic fluid model for a water-based mud of density 9.5 ppg to design the torque and drag considerations for the worst case. Figures 3.2a and 3.2b show the RSS and mud motor BHA for this horizontal well, which was designed to check the efficiency of these steerable tools.

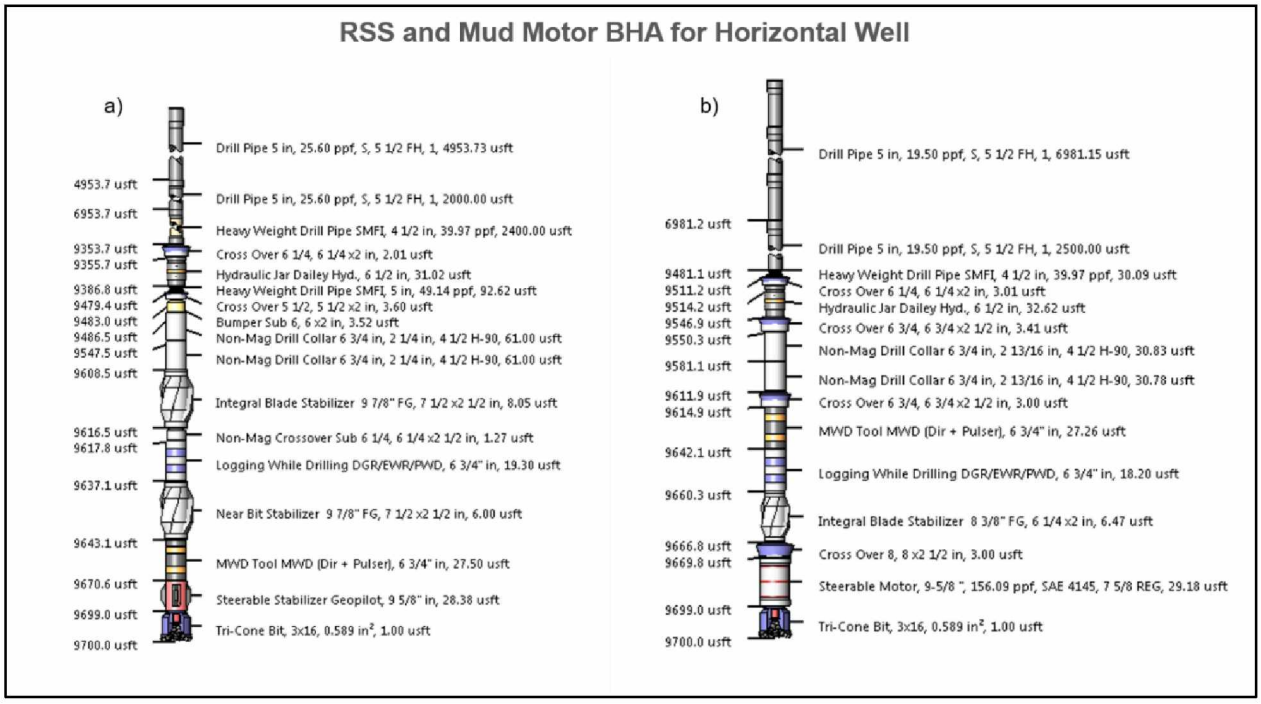

Figure 3.2: Drill string design for the horizontal well with a) RSS BHA b) Mud motor BHA.

The S-shaped well for a 9-7/8" vs. 7-5/8" hole section was planned for a MD/TVD ratio of 1.85 with a Directional Difficulty Index (DDI) of 6.263, indicating a short but tortuous well path. A 20", H-40, 94 ppf driver pipe was set at 112 ft MD. All the S-shaped offset wells in S-pad were drilled and cased with a single string from the surface to TD (AOGCC, 2017). We followed a similar approach and planned a 9-7/8" vs. 7-5/8" production hole

from the surface to TD using a water-based mud of density 9.5 ppg. Figures 3.3a and 3.3b show the RSS and mud motor BHA used for the S-shaped well.

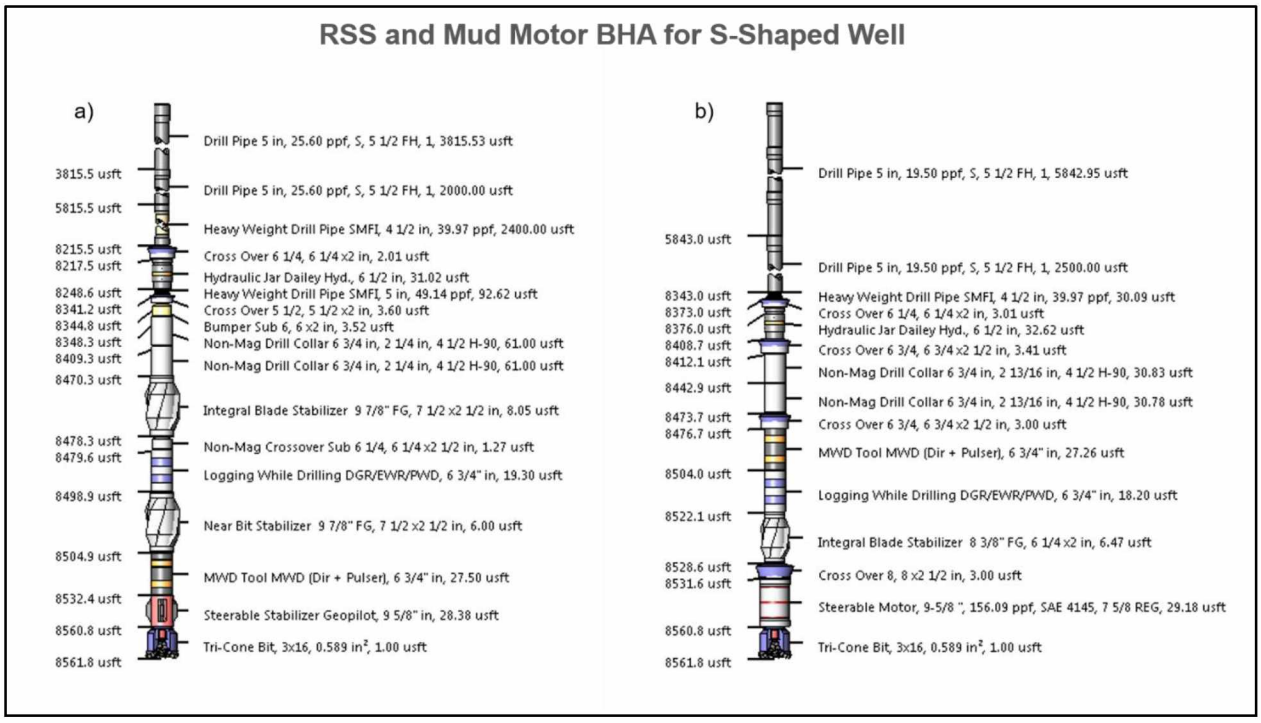

Figure 3.3: Drill string design for the s-shaped well with a) RSS BHA b) Mud motor BHA.

The slant well for a 9-7/8" vs. 7-5/8" hole section was planned for an Extended Reach Drilling (ERD) ratio of 1.51 with a DDI of 6.148, indicating a short but tortuous well path. Similar to the S-shaped wells, all the slant wells in S-pad were also drilled and cased with a single string from the surface to TD (AOGCC, 2017). On the similar basis, we planned a 9-7/8" vs. 7-5/8" production hole from the surface to TD using a water-based mud of density 9.5 ppg. Figures 3.4a and 3.4b show the RSS and mud motor BHA for the slant well.

Based on results given by Mason and Chen (2006) for wells in Alaska, we used an open hole friction factor of 0.4 and a cased hole friction factor of 0.3. The RSS BHA for the hole section used in this study was adopted from Chaudhary and others (2016), whereas the mud motor BHA was adopted from Sayers and others (2015). The initial drill string was designed for a horizontal well because 47% of the wells in S-pad are horizontal (AOGCC, 2017). For S-shaped and slant well profiles, the changes in terms of TD for the 9-7/8" hole

were incorporated in the length of the drill pipe from the surface. We used the Doyon 15 rig package for this study. The rig is pre-equipped with 5", 25.6 ppf, S-135 drill pipe (Abahusayn et al., 2012). In terms of mechanical specifications, the rig has a block rating of 1,000 klbf along with a Varco 8SA top drive capable of producing 63,000 ft-lbf continuous torque.

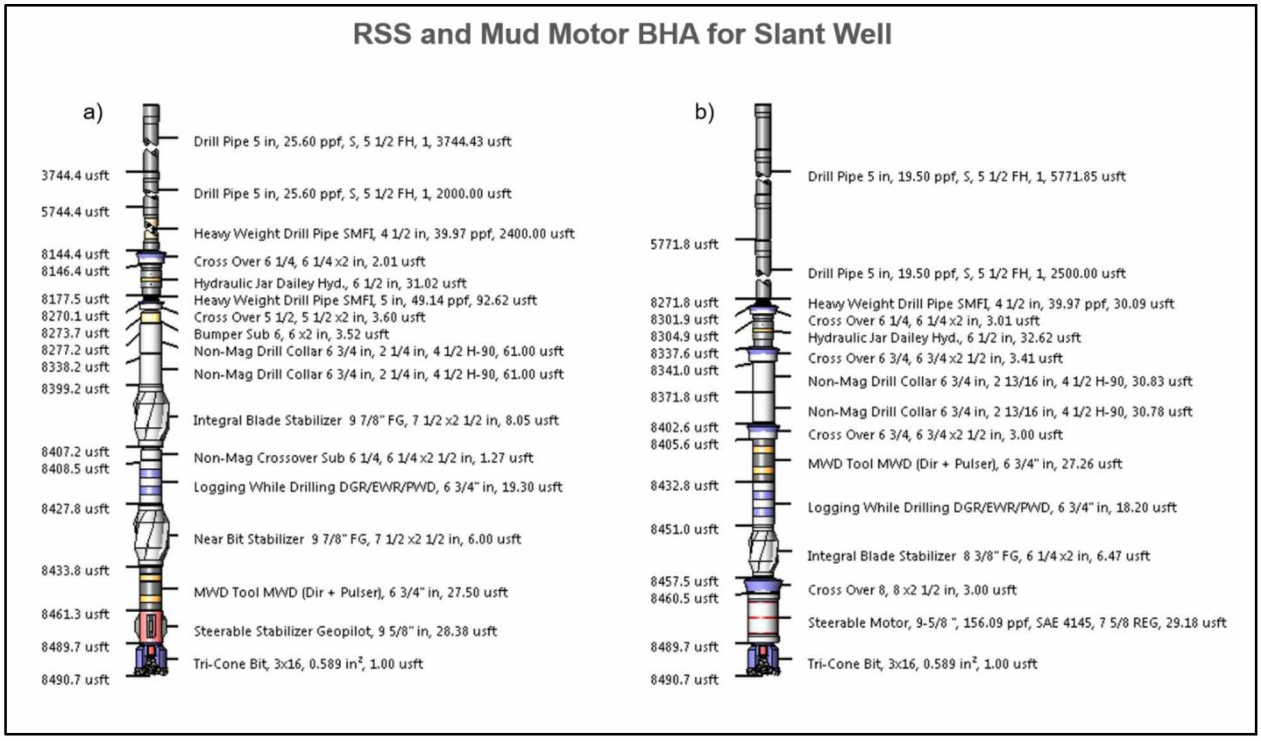

Figure 3.4: Drill string design for the slant well with a) RSS BHA b) Mud motor BHA.

3.6 Results and Discussion

3.6.1 Effect of Weight on Bit

In terms of the sequence of drilling operations, the first and the foremost objective of drilling a hole is achieved by applying compressive forces on the bit. In other words, a certain WOB is applied that will allow the given configuration of drill string to reach the desired depth. To follow this sequence, we chose WOB as the first parameter in the optimization process.

Figure 3.5 shows the variation of axial load as a function of WOB for a horizontal well with RSS BHA. As the WOB increases, the neutral point moves upward from the bit. During

this process, the compressive load acting on the drill string also increases, which makes it more susceptible to buckling. For example, for WOB of 59 klbf, the increase in the compressive load is large enough to cause the heavy weight drill pipe (HWDP) placed above the BHA to buckle. In terms of buckling, this is a critical location, as the HWDP provides support to the BHA for optimal directional control, which may not be achieved in this case. Figure 3.5 also indicates that for a horizontal well with RSS BHA in S-pad, Milne Point, the WOB can be varied safely until the value of WOB is 59 klbf. The limiting value of WOB is also acceptable from the standpoint of torque rating, as the surface torque generated using WOB of 59 klbf encompasses 73% of the MUT, which is less than the 80% suggested by API RP7G. Table 3.2 outlines the comparative results for all well profiles, including horizontal, S-shaped, and slant wells with RSS BHA. Table 3.2 indicates that as the DDI and, in turn, the well complexity decreases, higher values of WOB can be applied before causing buckling failure. This is attributed to the contact force (or side force) generated at the point where the drill string first buckles. The contact force is the force exerted by the wellbore on the drill string. This force acts to stabilize the string against buckling. Hence, higher the contact force, higher is the support exerted by the wellbore against buckling, which allows additional WOB to be applied on the drill string.

Table 3.2: Comparative results for effect of WOB for all well profiles with RSS BHA.

Well Profile	**Limiting value of WOB (klbf)**	**Location of Buckling**	**% of Make-Up-Torque (MUT)**	**Contact Force (lb/30 ft)**	**Directional Difficulty Index (DDI)**
Horizontal	59	HWDP above BHA	74%	1060	6.830
S-Shaped	67	HWDP above BHA	60%	1314	6.263
Slant	69	HWDP above BHA	57%	2015	6.148

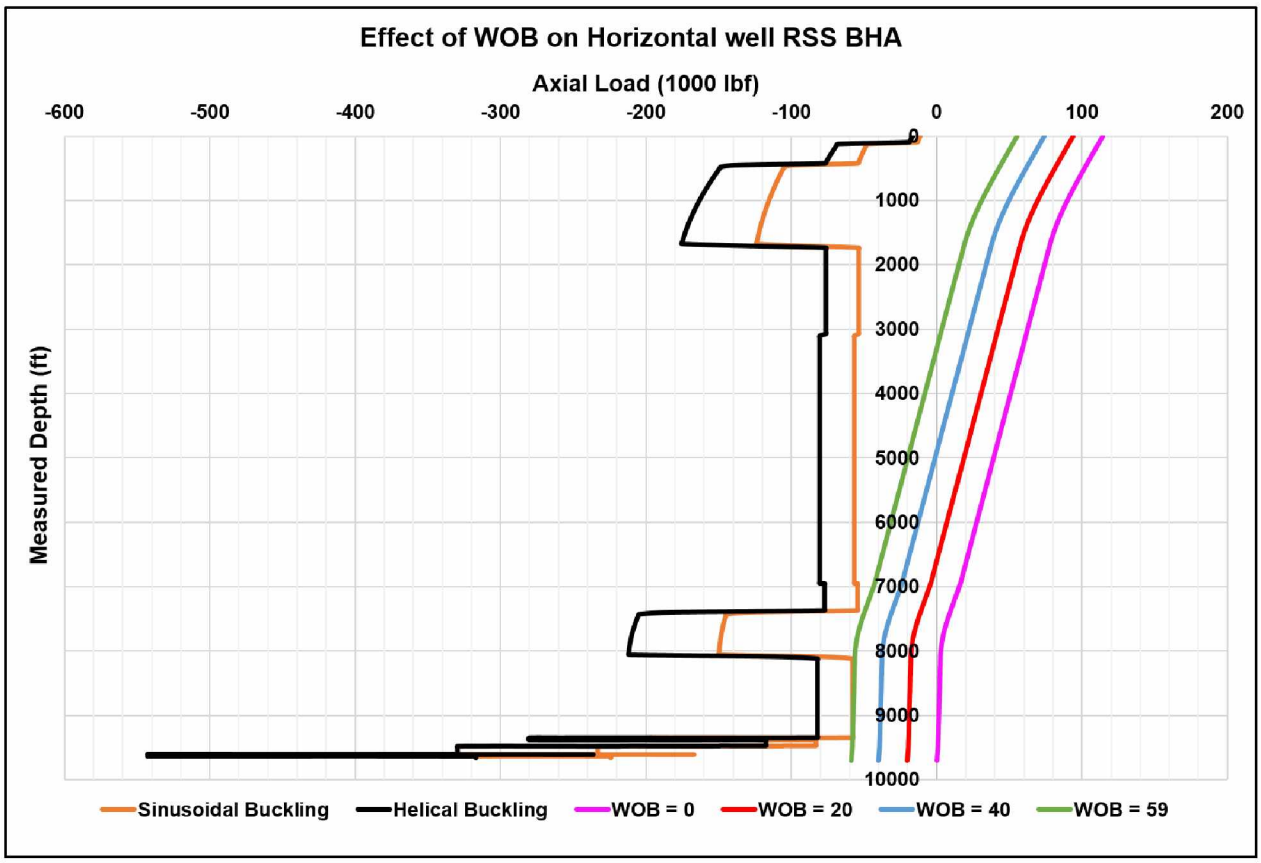

Figure 3.5: Variation of axial load as a function of WOB on horizontal well with RSS BHA.

Figure 3.6 shows the variation of axial load as a function of WOB for a horizontal well with mud motor BHA. Since there is no rotation compared to the RSS BHA, the main issue with the mud motor BHA is the ability to overcome drag forces. Hence, the results with mud motor BHA are focused on obtaining the workable WOB limits based on feasibility of slide drilling rather than the buckling criterion used in RSS BHA. Figure 3.6 shows that as the WOB increases, the cumulative drag force also increases, which lowers the measured axial load (or weight) of the drill string, causing negative axial load at the surface. This indicates a limiting value for WOB which causes negative weight at the surface. This situation prevents slide drilling due to inability of the mud motor BHA to overcome drag and advance the mud motor forward (Abahusayn et al., 2012). Thus, for a horizontal well with mud motor BHA, the maximum WOB of 15 klbf can be applied for conventional drilling to proceed. Table 3.3 outlines the comparative results for all well profiles, including horizontal, S-shaped, and slant wells with mud motor BHA. Similar to the RSS BHA, Table 3.3 indicates that as well complexity decreases, higher values of

WOB can be applied before the drill string enters the negative weight condition. During the same time, the increase in drag relative to the drag experienced for zero WOB also decreases due to the decrease in well complexity. It is important to note that the acceptable WOB values for RSS BHA are greater than the WOB values for mud motor. This phenomenon can be attributed to the magnitude of axial forces generated using both BHAs. When the magnitudes of axial forces are smaller, the drill string is oriented towards compression, which is responsible for buckling. As seen from Figure 3.6, the smaller magnitudes of axial forces generated using mud motor allow small margins for additional compressive forces to be applied as WOB. This results in smaller acceptable WOB magnitudes for mud motor BHA compared to RSS BHA.

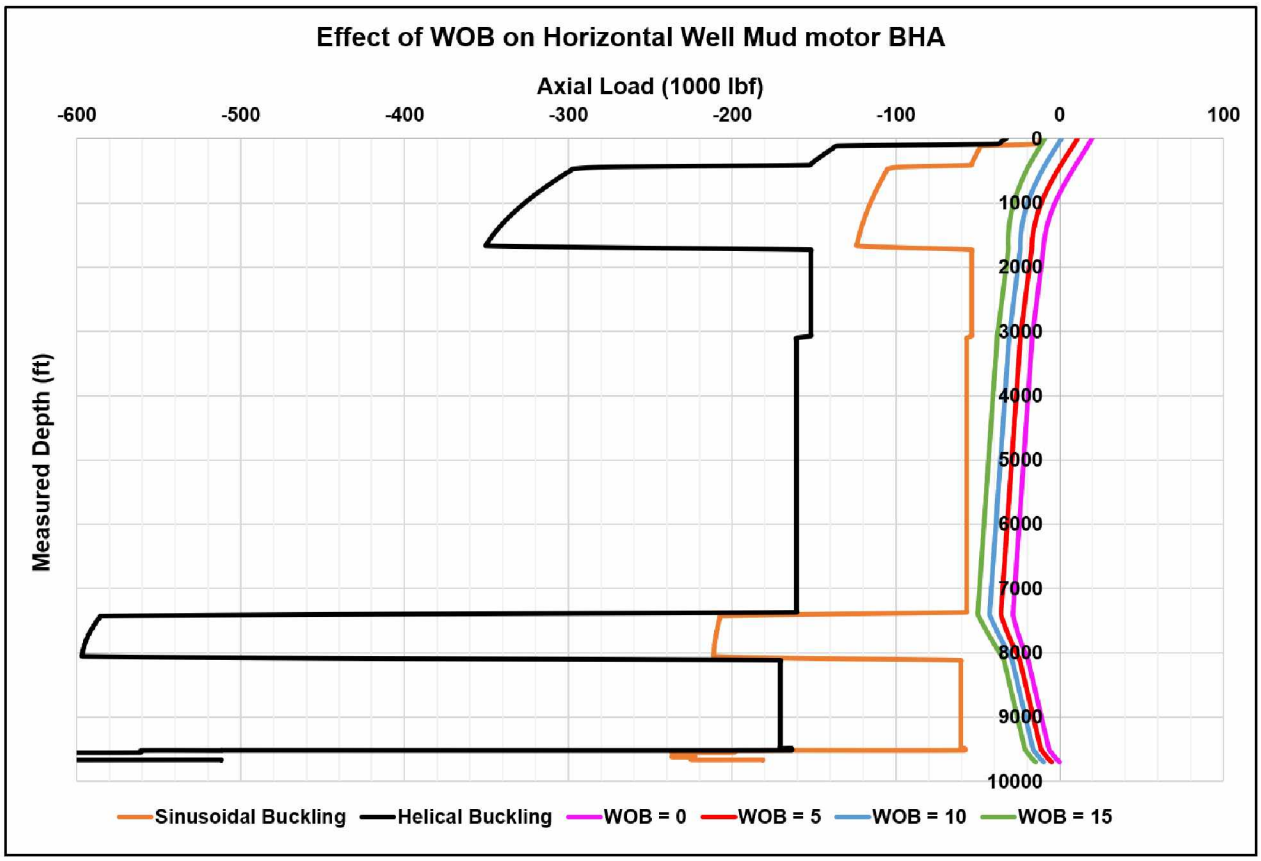

Figure 3.6: Variation of axial load as a function of WOB on horizontal well with mud motor BHA.

Table 3.3: Comparative results for effect of WOB for all well profiles with motor BHA.

Well Profile	Limiting value of WOB (kips)	% Increase in Drag	Directional Difficulty Index (DDI)
Horizontal	15	15%	6.830
S-Shaped	45	8%	6.263
Slant	47	7%	6.148

According to Cunningham (1960), the relationship between the rate of penetration (ROP) and applied WOB is given by Eq. 3.1:

$$ROP = K * W^{a} * N \tag{3.1}$$

where, ROP is the rate of penetration in ft/hr, W is WOB in kips, N is the rotary speed in rpm, and K and a are constants of proportionality.

Eq. 3.1 indicates that ROP is directly proportional to WOB. Our results show that higher WOB for RSS BHA will provide higher ROP, which points out the superiority of RSS BHA over the motor BHA.

3.6.2 Effect of Combined Motion

The next step in the drilling sequence was to analyze the tripping out process and select the optimum parameters that will allow the drill string to be pulled out from the hole without undergoing drill string failures.

In the previous years, the tripping out process was carried out using variable trip speed as the only parameter, with the motive that the drill string should not undergo tensile failures. However, this method caused problems like higher drag and subsequently higher measured hook loads at the surface as the trip speed was increased. During tripping out, the higher measured hook load is due to the higher effective tension in the string (Aadnoy et al., 2010). Figure 3.7 illustrates this problem for a horizontal well with RSS BHA. Figure 3.7 shows that as the tripping speeds are increased, the effective tension in the string

also increases. The main purpose of selecting a particular tripping speed was not only to maximize the margin of overpull (MOP) but also reduce the effective tension, which in turn decreases the measured hook loads at the surface. However, for all the trip speeds shown in Figure 3.7, there is no significant change in the effective tension at the surface. Also, the average change in the MOP during such scenarios was very small (2.42%).

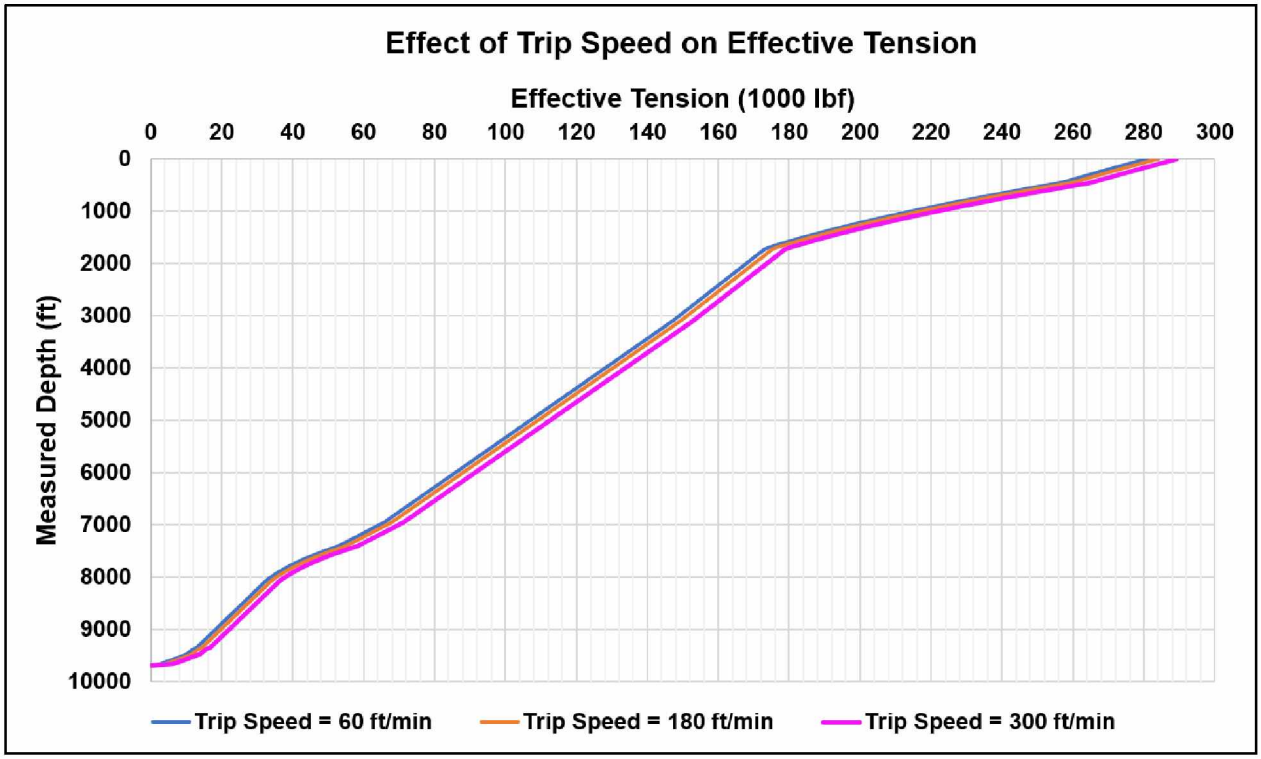

Figure 3.7: Variation of effective tension as a function of trip speed.

To overcome the problem of higher hook load and smaller MOP, Aadnoy and others (2010) suggested a combined motion solution, wherein trip speed is combined with pipe rotation. During combined motion, the tripping out process of the drill string consists of two operational components: first, trip speed in ft/min, and second, pipe rotation in rpm. In previous studies, Aadnoy and Anderson (2001) found that the total drag during combined motion is a function of axial drag caused by tripping speed and rotational drag caused by pipe rotation. They showed that during such motion, for a constant trip speed, the rotational speed helps reduce the effective tension by reducing the axial drag, which also reduces the measured hook load. However, there was a need to study the combined effect of varying trip and rotational speeds, which would aid in selection of their optimal

values to not only reduce the measured hook load but also increase the MOP, which will help overcome scenarios like stuck pipe, slip/stick, etc. To achieve this, the RSS and mud motor BHA for each of the three well profiles were simulated for all the combinations of trip speed and rotational speed, as outlined in Table 3.1.

Figures 3.8a, 3.8b, and 3.8c show the effect of rotational speeds combined with trip speeds of 60 ft/min, 180 ft/min, and 300 ft/min, respectively, on effective tension of a horizontal well with RSS BHA. These figures indicate that using combined motion, the effective tension can be reduced significantly compared to the effective tension measured for the same trip speed without rotation. These figures also indicate that for a particular rotary speed, as the tripping speed increases, the effective tension also increases. For example, the effective tension measured at the surface for a combination of 300 ft/min and 50 rpm is 44% greater than the effective tension for a combination of 60 ft/min and 50 rpm. In other words, for the same rotary speed, higher the trip speed, lower is the reduction in effective tension as compared to the effective tension measured with same trip speed without rotation.

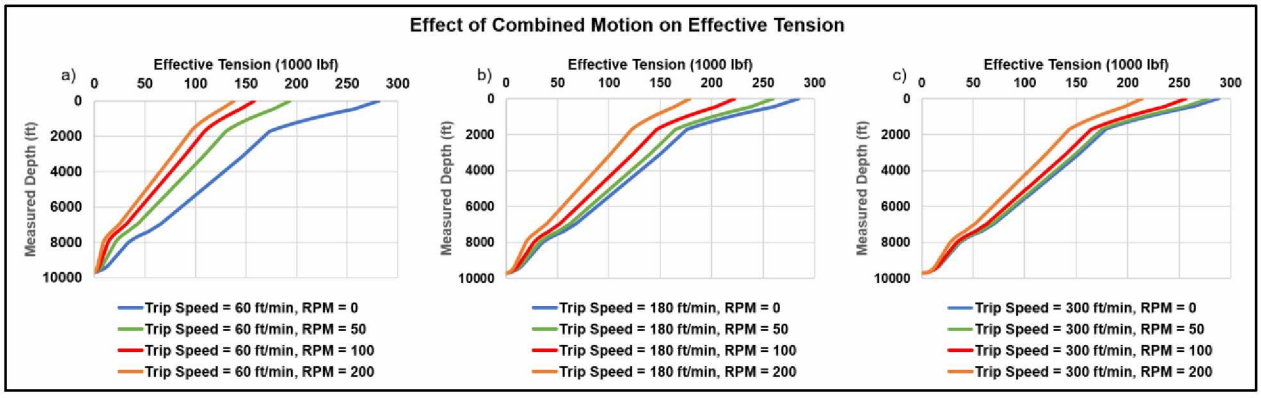

Figure 3.8: Effect of rotational speeds on effective tension combined with trip speed of a) 60 ft/min b) 180 ft/min c) 300 ft/min.

Figures 3.9a, 3.9b, and 3.9c show the effect of rotational speeds combined with trip speed of 60 ft/min, 180 ft/min, and 300 ft/min, respectively, on torque limits of the same horizontal well as above. These figures indicate that for a particular rotary speed, as the tripping speed increases, the rotary table torque decreases significantly. For example, the torque required at the rotary table for a combination of 300 ft/min and 50 rpm is 56% less

than the torque required for a combination of 60 ft/min and 50 rpm. In other words, for the same rotary speed, higher the trip speed, lower is the torque requirement.

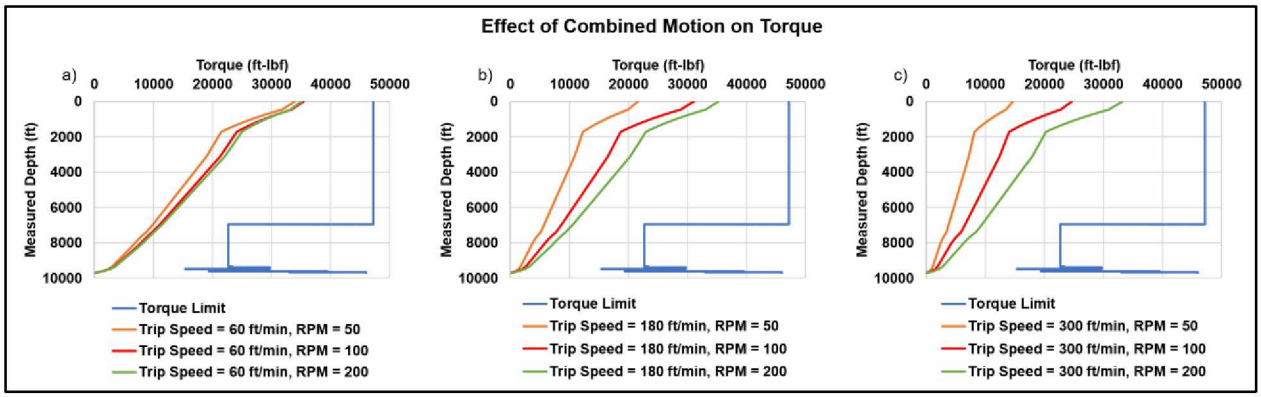

Figure 3.9: Effect of rotational speeds on torque combined with trip speed of a) 60 ft/min b) 180 ft/min c) 300 ft/min.

The reason for such behavior can be attributed to the angle made by the resultant of axial and tangential velocities. This angle is defined by Eq. 3.2 (Aadnoy et al. 2010):

$$\psi = \tan^{-1}\left(\frac{V_h}{V_r}\right) = \tan^{-1}\left(\frac{V_h}{2\pi * N * r}\right) \tag{3.2}$$

where, Ψ is the angle between the axial and tangential velocities, V_h is the axial velocity (or trip speed) in ft/min, N is the pipe rotary speed in rpm, and r is the pipe radius in ft.

Aadnoy and others (2010) have shown the dependency of this resultant angle on torque and drag calculations during tripping out operations in straight and curved sections of the well through Eq. 3.3 and Eq. 3.4, respectively:

$$T = r * \mu * \beta * w * \Delta L * sin\alpha * cos\psi \tag{3.3a}$$

$$F_2 = F_1 + \beta * w * \Delta L * cos\alpha + \mu * \beta * w * \Delta L * sin\alpha * sin\psi \tag{3.3b}$$

$$T = r * \mu * F_1 * |\theta_2 - \theta_1| * cos\psi \tag{3.4a}$$

$$F_2 = F_1 + F_1\left(e^{|\theta_2 - \theta_1|} - 1\right) * sin\psi + \beta * w * \Delta L * \left(\frac{\sin\alpha_2 - \sin\alpha_1}{\alpha_2 - \alpha_1}\right) \tag{3.4b}$$

where, T is the torque in the string in ft-lbf, F_2 is the force due to static weight at the top of the string element in consideration in lbf, F_1 is the force due to static weight at the bottom of the string element in consideration in lbf, r is the pipe radius in ft, μ is the coefficient of friction, β is the buoyancy factor, w is unit pipe weight in lb/ft, ΔL is length of pipe segment in consideration in ft, α is wellbore inclination, Ψ is the angle between axial and tangential velocities, and $|\theta_2 - \theta_1|$ is the absolute change in direction.

In our study, for a trip speed of 300 ft/min and rotational speed of 50 rpm, the resultant angle, Ψ, is 77°, whereas for a trip speed of 60 ft/min and rotational speed of 50 rpm, the resultant angle, Ψ, is 42°. Since both combinations are analyzed for the same well profile, hole section, drill string, and mud weight, all the properties defined in Eqs. 3.3a, 3.3b and Eqs. 3.4a, 3.4b are constant except for the resultant angle. This points out that for our case, the torque is directly proportional to the cosine of the resultant angle and drag is directly proportional to the sine of the resultant angle. Hence, based on the mathematical properties of the sine and cosine functions, the drag for a combination of 300 ft/min and 50 rpm will be greater than that for a combination of 60 ft/min and 50 rpm, which is reflected by the behavior of effective tension. On a similar basis, the torque for a combination of 300 ft/min and 50 rpm will be smaller than that for a combination of 60 ft/min and 50 rpm.

The optimal combination of trip and rotational speed should result in higher reduction in effective tension and lower torque requirements. However, the results presented in the study show that the effects of combined motion on effective tension and torque are opposite to each other. Hence, it was necessary to add a third parameter in this process to narrow down the design domain for the number of combinations. This parameter was the fatigue ratio, which is defined as the summation of bending and buckling stress divided by the fatigue endurance limit of the drill string section under consideration. Since the results of this section are focused on the tripping out process, the buckling stress is zero. Hence, the fatigue ratio for the tripping out process signifies the location and relative magnitude of the bending stress that will cause fatigue failure of the drill pipe.

Figures 3.10a, 3.10b, and 3.10c show the variation of the fatigue ratio with the rotational speeds and trip speeds considered in the study for the same horizontal well as above.

These figures are useful in reducing the acceptable design domain for the number of combinations of trip and rotational speed because they indicate all the combinations which cause the fatigue ratio to be greater than 1 which will ultimately lead to fatigue failures of the drill pipe. Hence using this criterion, the design domain for the number of combinations reduces to that shown in Table 3.4.

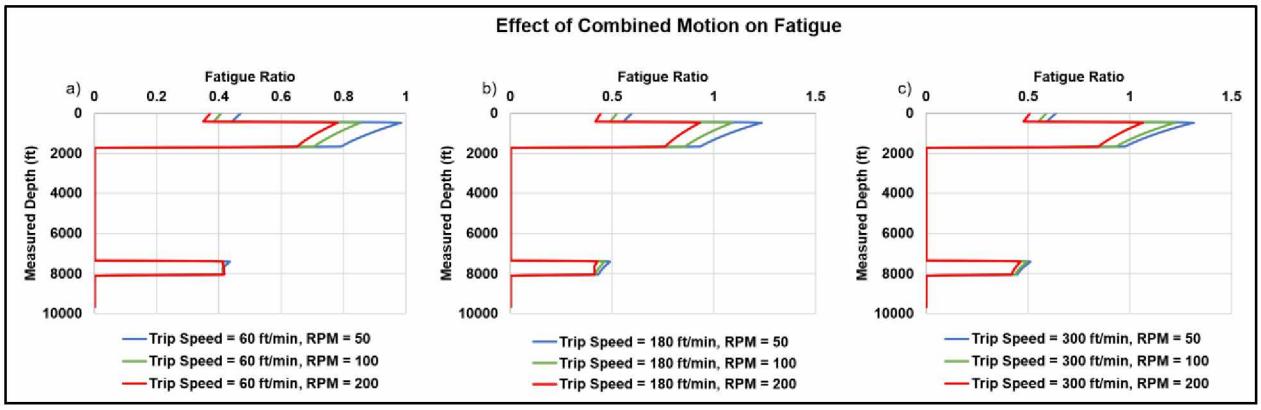

Figure 3.10: Effect of rotational speeds on fatigue ratio combined with trip speed of a) 60 ft/min b) 180 ft/min c) 300 ft/min.

Table 3.4 Possible combinations and their properties for a horizontal well with RSS BHA. Favorable values in red.

Combination	Max. Fatigue Ratio	Dec. in Effective Tension	Torque utilized	Inc. in MOP
		(%)	(%)	(%)
60 ft/min, 50 RPM	0.98	31.2	71.9	37.3
60 ft/min, 100 RPM	0.85	43.8	74.9	52.4
60 ft/min, 200 RPM	0.78	50.8	74.1	60.8
180 ft/min, 200 RPM	0.93	37.1	74.6	45.5

Table 3.5: Possible combinations and their properties for a horizontal well with mud motor BHA. Favorable values in red.

Combination	Max. Fatigue Ratio	Dec. in Effective Tension	Torque utilized	Inc. in MOP
		(%)	(%)	(%)
60 ft/min, 40 RPM	0.97	25.8	63.7	15.5
60 ft/min, 80 RPM	0.84	39.4	69.0	23.7

In other words, Table 3.4 shows the combinations that will not cause fatigue failure of the drill string. Similarly, Table 3.5 shows the combinations for a horizontal well with mud motor BHA. The optimal combination should have maximum increase in MOP along with minimum fatigue ratio, indicating small chances of the drill string undergoing fatigue failure; maximum reduction in effective tension, indicating reduction in axial drag; and minimum torque utilized, indicating small chances of drilling undergoing twist off failure. From Tables 3.4 and 3.5, the combinations of 60 ft/min and 200 rpm and 60 ft/min and 80 rpm give the required results for a horizontal well with RSS BHA and mud motor BHA, respectively, except for the torque ratings. However, the torque at the rotary table satisfies the API RP7G recommendation, hence, the torque rating results are considered acceptable. A similar trend was observed for slant and S-shaped well profiles. These results show that optimal combinations are possible with low trip speeds and high rotational speeds as long as the drill string does not undergo fatigue and twist off failures. Furthermore, the RSS BHA outperforms the motor BHA because of higher reduction in effective tension and higher increase in MOP.

3.6.3 Effect of Hydrodynamic Viscous Forces

In continuation of the tripping out sequence, Maidla and Wojtanowicz (1987b) showed that the hydrodynamic viscous forces resulting due to the properties of drilling fluid affect the drag forces which arise due to the pipe movement in opposite direction to that of the drilling fluid. They presented a procedure for calculating the viscous pressure gradient for

each pipe element based on the fluid model, which was then translated into calculating the hydrodynamic viscous forces given by Eq. 3.5:

$$F_D = \frac{\pi}{4} * \sum \left(\frac{\Delta P}{\Delta L}\right) * \Delta L * d^2 \tag{3.5}$$

where, F_D is the hydrodynamic viscous drag force in lb, $\frac{\Delta P}{\Delta L}$ is the viscous pressure gradient in psi/ft, ΔL is the length of pipe segment in ft, and d is the outer diameter of the pipe segment in inches.

In our study, we interpreted the effect of hydrodynamic viscous forces as a way to enhance the results of the tripping out process. To achieve this, previous results of optimum combinations of trip and rotational speeds were coupled with the Bingham Plastic drilling fluid model with three different plastic viscosities (mentioned in Table 3.1), keeping the mud weight of 9.5 ppg constant at all times. Figures 3.11 and 3.12 show the variation of hydrodynamic viscous force as a function of plastic viscosity for a horizontal well with RSS BHA and mud motor BHA, respectively. These figures indicate that as the viscosity of the drilling fluid increases, the viscous drag associated with it also increases. Since the fluid model, mud weight, hole section, and trip speed are constant, the increase in viscosity causes the Reynold's number to decrease. As a result, flow becomes laminar, which causes the friction factor and subsequently the viscous pressure gradient to increase, leading to increased viscous drag. The simultaneous analysis of Figures 3.11 and 3.12 for a particular value of plastic viscosity and drill string element points out that the length of the drill string element and the clearance between the wellbore diameter and outer pipe radius are additional critical parameters causing increases in viscous drag forces. The smaller clearance implies a higher viscous pressure gradient and the longer length implies a larger spread of viscous drag forces over the length of the drill string. In terms of performance comparison, the RSS BHA is considered better than the motor BHA, as it generates smaller viscous forces. However, it is important to note that though the magnitude of the viscous drag is very small, it should not be neglected because it increases the robustness of the soft string model.

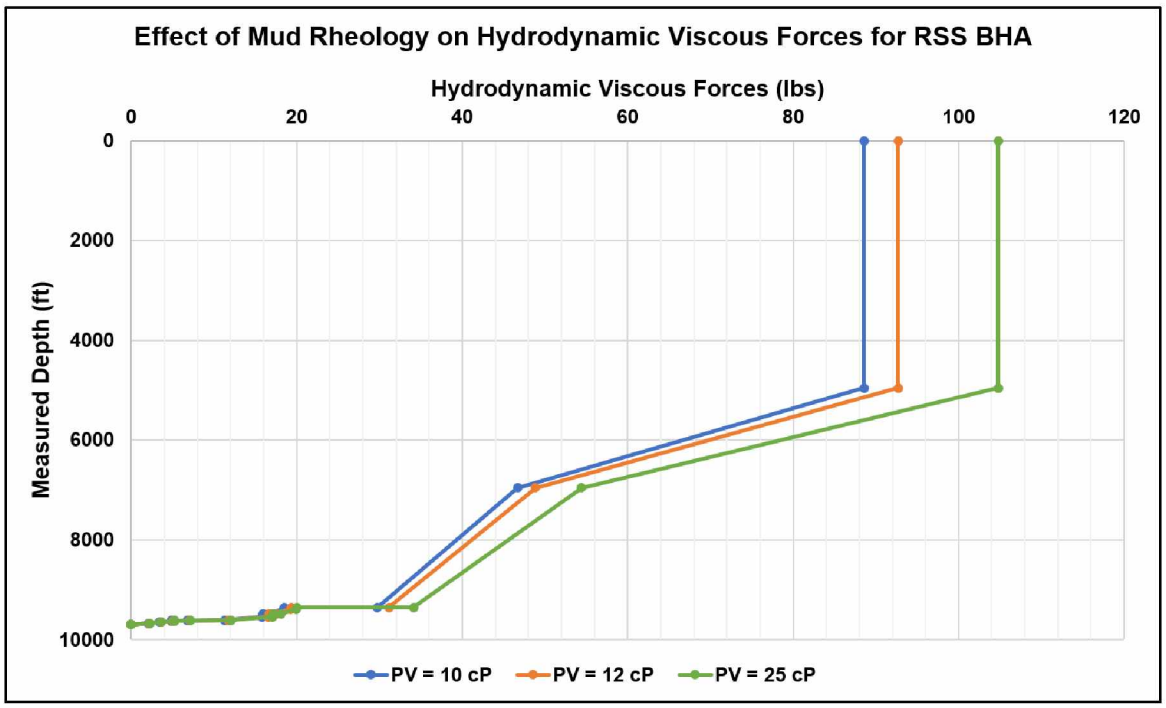

Figure 3.11: Variation of hydrodynamic viscous forces as a function of mud rheology on the horizontal well with RSS BHA.

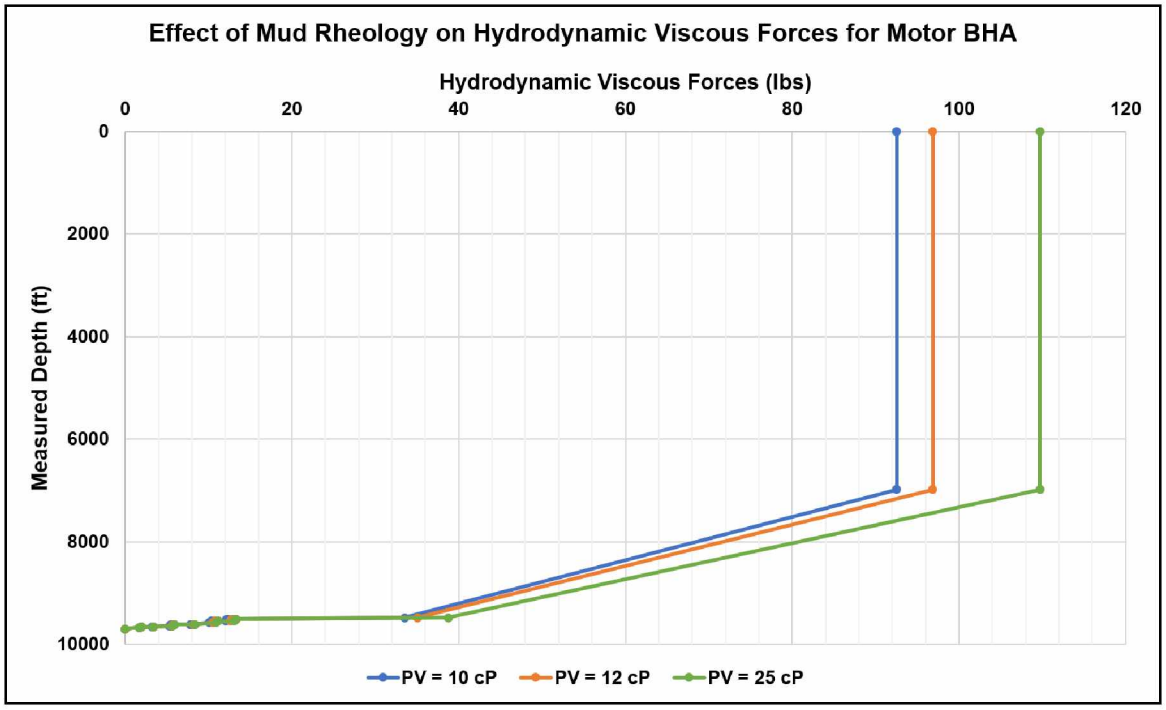

Figure 3.12: Variation of hydrodynamic viscous forces as a function of mud rheology on the horizontal well with mud motor BHA.

3.6.4 Effect of Drill Pipe Size

As a final step in the drill string optimization process, we checked the effect of drill pipe size on drilling and tripping out operations and asked whether the estimated torque and drag could be reduced. We selected a 4-1/2", 22.82 ppf, S-135 drill pipe with NC 50 connection for comparison with the previous results which were generated using a 5", 25.6 ppf, S-135 drill pipe with 5-1/2 FH connection. We also selected a 6-5/8", 27.70 ppf, S-135 drill pipe with FH connection to check the validity of the results. Tables 3.6 and 3.7 compare the results for a horizontal well with RSS and mud motor BHA, respectively.

Table 3.6: Comparison of 5" drill pipe vs. 4½" drill pipe for a horizontal well with RSS BHA. Favorable values in red.

Parameter	6 5/8", S-135, 27.7 ppf, FH	5", S-135, 25.6 ppf, 5 ½ FH	4 ½", S-135, 22.82 ppf, NC 50
Drilling			
WOB Limit	59 kips	59 kips	55 kips
Drilling torque rating	63.8 %	74.6 %	84 %
Tripping Out			
Combined Motion	60 ft/min, 200 RPM	60 ft/min, 200 RPM	60 ft/min, 200 RPM
Reduction in Effective Tension	50.8 %	50.8 %	51.1 %
Increase in MOP	64.6 %	60.8 %	56.3 %
Tripping torque rating	62.8 %	74.1 %	80.3 %

Table 3.7: Comparison of 5" drill pipe vs. 4½" drill pipe for a horizontal well with mud motor BHA. Favorable values in red.

Parameter	6 5/8", S-135, 27.7 ppf, FH	5", S-135, 25.6 ppf, 5 ½ FH	4 ½", S-135, 22.82 ppf, NC 50
Drilling			
WOB Limit	15 kips	15 kips	10 kips
Increase in Drag	19.1 %	15.8 %	11.6 %
Tripping Out			
Combined Motion	60 ft/min, 80 RPM	60 ft/min, 80 RPM	60 ft/min, 80 RPM
Reduction in Effective Tension	41.9 %	39.4 %	38.1 %
Increase in MOP	26.8 %	23.7 %	22.1 %
Tripping torque rating	59.7 %	69.0 %	66.5 %

Eq. 3.6a, 3.6b and Eq. 3.7a, 3.7b are the modified forms of Eq. 3.3a, 3.3b and Eq. 3.4a, 3.4b, respectively, and are considered to be the governing equations for torque and drag during drilling operations.

$$T = r * \mu * \beta * w * \Delta L * sin\alpha \tag{3.6a}$$

$$F_2 = F_1 + \beta * w * \Delta L * cos\alpha - \mu * \beta * w * \Delta L * sin\alpha \tag{3.6b}$$

$$T = r * \mu * F_1 * \ |\theta_2 - \ \theta_1| \tag{3.7a}$$

$$F_2 = F_1 + F_1\left(e^{-|\theta_2 - \theta_1|} - 1\right) + \ \beta * w * \Delta L * \left(\frac{\sin\alpha_2 - \sin\alpha_1}{\alpha_2 - \ \alpha_1}\right) \tag{3.7b}$$

The first modification is that the drilling operations considered in the study are independent of the resultant angle, Ψ, because the pipe rpm and speed are exclusive properties of tripping out operation. Second, the force *F* in the string is not the static weight but the static weight minus the WOB (Aadnoy et al., 2010).

Our results show that the 5" drill pipe performs better than the 4-1/2" drill pipe for both BHAs. In terms of drilling performance for both BHAs, the 5" drill pipe provides higher WOB limits because of its larger size, which increases the resistance to buckling forces, ultimately preventing failure. However, for both BHAs, the WOB limit for 5" and 6-5/8" drill pipe is the same. In the case of RSS BHA, this can be attributed to the location of buckling. For RSS BHA, the WOB limit is reached at the first point of buckling, in which case the axial force (F_{axial}) generated using that value of WOB is greater than the resisting sinusoidal buckling force (F_{sin}). In our study, all the changes for the drill pipe are made by keeping the BHA and HWDP above the BHA constant. In other words, F_{axial} and F_{sin} are independent of drill pipe change up to 2750 ft from the bottom. The location of buckling for both 5" and 6-5/8" drill pipe occurs at 347 ft from bottom, which means that, theoretically, the same amount of WOB must be applied to cause the buckling at the same point where F_{axial} and F_{sin} do not change. Since these are the first points of buckling for both drill pipes, the WOB limit remains the same. In the case of mud motor BHA, the WOB limit is the value which causes F_{axial} to be negative, because at this condition, the drag is large enough to lower the measured weight at the surface, causing it to experience compression throughout the entire length of the drill string. Hence, the resisting force in this case is F_{axial}, whose maximum value is achieved when the applied WOB is zero. For 5" and 6-5/8" drill pipes, the change in F_{axial} for a zero WOB is 0.8 klbf. Since this difference is very small, they offer the same resisting forces, reflected by their equal WOB limits.

Based on Eq. 3.6b and Eq. 3.7b, for mud motor BHA, the increase in drag is higher for a 5" drill pipe because of higher WOB capabilities, larger radius, and higher unit weight. The 5" drill pipe, being larger in size and heavier in unit weight, has a higher MUT. The higher MUT indicates higher resistance to drilling and/or tripping torque (Boonsri, 2014). Hence, for a RSS BHA, it is important to note that even though the 4-1/2" drill pipe generates smaller drilling torque due to smaller radius and unit weight (Eq. 3.6a and Eq. 3.7a), its torque rating, defined as the ratio of drilling and/or tripping torque to MUT, is higher due to small MUT.

The comparison of the tripping out performance also indicates the superiority of the 5" drill pipe. In the case of RSS BHA, the 4-1/2" drill pipe has a greater reduction in the

effective tension due to the smaller initial value generated for no rotation. The 4-1/2" drill pipe will have smaller initial effective tension because of small drag due to its smaller unit weight compared to 5" drill pipe. Even though this case is favorable for the 4-1/2" drill pipe, the marginal difference is very small. On the other hand, the 5" drill pipe increases the MOP significantly at a lower torque rating. In the case of mud motor BHA, the 5" drill pipe outperforms the 4-1/2" drill pipe due to larger reduction in effective tension and greater increase in MOP. Even though the tripping torque rating for the 5" drill pipe was comparatively higher, it was considered acceptable from the standpoint of the API RP7G torque recommendation.

In all cases, the validity of the results generated using a 5" and 4-1/2" drill pipe is confirmed by a 6-5/8" drill pipe, wherein the results generated using a 6-5/8" drill pipe are greater than the 5" drill pipe owing to its larger radius and unit weight.

3.7 Optimization of Well Path for Inclination and Dogleg

The results in the above section indicate that the optimized drill string consists of RSS BHA as the steering unit coupled with a 5", 25.6 ppf, S-135 drill pipe. The WOB limits generated using this optimized drill string vary with the well profile. During tripping out, the optimized operating parameters for this drill string were found to be 60 ft/min as the trip speed and 200 rpm as the rotating speed. The next step was to check the drillability of the three well profiles, viz., horizontal, S-shaped, and slant wells, with this optimized drill string. Since the optimized drill string consisted of RSS BHA, we identified surface torque as the validating parameter for this process.

The results shown for 5", 25.6 ppf, S-135 drill pipe in Table 3.7 were obtained for the horizontal well with the optimized drill string. These results confirm the drillability of the horizontal well, as the surface torque for both drilling and tripping operations was acceptable from the standpoint of API recommendations. Table 3.8 shows the variation of drilling and tripping torque for all three well profiles generated using the optimized drill string. In terms of drilling operations, the torque required at the rotary table increases with well complexity because of the smaller WOB limits. Based on Eq. 3.7a, which gives the torque required in the curved section, smaller WOB limits will cause higher static force

during drilling, leading to higher torque. A similar trend for torque behavior was expected for tripping out, because during such operations, the entire static weight, a function of the length of the drill pipe, is used in Eq. 3.7a. However, based on the well design for the horizontal well, 44% of the drill pipe experiences a smaller cased hole friction factor (μ = 0.3). This results in lower torque values. On the other hand, Table 3.8 also shows that for S-shaped and slant wells, the optimized drill string generates excessive torque. This suggests that to reduce the torque requirements, there was a need to optimize the well path for S-shaped and slant wells.

Table 3.8: Variation of drilling and tripping out torque for all well trajectories generated using optimized drill string.

Well Profile	Drilling torque (ft-lbf)	Tripping out torque (ft-lbf)	WOB limits (kips)	Drill pipe length (ft)	DDI
Horizontal	35256	35015	59	6953	6.830
S-shaped	28387	43004	67	5815	6.263
Slant	27881	41265	69	5744	6.148

Based on the previous anti-collision study, we optimized the well path by varying the inclination, dogleg, and azimuth. The main objective of this process was to set end point limits for the variation of inclination, dogleg, and azimuth such that within these limits, the well path will not only satisfy the anti-collision considerations but also be drillable from the standpoint of torque and drag considerations. Eqs. 3.3a, 3.3b, Eqs. 3.4a, 3.4b, Eqs. 3.6a, 3.6b, and Eqs. 3.7a, 3.7b show that torque increases as inclination increases. Hence, we adopted the following trial and error approach to determine the limits:

Step 1: Keeping the dogleg constant, reduce the inclination to a critical inclination (α_c) which passes the anti-collision criterion measured by the separation factor plot. Hence, the inclination values from the initial value to α_c become the range for varying inclination. If, due to the existing wells, the inclination cannot be reduced, then the initial value becomes α_c. In such a scenario, the range for inclination cannot be determined. Since the

inclination is being reduced, the torque for drilling and tripping out operations should decrease.

Step 2: Keeping the inclination constant at α_c, step 1 was repeated for dogleg. Hence, all the dogleg values satisfying the anti-collision criterion will act as a range for dogleg variation. Similar to inclination, as the dogleg decreases, the torque also decreases.

The above procedure can be applied to all sections of well design. However, in our study, we applied this procedure in the initial section above the KOP because of the large side forces generated in this section during the tripping out operations. During this process, it is important to note that both inclination and dogleg are azimuth dependent. In other words, as the direction of the wellbore changes, the inclination and dogleg values that the wellbore can achieve also change. Hence, the range for inclination and dogleg will exist for every azimuth that satisfies the separation factor plot.

Figure 3.13 shows the variation of torque at 0° azimuth as a function of α_c and dogleg for S-shaped and slant wells. In both cases, α_c is equal to the initial planned inclination. Hence, there was no range for variation of inclination. The dogleg variation for an S-shaped well ranged from 1.8 °/100 ft to 2 °/100 ft and that for a slant well ranged from 1.05 °/100 ft to 2.05 °/100 ft. The torque values generated using α_c and smallest dogleg represent the maximum reduced torque values obtained by optimizing the well path at 0° azimuth. However, Figure 3.13 also shows that even with optimized drill string and well path, the tripping out torque in both S-shaped and slant wells exceeds the API recommendation. This points out that additional torque-reducing equipment is necessary for the drill string design of S-shaped and slant wells in Milne Point.

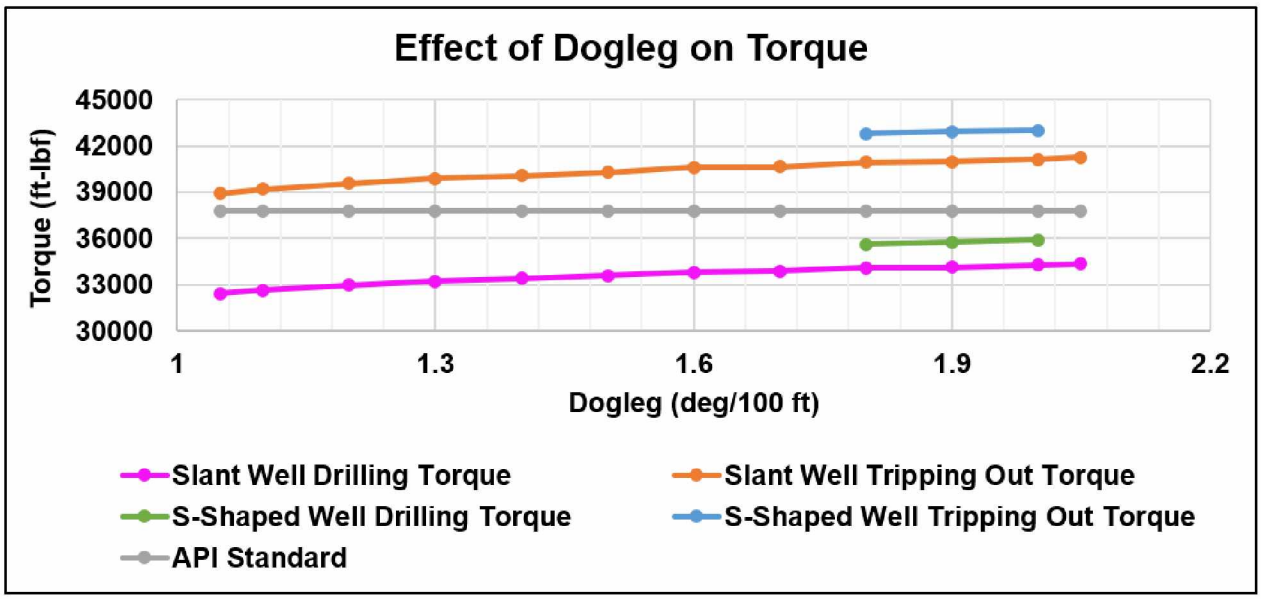

Figure 3.13: Torque variation as a function of dogleg for slant well (0° azimuth, critical inclination 4.25°) and for S-shaped well (0° azimuth, critical inclination 6°).

In Alaska, non-rotating drill pipe protectors (NRDPP) are the most commonly used friction reducing devices because of their ability to reduce the effective diameter, which ultimately lowers the torque (Moore et al., 1996; Aston et al., 1998). In some cases, non-rotating subs are also used, however, their applicability is limited to cased hole lengths (Thomas et al., 2008). Figure 3.14 shows a schematic of NRDPP, which is a sleeve placed on a bearing surface that becomes the point of contact for torque generation (WellPlan User Guide, 2014). The outer diameter of the sleeve is greater than that of the drill pipe, which creates the required standoff, and the diameter of the bearing surface becomes the effective diameter considered in torque calculations.

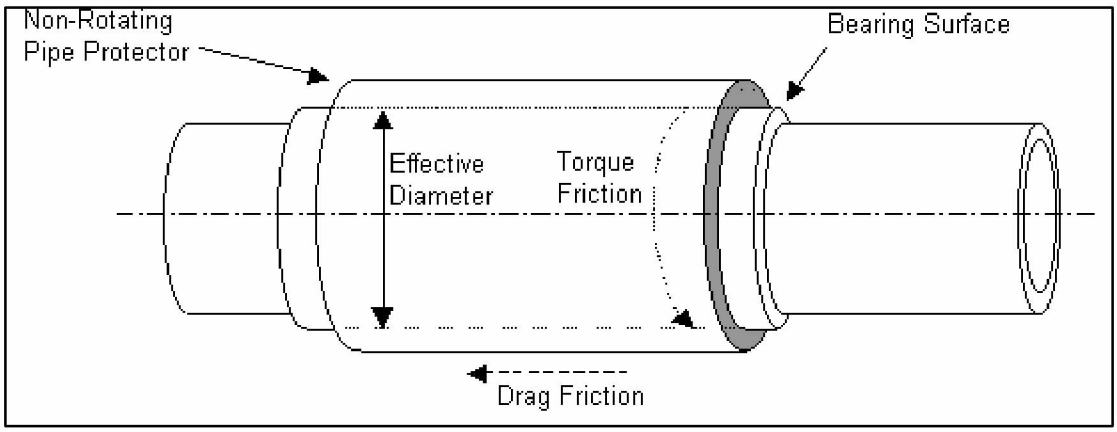

Figure 3.14: Schematic of NRDPP (WellPlan User Guide, 2014).

In this study, we used a WWT Super Slider 3 as the NRDPP. The selection was based upon the tool's usability in open hole applications, small (less than one minute) connection time, and ability to withstand a rotary speed of 200 rpm as designed for the optimized drill string. The NRDPPs were placed in the initial build section, as well as in the final drop-off section for S-shaped wells, to overcome the high contact forces generated in this section. For slant wells, they were placed between 416 ft MD and 2140 ft MD with 1 unit per 3 joints. In the case of S-shaped wells, they were placed between 358 ft MD and 1907 ft MD in the initial build section and from 6444 ft MD and 7465 ft MD in the final drop-off section, with 1 unit per 3 joints in both sections. Figure 3.15 shows the torque variation as a function of the NRDPP's effective friction factor for slant and S-shaped wells. The reduction in the torque is due to relative radial friction of the bearing surface, which acts as a multiplier to reduce the hole friction factor, which in this case is 0.4. For WWT SS3, the relative radial friction of the bearing surface ranges from 0.5 to 0.1 (WWT International, 2015). The results shown in Figure 3.15 show that by using NRDPP with the optimized drill string, the torque rating for both S-shaped and slant wells can be decreased, as per API recommendations. Moreover, since NRDPP is only additional equipment and does not have any impact on dogleg and inclination, we can conclude that the range defined for variation of dogleg for S-shaped and slant wells satisfies both the anti-collision considerations and the torque and drag requirements.

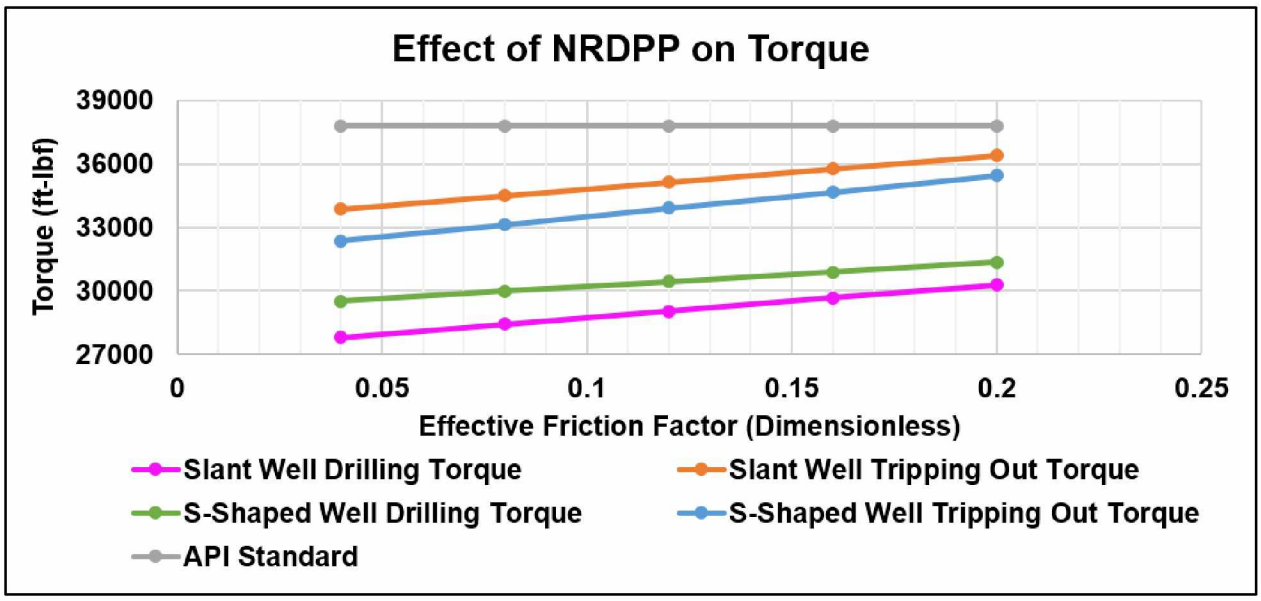

Figure 3.15: Torque variation as a function of effective friction factor generated by NRDPP for slant well with DLS of 1.05°/100 ft and 4.25° inclination and for S-shaped well with DLS of 1.8°/100 ft and 6° inclination, in the final drop-off section, when relative radial friction in the build section was set at 0.5.

3.8 Conclusions

The following conclusions can be made for the soft string model used in the study:

1. As the well complexity measured by DDI decreases, higher WOB can be applied on the same bit type, indicating higher ROP.
2. During tripping out with combined motion, the optimal combination is achieved for low trip speeds and high rotational speed.
3. The magnitude of hydrodynamic viscous forces and, in turn, the effect of mud rheology is very small to affect the tripping out drag for both the RSS and the motor BHA. However, they should still be considered in the soft string model for realistic and practical purposes.
4. Higher reduction in effective tension and greater MOP is achieved for a larger and heavier drill pipe.
5. The optimized drill string in terms of operational parameters consists of:
    a. RSS BHA as the steerable tool

b. 5", 25.6 ppf, S-135 drill pipe
c. 60 ft/min and 200 rpm as the optimal tripping and rotational speeds respectively

6. A generalized trial and error approach has been proposed for optimizing the range for variation of inclination and dogleg as a function of azimuth.
7. Based on the existing well paths and well design in Schrader Bluff, a 9-7/8" hole section can be drilled for all well profiles, with their respective RSS BHAs used in the study. However, in the case of S-shaped and slant well profiles, NRDPPs must be used in the build sections to reduce the torque ratings as per API standards.

3.9 Acknowledgement

The authors would like to extend their sincere thanks to Landmark Solutions, Halliburton for the software support throughout the process, and the Oil and Gas Division of the Department of Natural Resources (DNR) for providing the data for the study.

CHAPTER 4: GENERAL CONCLUSIONS AND RECOMMENDATIONS

4.1 Conclusions

This research focused on two of the most important aspects of directional well planning, namely, anti-collision and torque and drag analysis.

Chapter 2 shows that using nudging and optimum align technique can overcome wellbore collision scenarios during the well planning phase. Furthermore, the performance of the newly developed OWSG error model was compared to the long term industry standard, the ISCWSA error model. These results demonstrate that the OWSG error model performs better and should be preferred during the anti-collision study based on its conciseness. The results of sensitivity analysis on location highlight the fact that positional uncertainty degrades approximately by a factor of 2 in high latitude areas like Alaska, the North Sea, the Barents Sea, and the Beaufort Sea. Moreover, these results highlight that the improved MWD tool generates 73% smaller uncertainties than the gyroscopic tools which were the preferred option in such areas. The poor quality of wellbore positioning led to the investigation of the risk-based collision avoidance model in such areas. The results showed that for enhanced safety of drilling operations, well planners working in high latitude areas should increase the cut-off limits for the risk-based collision avoidance model. The results presented in this chapter led to the formulation of an improved and detailed anti-collision risk management workflow for Arctic areas, including the crucial steps of selection of survey tool, error model, and SF magnitude.

Chapter 3 was a follow-up study to understand the torque and drag perspective of the well paths planned using the improved anti-collision workflow. The drill string design required to understand this behavior was optimized in terms of operational parameters for WOB, trip and rotational speed, mud rheology, drill pipe size, and steerable tool. The results indicate that the RSS BHA performs better than mud motor BHA because of higher WOB capabilities, higher reduction in effective tension and higher increase in MOP at comparatively lower torque ratigs, and lower hydrodynamic viscous loss. The overall optimization results demonstrate that RSS BHA with 5”, 25.6 ppf, S-135 drill pipe should be used to drill most common 9-7/8” intermediate hole section in Schrader Bluff and the

drill string should be pulled out at the 60 ft/min and 200 rpm to minimize the effective tension and increase the MOP. To reduce the torque requirements of this optimized drill string as per API standards, a generalized procedure to optimize the well path as a function of azimuth was proposed. Using this process, a range of inclination and dogleg for a particular azimuth was generated. Since the acceptable values of inclination and dogleg are generated by keeping anti-collision as the focal point, this process will reduce a significant amount of time required by the well planners to finalize a well plan. Furthermore, in cases where optimization of well path does not reduce torque ratings, this procedure shows the corrective measures, via the use of NRDPP, that can maintain the safety standards as per API recommendations.

In summary, the results of this research highlight the planning considerations required for horizontal, slant, and S-shaped wells, and demonstrates how each of these wells can be drilled and tripped out as per API recommendations.

4.2 Recommendations

The scope for further research in this area includes:

1. During the anti-collision study, only mother wellbores from S-pad were classified as existing wellbores. However, the presence of laterals from these wellbores can be considered to evaluate the hazard and risk management model at higher locations.

2. The torque and drag analysis in this study was carried out using the soft string model. It would be interesting to compare these results to those generated by a stiff string model.

3. The initial drill string used in Chapter 3 was adapted from the literature. However, using the actual drill string design for Milne Point would give more realistic and accurate results for the torque and drag analysis.

4. A complete economic evaluation is required for selection of the survey tool in anti-collision study and feasibility of the optimized drill string in torque and drag study.

5. Using the results of trip and rotational speed presented in Chapter 3, along with the actual drill string design, the hydraulics of the system, including flow rate and pressure losses, can also be optimized.

6. To complete the study from well planning to well construction, the thermal effects of permafrost on well design should also be analyzed. This can be achieved using WellCat©, which will simulate a downhole temperature profile and the corresponding loads and stresses on casing during drilling operations.

REFERENCES

Aadnoy, B.S., and Andersen, K. 2001. Design of Oil Wells Using Analytical Friction Models. *J. Petrol. Sci. Eng.* **32** (01): 53-71. https://doi.org/10.1016/S0920-4105(01)00147-4.

Aadnoy, B. S., Fazaelizadeh, M., & Hareland, G. 2010. A 3D Analytical Model for Wellbore Friction. *J. Can. Petrol. Technol.* **49** (10): 25-36. SPE-141515-PA. http://doi.org/10.2118/141515-PA.

Aarrestad, T. V., & Blikra, H. 1994. Torque and Drag-Two Factors in Extended-Reach Drilling. *J. Petrol. Technol.* **46** (09): 800-803. SPE-27491-PA. http://doi.org/10.2118/27491-PA.

Abahusayn, M., Foster, B., Brink, J., Kuck, M., & Longo, J. 2012. Nikaitchuq Extended-Reach Drilling: Designing for Success on the North Slope of Alaska. *SPE Drill. and Comp.* 27 (04): 501-515. SPE-149778-PA. http://doi.org/10.2118/149778-PA.

Adams, N. J. 1985. *Drilling Engineering: A complete Well Planning Approach*. First edition. Tulsa, Oklahoma: PenWell Corporation.

Adewuya, O. A., & Pham, S. V. 1998. A Robust Torque and Drag Analysis Approach for Well Planning and Drillstring Design. Presented at the SPE/IADC Drilling Conference and Exhibition, Dallas, Texas, 3-6 March. SPE-39321-MS. http://doi.org/10.2118/39321-MS.

Alvord, C., Noel, B., Galiunas, L., Johnson, V., Holtzman, K., Dennis, J., Smith, L. 2007. Onshore ERD Wells prove RSS effectiveness for Alaska. *World Oil*, June 2007. pp. 47-54.

AOGCC. 2017. Well history file. http://aogweb.state.ak.us/WebLink/0/doc/29730/Page1.aspx (accessed 1 March 2017).

Aslaksen, H., Annand, M., Duncan, R., Fjaere, A., Paez, L., & Tran, U. 2006. Integrated FEA Modeling Offers System Approach to Drillstring Optimization. Presented at the SPE/IADC Drilling Conference, Miami, Florida, 21-23 February. SPE-99018-MS. http://doi.org/10.2118/99018-MS.

Aston, M. S., Hearn, P. J., & McGhee, G. 1998. Techniques for Solving Torque and Drag Problems in Today's Drilling Environment. Presented at the SPE Annual Technical Conference and Exhibition, New Orleans, Louisiana, 27-30 September. SPE-48939-MS. http://doi.org/10.2118/48939-MS.

Azar, J. J., & Samuel, R. G. 2007. *Drilling Engineering*. First edition. Tulsa, Oklahoma: PenWell Corporation.

Bang, J., Torkildsen, T., Bruun, B. T., & Havardstein, S. T. 2009. Targeting Challenges in Northern Areas due to Degradation of Wellbore Positioning Accuracy. Presented at the SPE/IADC Drilling Conference and Exhibition, Amsterdam, Netherlands, 17-19 March. SPE-119661-MS. https://doi.org/10.2118/119661-MS.

Bang, J., & Torkildsen, T. 2011. Wellbore Anti-Collision Safety: Separation Distances Must Be Increased Due To Degraded Positioning Accuracy In Northern Areas. Presented at the SPE Arctic and Extreme Environments Conference and Exhibition, Moscow, Russia, 18-20 October. SPE-149699-MS. https://doi.org/10.2118/149699-MS.

Boonsri, K. 2014. Torque Simulation in the Well Planning Process. Presented at the SPE/IADC Asia Pacific Drilling Technology Conference, Bangkok, Thailand, 25-27 August. SPE-170500-MS. http://doi.org/10.2118/170500-MS.

Buchanan, A., Finn C.A., Love J.J., Worthington E.W., Lawson F., Maus S., Okewunmi S., Poedjono A. 2013. Geomagnetic Referencing - The Real-Time Compass for Directional Drillers. Oilfield Review **25** (03): 32–47.

Caglayan, K., B. 2014 Torque and Drag Applications for Deviated and Horizontal Wells: A Case Study. Master's Thesis. Middle East Technical University, Ankara, Turkey.

Cernocky, E. P., & Scholibo, F. C. 1995. Approach to Casing Design for Service in Compacting Reservoirs. Presented at the SPE Annual Technical Conference and Exhibition, Dallas, Texas, 22-25 October. SPE-30522-MS. http://doi.org/10.2118/30522-MS.

Chatar, C., Beck, N., Simeone, D., Buchanan, A., Borri, L., & Occhionero, L. 2015. Anti-Collision Considerations for Arctic and Other High Latitude Locations. Presented at the SPE/IADC Drilling Conference and Exhibition, London, England, UK, 17-19 March. SPE-173047-MS. https://doi.org/10.2118/173047-MS.

Chaudhry, A., Sallee, A., Burton, J., Lazzari, A., Kuck, M., Ravagli, B., Simeone, D., Kuwairi, A. 2016. Operational Improvements Drilling One Million Feet at Nikaitchuq. Presented at the SPE Western Regional Meeting, Anchorage, Alaska. SPE-180443-MS. http://doi.org/10.2118/180443-MS.

Chia, C. R., & de Lima, B. C. 2004. MWD Survey Accuracy Improvements Using Multistation Analysis. Presented at the SPE/IADC Asia Pacific Drilling Technology Conference and Exhibition, Kuala Lumpur, Malaysia, 13-15 September. SPE-87977-MS. https://doi.org/10.2118/87977-MS.

Compass User Guide. 2011. Halliburton Landmark Software & Services, Houston, Texas.

Costeno, H., Djohor, M., Raziyev, M., Sessarego, H. L., Subroto, B., Ismail, A., Mond, M. 2014. Improving Collision Avoidance and Target Accuracy in an Offshore Brownfield Redevelopment Combining Gyros and In-Field Referencing. Presented at the International Petroleum Technology Conference, Doha, Qatar, 19-22 January. IPTC-17363-MS. https://doi.org/10.2523/IPTC-17363-MS.

Cunningham, R. A. 1960. Laboratory Studies of the Effect of Rotary Speed on Rock-bit Performance and Drilling Cost. *API Drill. and Prod. Practice*. API-60-007.

Davies, B. E., Newby, N., & Smart, A. B. 1979. Deep Permafrost Oil Production: The First Two Years. Presented at the World Petroleum Congress, Bucharest, Romania, 9-14 September. WPC-18201.

Dhar, D., K. & Gandhi S., D. 1994. Well Planning. In *ONGC Drilling Operations Manual*. ed. Bias, P, Chap. 7. Parel, Bombay: Goodprint.

Dunn, D., M., Crane, R., L., & Thomas, L., R. 2005. North Slope Drilling Practices – Ever Adapting to New Challenges. Presented at the American Association of Drilling Engineers National Technical Conference, Houston, Texas, 5-7 April. AADE-05-NTCE-07.

Everdingen, R. O. 1998. *Multi-language Glossary of Permafrost and Related Ground-Ice Terms*. The Arctic Institute of North America, The University of Calgary, Calgary, Alberta, Canada. T2N 1N4.

Fazaelizadeh, M., Hareland, G., & Aadnoy, B. S. 2010. Application of New 3-D Analytical Model for Directional Wellbore Friction. *Modern Applied Science* **04** (02): 2-22. http://doi.org/10.5539/mas.v4n2p2.

Fletcher, H. G. 2011. Arctic Drilling Operations Planning and Execution: Feedback from Kharyaga Field, Russia. Presented at the SPE Arctic and Extreme Environments Conference and Exhibition, Moscow, Russia, 18-20 October. SPE-149765-MS. http://doi.org/10.2118/149765-MS.

Goodman, Malcolm A. 1978. *World Oil's Handbook of Artic Well Completions*, World Oil, Houston, Texas.

Grindrod, S. J., Clark, P. J., Lightfoot, J. D., Bergstrom, N., & Grant, L. S. 2016. OWSG Standard Survey Tool Error Model Set for Improved Quality and Implementation in Directional Survey Management. Presented at the SPE/IADC Drilling Conference and Exhibition, Fort Worth, 1-3 March. SPE-178843-MS. https://doi.org/10.2118/178843-MS

Grindrod, S. OWSG Set A: Standard Error Model (28 April 2017, Revision No. 2. https://copsegrove.sharepoint.com/Documents/OWSG_Set_A_Standard_Error_Model_Set_Rev2_28Apr 2017.xlsx (accessed 7 May 2017).

G, R., Samuel, X., Liu. 2009. *Advanced Drilling Engineering: Principles and Designs*, first edition. Houston, Texas: Gulf Publication.

Hawkinson, B., & Mullin, S. 2014. Presentation given at 39th SPE WPTS Meeting, Long Beach, California, May 9, 2014.

Hawkinson, B. 2014. Presentation given for Scientific Drilling International, September 30, 2014.

Ho, H.-S. 1988. An Improved Modeling Program for Computing the Torque and Drag in Directional and Deep Wells. Presented at the SPE Annual Technical Conference and Exhibition, Houston, Texas, 2-5 October. SPE-18047-MS. http://doi.org/10.2118/18047-MS.

Hoan Van Luu. 2015. Presentation given at SPE Rotary Steerable System Workshop, Queensland, Australia, October 21, 2015.

Huracan. 2017. Continuous Gyro Brochure. http://huracan.com.au/wordpress/wp-content/uploads/2017/11/Huracan_Continuous_Gyro_Brochure.pdf (accessed 3 December 2017).

ICF International. 2016. Recommendations for Improvements to Wellbore Surveying and Ranging Regulations. Final Report, BPA No. E13PA00010, US-BSEE, Sterling, VA (August 2016).

Inglis, A., T. 1987. *Directional Drilling*. First Edition. London, United Kingdom: Graham & Trotman Limited.

Ismayilov, O. 2012. Application of 3-D Analytical Model for Wellbore Friction Calculation in Actual wells. Master's Thesis. Norwegian University of Science and Technology, Trondheim, Norway.

Jamieson, A. 2012. *Introduction to Wellbore Positioning*, first edition. Inverness: Research Office of University of Highlands and Islands.

Johancsik, C. A., Friesen, D. B., & Dawson, R. 1994. Torque and Drag in Directional Wells-Prediction and Measurement. *J. Pet. Technol.* **36** (6): 987-992. SPE-11380-PA. http://doi.org/10.2118/11380-PA.

Kutasov, I. M., & Caruthers, R. M. 1988. Hole Enlargement Control During Arctic Drilling. Presented at the SPE California Regional Meeting, Long Beach, California, 23-25 March. SPE-17442-MS. http://doi.org/10.2118/17442-MS.

Lesage, M., Falconer, I. G., & Wick, C. J. 1988. Evaluating Drilling Practice in Deviated Wells With Torque and Weight Data. *SPE Drill. Eng.* **03** (03): 248-252. SPE-16114-PA. http://doi.org/10.2118/16114-PA.

Lowdon, R. M., & Chia, C. R. 2003. Multistation Analysis and Geomagnetic Referencing Significantly Improve Magnetic Survey Results. Presented at the SPE/IADC Drilling Conference and Exhibition, Amsterdam, Netherlands, 19-21 February. SPE-79820-MS. https://doi.org/10.2118/79820-MS.

Maidla, E. E., & Wojtanowicz, A. K. 1987b. Field Comparison of 2-D and 3-D Methods for the Borehole Friction Evaluation in Directional Wells. Presented at the SPE Annual Technical Conference and Exhibition, Dallas, Texas, 27-30 September. SPE-16663-MS. http://doi.org/10.2118/16663-MS.

Mason, C., & Chen, D. C.-K. 2006. The Drilling and Casing Running Enigma. Presented at the SPE Annual Technical Conference and Exhibition, San Antonio, Texas, 24-27 September. SPE-100749-MS. http://doi.org/10.2118/100749-MS.

Mason, C., & Chen, D. C.-K. 2007. Step Changes needed to Modernise T&D Software. Presented at the SPE/IADC Drilling Conference and Exhibition, Amsterdam, Netherlands, 20-22 February. SPE-104609-MS. http://doi.org/10.2118/104609-MS.

Maus, S., & DeVerse, S. 2015. Enhanced Wellbore Placement Accuracy Using Geomagnetic In-Field Referencing and Multi-Station Correction. Presented at the Unconventional Resources Technology Conference, San Antonio, 20-22 July. URTEC-2173526-MS. https://doi.org/10.15530/URTEC-20152173526.

McCormick, J. E., Frilot, M. A., & Chiu, T. 2011. Torque and Drag Software Model Comparison: Impact on Application and Calibration of Field Data. Presented at the Brazil Offshore Conference and Exhibition, Macae, Brazil, 14-17 June. SPE-143623-MS. http://doi.org/10.2118/143623-MS.

McNair, G. A., Lance, S. J., Codling, J., & Watson, R. 2005. Implementation of a New Risk Based Well Collision Avoidance Method. Presented at the SPE/IADC Drilling

Conference and Exhibition, Amsterdam, Netherlands, 23-25 February. SPE-92554-MS. https://doi.org/10.2118/92554-MS.

McSpadden, A. R., Coker, O. D., & Ruan, G. C. 2012. Advanced Casing Design With Finite-Element Model of Effective Dogleg Severity, Radial Displacements, and Bending Loads. *SPE Drill & Compl* **27** (03): 436-448. SPE-141458-PA. http://doi.org/10.2118/141458-PA.

Menand, S., Sellami, H., Tijani, M., Stab, O., Dupuis, D. C., & Simon, C. 2006. Advancements in 3D Drillstring mechanics: From the Bit to the Topdrive. Presented at the SPE/IADC Drilling Conference, Miami, Florida, 21-23 February. SPE-98965-MS. http://doi.org/10.2118/98965-MS.

Miller, R., Terpening, M., Conran, G. 2003. Survey Management Provides a Safer Drilling Environment with Reduced Drilling Costs. Presented at the American Association of Drilling Engineers National Technical Conference, Houston, 1-3 April. AADE-03-NTCE-19.

Mims, M., & Krepp, T. 2003. *Drilling design and Implementation for Extended Reach and Complex Wells.* Third Edition. Houston, Texas: K&M Technology Group LLC.

Mitchell, B. 1995. *Advanced Oilwell Drilling Engineering Handbook & Computer Programs*. Tenth Edition. Lakewood, Colorado: Mitchell Engineering.

Moore, N. B., Mock, P. W., & Krueger, R. E. 1996. Reduction of Drill String Torque and Casing Wear in Extended Reach Wells Using Non-Rotating Drill Pipe Protectors. Presented at the SPE Western Regional Meeting, Anchorage, Alaska, 22-24 May. SPE-35666-MS. http://doi.org/10.2118/35666-MS.

Nyrnes, E., Torkildsen, T., & Wilson, H. 2009. Minimum Requirements for Multi-Station Analysis of MWD Magnetic Directional Surveys. Presented at the SPE/IADC Drilling Conference and Exhibition, Manama, Bahrain, 26-28 October. SPE-125677-MS. https://doi.org/10.2118/125677-MS.

Okewunmi, S., & Brooks, A. G. 2011. A Comparison of Collision Avoidance Calculations. Presented at the SPE/IADC Drilling Conference and Exhibition, Amsterdam, Netherlands, 1-3 March. SPE-140183-MS. https://doi.org/10.2118/140183-MS.

Payne, M. L., & Abbassian, F. 1997. Advanced Torque and Drag Considerations in Extended-Reach Wells. *SPE Drill & Compl* **12** (01): 55-62. SPE-35102-PA. http://doi.org/10.2118/35102-PA.

Poedjono, B., Akinniranye, G., Conran, G., Spidle, K., & San Antonio, T. A. 2006. Well-Collision Risk in Congested Environments. Presented at the SPE Asia Pacific Oil & Gas Conference and Exhibition, Adelaide, Australia, 11-13 September. SPE-101719-MS. http://doi.org/10.2118/101719-MS.

Poedjono, B., Akinniranye, G., Conran, G., Spidle, K., San Antonio, T., A. 2007a. A Comprehensive Approach to Well-Collision Avoidance. Presented at the American Association of Drilling Engineers National Technical Conference, Houston, 10-12 April. AADE-07-NTCE-28.

Poedjono, B., Conran, G., Akinniranye, G., Phillips, W. J., & San Antonio, T. A. 2007b. Minimizing the Risk of Well Collisions in Land and Offshore Drilling. Presented at the SPE/IADC Middle East Drilling and Technology Conference, Cairo, Egypt, 22-24, October. SPE-108279-MS. http://doi.org/10.2118/108279-MS.

Poedjono, B., Phillips, W. J., & Lombardo, G. J. 2009. Anti-Collision Risk Management Standard for Well Placement. Presented at the SPE Americas E&P Environmental and Safety Conference, 23-25 March, San Antonio, Texas. SPE-121040-MS. http://doi.org/10.2118/121040-MS.

Poedjono, B., Adly, E. E., Terpening, M., & Li, X. 2010. Geomagnetic Referencing Service - A Viable Alternative for Accurate Wellbore Surveying. Presented at the SPE/IADC Drilling Conference and Exhibition, New Orleans, 2-4 February. SPE-127753-MS. https://doi.org/10.2118/127753-MS.

Rabia, H. 1985. *Well Engineering and Construction*. First edition. London, United Kingdom: Entrac Petroleum.

Rae, G., Lesso, W. G., & Sapijanskas, M. 2005. Understanding Torque and Drag: Best Practices and Lessons Learnt from the Captain Field's Extended Reach Wells. Presented at the SPE/IADC Drilling Conference and Exhibition, Amsterdam, Netherlands, 23-25 February. SPE-91854-MS. http://doi.org/10.2118/91854-MS.

Rezmer-Cooper, I., Chau, M., Hendricks, A., Woodfine, M., Stacey, B., & Downton, N. 1999. Field Data Supports the Use of Stiffness and Tortuosity in Solving Complex Well Design Problems. Presented at the SPE/IADC Drilling Conference, Amsterdam, Netherlands, 9-11 March. SPE-52819-MS. http://doi.org/10.2118/52819-MS.

Sayers, Z., Sallee, A., Burton, J., & Francis, M. 2015. Unlocking a Frozen Resource: Horizontal Milestone in Permafrost Drilled at -80°Fahrenheit. Presented at the SPE Western Regional Meeting, Garden Grove, California. SPE-174036-MS. http://doi.org/10.2118/174036-MS.

Schlumberger Glossary. 2017. http://www.glossary.oilfield.slb.com/Terms/w/well_plan.aspx (accessed 1 May 2016).

Shanker, S., & Saktavat, S., K. 1994. Well Planning. In *ONGC Drilling Operations Manual*. ed. Bias, P, Chap. 3. Parel, Bombay: Goodprint.

Sheppard, M. C., Wick, C., & Burgess, T. 1987. Designing Well Paths To Reduce Drag and Torque. *SPE Drill. Eng.* **02** (04): 344-350. SPE-15463-PA. http://doi.org/10.2118/15463-PA.

Shur, Y. L. 2016. Introduction of Permafrost Engineering Coursework. College of Engineering and Mines, University of Alaska Fairbanks.

Siddiqui, M., A, Mangla, V, K. & Pandey, A., K. 1994. Well Planning. In ONGC Drilling Operations Manual. ed. Bias, P, Chap. 9. Parel, Bombay: Goodprint.

Smith, R. E., & Clegg, M. W. 1971. Analysis and Design of Production Wells Through Thick Permafrost. Presented at the World Petroleum Congress, Moscow, USSR, 13-18 June. WPC-14244.

Stockholm Precision Tools. 2017. Continuous Gyro Brochure.

http://www.stockholmprecisiontools.com/res/uploads/20140331140733-spt-continous-gyro.pdf (accessed 3 December 2017).

Thomas, R. L., McKeever, S. O., Hartwig, D. D., Egedahl, D. B., Patton, J., Holtzman, K., & Smith, L. 2008. Overcoming Weight Transfer Challenges in Complex, Shallow, Extended Reach Wells on Alaska's North Slope. Presented at the Offshore Technology Conference, Houston, Texas, 5-8 May. OTC-19550-MS. http://doi.org/10.4043/19550-MS.

Tikhonov, V., Valiullin, K., Nurgaleev, A., Ring, L., Gandikota, R., Chaguine, P., & Cheatham, C. 2014. Dynamic Model for Stiff-String Torque and Drag. *SPE Drill & Compl* **29** (03): 279-294. SPE-163566-PA. http://doi.org/10.2118/163566-PA.

Torkildsen, T., Havardstein, S. T., Weston, J. L., & Ekseth, R. 2008. Prediction of Wellbore Position Accuracy When Surveyed with Gyroscopic Tools. *SPE Drill & Compl* **23** (1): 5-12. SPE-90408-PA. https://doi.org/10.2118/90408-PA.

Ugochukwu, O., & Verity, S. 2014. Using Robust Torque and Drag Modelling Software for Efficient Well Planning and Operations Monitoring. Paradigm Sysdrill for OML 126 Wells - A Case Study. Presented at the SPE Nigeria Annual International Conference and Exhibition, Lagos, Nigeria, 5-7 August. SPE-172388-MS. http://doi.org/10.2118/172388-MS.

Ulterra. 2017. Bit Calculations. http://ulterra.com/pdfs/resources/Bit%20Calculations.pdf (accessed 21 November 2017).

USGS. 2017a. Permafrost distribution of Alaska. https://pubs.usgs.gov/ha/ha730/ch_n/N-AKsummary4.html. (accessed 1 November 2017).

USGS. 2017b. Magnetic Observatories. https://geomag.usgs.gov/monitoring/observatories/ (accessed 29 November 2017).

WellPlan User Guide. 2014. Halliburton Landmark Software & Services, Houston, Texas.

Williamson, H. S. 2000. Accuracy Prediction for Directional Measurement While Drilling. *SPE Drill & Compl* **15** (04): 221-233. SPE-67616-PA. https://doi.org/10.2118/67616-PA.

WWT International. 2015. WWT Non-Rotating Protectors Brochure http://wwtinternational.com/pdf/WWT_NRP_Benefits_Brochure_1_2015.pdf (accessed 20 November 2017).

Zarling, J. P. 2016. Arctic Engineering Coursework. College of Engineering and Mines, University of Alaska Fairbanks.